THE UNIVERSITY OF QUEENSLAND

AUSTRALIA

Drainage and Stability of Foam Films during Bubble Coalescence in Aqueous Salt Solutions

Mahshid Firouzi

B.Eng., M.Eng. Chemical Engineering

A thesis submitted for the degree of Doctor of Philosophy at

The University of Queensland in 2014

School of Chemical Engineering

Abstract

Bubble coalescence and thin liquid films (TLFs) between bubbles known as foam films, are central to many daily activities, both natural and industrial. They govern a number of important processes such as foam fractionation, oil recovery from tar sands and mineral recovery by flotation using air bubbles. TLFs are known to be stabilized by some salts and bubble coalescence in saline water can be inhibited at salt concentrations above a critical (transition) concentration. However, the mechanisms of the inhibiting effect of these salts are as yet contentious. The aim of this work is to characterise the behaviour of saline liquid films both experimentally and theoretically to better understand the mechanisms.

The effect of sodium halide and alkali metal salts including NaF, NaBr, NaI, NaCl, KCl and LiCl on the stability of a foam film was investigated by applying the TLF interferometry method. To mimic realistic conditions of bubble coalescence in separation processes, the drainage and stability of TLFs were studied under non-zero bubble (air-liquid interface) approach speeds (10-300 µm/s) utilizing a nano-pump. For each of the salts studied, a critical concentration (C_{cr}) above which liquid films lasted for up to 50 s depending on the salt type, concentration and the interface approach speed, was determined. For concentrations below C_{cr}, the saline liquid films either ruptured instantly or lasted for less than 0.2 s. C_{cr} follows the order NaF<LiCl<NaCl<KCl<NaBr<NaI and was found to be independent of the bubble approach speed in the investigated range of speeds. For TLFs of deionised water, a critical speed of 35 µm/s, above which water films ruptured rapidly, was obtained.

To develop insight into mechanisms of the inhibiting effect of salts, a theoretical investigation was also undertaken. Three models available in the literature to predict C_{cr} were critically examined. The first two models employed the non-retarded and retarded van der Waals attractions to evaluate the C_{cr} from the discriminant of quadratic or cubic polynomials. The third model modified the previous models following the same approach, and replaced van der Waals attractions with hydration repulsions of water molecules. Their model predictions depend on the rupture thickness of liquid films which is usually unknown and requires further experimental work to be determined. To resolve the uncertainty in the first two models concerning the non-retarded and retarded Hamaker constants, the Lifshitz theory on the van der Waals interaction energy and the available spectrum for water dielectric permittivity was

applied to determine the Hamaker constants for saline liquid films. Values of $A = 3.979 \times 10^{-20}\,\mathrm{J}$ and $B = 3.492 \times 10^{-29}\,\mathrm{J \cdot m}$ were obtained for non-retarded and retarded Hamaker constants respectively. The value for the retarded Hamaker constant is almost one order of magnitude larger than what was considered in the second model. Employing the new values for Hamaker constants in the models, it was shown that the role of van der Waals attractions in bubble coalescence in salt solutions is much less significant than previously hypothesized. Therefore another attractive disjoining pressure which is stronger than the van der Waals attraction is required to predict the experimental $C_{cr.}$ To modify the models a novel methodology was proposed which resolves the mathematical uncertainties in modelling the C_{cr} and can explicitly predict it from any relevant intermolecular forces. The generality of the novel methodology was validated by re-applying the theory to establish the previous models obtained by the discriminant method. It was shown further that the third mode is physically inconsistent and not only the repulsive hydration disjoining pressure, but any other repulsive disjoining pressure, cannot be the main driving force for inhibiting bubble coalescence in salt solutions.

Using the novel methodology the model was modified by incorporating hydrophobic attractions. The model suggested by Eriksson et al. (1989) for hydrophobic attractions was employed in the modelling to predict the experimental C_{cr}. The hydrophobic strength and decay length in Eriksson et al.'s model were determined by using the experimental results for the C_{cr} and thickness. A power law correlation was proposed for the hydrophobic constant of different salt types as a function of the salting-out coefficient as representative of salt type. The predicted C_{cr} values are in a good agreement with the experimental data obtained in this thesis and in the literature.

It is envisaged that the outcomes of this work will contribute to a better understanding of the mechanisms responsible for the stability of foam films between two bubbles in saline water. The proposed novel methodology allows further improvements to the models for predicting C_{cr} values, for example, by incorporating the effect of inertia. The proposed correlation for the hydrophobic constant could also be modified based on the force measurement data for foam films of salt solutions.

Declaration by author

This thesis is composed of my original work, and contains no material previously published or written by another person except where due reference has been made in the text. I have clearly stated the contribution by others to jointly-authored works that I have included in my thesis.

I have clearly stated the contribution of others to my thesis as a whole, including statistical assistance, survey design, data analysis, significant technical procedures, professional editorial advice, and any other original research work used or reported in my thesis. The content of my thesis is the result of work I have carried out since the commencement of my research higher degree candidature and does not include a substantial part of work that has been submitted to qualify for the award of any other degree or diploma in any university or other tertiary institution. I have clearly stated which parts of my thesis, if any, have been submitted to qualify for another award.

I acknowledge that an electronic copy of my thesis must be lodged with the University Library and, subject to the General Award Rules of The University of Queensland, immediately made available for research and study in accordance with the *Copyright Act 1968*.

I acknowledge that copyright of all material contained in my thesis resides with the copyright holder(s) of that material. Where appropriate I have obtained copyright permission from the copyright holder to reproduce material in this thesis.

Publications during candidature

Book chapter:

1 Anh V. Nguyen, **Mahshid Firouzi**," Collision and Attachment Interactions of Single Air Bubbles with Flat Surfaces in Aqueous Solutions", Drops and Bubbles in Contact with Solid Surfaces, (2012). In: M. Ferrari, L. Liggieri and R. Miller (Editors), Drops and Bubbles in Contact with Solid Surfaces (Book series: Progress in Colloid and Interface Science, Vol. 3), Brill, Leiden (the Netherlands), Chapter 9, pp. 211-240.

Peer-reviewed papers:

2 **Mahshid Firouzi**, Anh Nguyen, S.H. Hashemabadi "The Effect of Micro Hydrodynamics on Bubble-Particle Collision Interaction", *Minerals Engineering*, (2011) 24(9):973–986.

3 **Mahshid Firouzi**, Anh Nguyen, "Different Effects of Monovalent Anions and Cations on the Bubble Coalescence and Lifetime of Aqueous Films between Air Bubbles", In *Chemeca conference proceedings*, Brisbane, Australia, 29 September – 2 October, 2013, Paper No. 29706.

4 **Mahshid Firouzi**, Anh Nguyen, "On the Effect of Van der Waals Attractions on the Critical Salt Concentration for Inhibiting Bubble Coalescence", *Minerals Engineering*, (2014) 58:108-112.

5 **Mahshid Firouzi**, Anh Nguyen, "A Novel Methodology for Predicting Critical Salt Concentration of Bubble Coalescence Inhibition", *The Journal of Physical Chemistry C*, (2014) 118:1021-1026.

6 **Mahshid Firouzi**, Anh Nguyen, "Effects of Monovalent Anions and Cations on Drainage and Lifetime of Foam Films at Different Interface Approach Speeds", *Advanced Powder Technology*, (2014) 25: 1212-1219

7 **Mahshid Firouzi**, Tony Howes and Anh Nguyen, "A Quantitative review of the transition salt concentration for inhibiting bubble coalescence", *Advances in Colloid and Interface Science*, (2014), DOI: 10.1016/j.cis.2014.07.005.

8 **Mahshid Firouzi**, Anh Nguyen, "Critical salt concentration of bubble coalescence inhibition: effect of dissolved gases and hydrophobic attraction", Submitted to *The Journal of Physical Chemistry C*, July (2014)

Conference abstracts:

9 **Mahshid Firouzi**, Anh Nguyen, “Novel Analysis of the Topology of Liquid Films between Air Bubbles”, presented at UQ Engineering Postgraduate Research Conference, June (2013).

10 **Mahshid Firouzi**, Anh Nguyen, “A Novel Methodology for Predicting Critical Salt Concentration of Bubble Coalescence Inhibition”, presented at UQ Engineering Postgraduate Research Conference, June (2014).

Publications included in this thesis

Anh V. Nguyen, Mahshid Firouzi,” Collision and Attachment Interactions of Single Air Bubbles with Flat Surfaces in Aqueous Solutions”, Drops and Bubbles in Contact with Solid Surfaces, (2012) CRC Press: 10% of this book chapter is incorporated as Chapter 2.

Contributor	Statement of contribution
Mahshid Firouzi (Candidate)	Wrote the chapter (55%)
Anh V. Nguyen	Wrote and edited the chapter (45%)

Mahshid Firouzi, Tony Howes and Anh Nguyen, “A Quantitative review of the transition salt concentration for inhibiting bubble coalescence”, *Advances in Colloid and Interface Science*, (2014) incorporated as Chapter 2.

Contributor	Statement of contribution
Mahshid Firouzi (Candidate)	Analysed the results (100%) Wrote the paper (85%)
Tony Howes	Analysed the results (0%) Edited the paper (5%)
Anh V. Nguyen	Analysed the results (0%) Edited the paper (10%)

Mahshid Firouzi, Anh Nguyen, “Effects of Monovalent Anions and Cations on Drainage and Lifetime of Foam Films at Different Interfacial Approach Speeds”, *Advanced Powder Technology*, (2014) 25: 1212-1219, incorporated as Chapter 3.

Contributor	Statement of contribution
Mahshid Firouzi (Candidate)	• Designed experiments (90%) • Conducted experiments (100%) • Wrote the paper (85%)
Anh V. Nguyen	• Designed experiments (10%) • Conducted experiments (0%) • Wrote and edited the paper (15%)

Mahshid Firouzi, Anh Nguyen, “On the Effect of Van der Waals Attractions on the Critical Salt Concentration for Inhibiting Bubble Coalescence”, Minerals Engineering, (2014) 58:108-112, incorporated as Chapter 4.

Contributor	Statement of contribution
Mahshid Firouzi (Candidate)	• Examined models and collected results (85%) • Wrote the paper (65%)
Anh V. Nguyen	• Examined models and collected results (15%) • Wrote and edited the paper (35%)

Mahshid Firouzi, Anh Nguyen, “A Novel Methodology for Predicting Critical Salt Concentration of Bubble Coalescence Inhibition”, *The Journal of Physical Chemistry C*, (2014) 118:1021-1026, incorporated as Chapter 5.

Contributor	Statement of contribution
Mahshid Firouzi (Candidate)	• Derived the model and collected results (70%) • Wrote the paper (60%)
Anh V. Nguyen	• Deriving the model and collecting results (30%) • Wrote and edited the paper (40%)

Mahshid Firouzi, Anh Nguyen, “Critical salt concentration of bubble coalescence inhibition: effect of dissolved gases and hydrophobic attraction”, Submitted to *The Journal of Physical Chemistry C*, July (2014) incorporated as Chapter 6.

Contributor	Statement of contribution
Mahshid Firouzi (Candidate)	• Designed experiments (95%) • Conducted experiments (100%) • Derived the model and collected results (95%) • Wrote the paper (85%)
Anh V. Nguyen	• Designed experiments (5%) • Conducted experiments (0%) • Derived the model and collected results (5%) • Wrote and edited the paper (15%)

Contributions by others to the thesis

None.

Statement of parts of the thesis submitted to qualify for the award of another degree

None.

Acknowledgements

First, I would like to express my deepest appreciation to my supervisor Prof. Anh Nguyen without whom, it would have not been possible for me to complete this journey. Your patience, time, help and encouragement along the way are greatly appreciated. Your advices have been priceless.

I would like to thank my co-supervisor A/Prof. Tony Howes for the helpful feedback and assistance.

I would like to thank my committee members, Prof. Joe Da Costa and Prof. Jason Stokes for their guidance and support at each milestone.

A special gratitude I give to Dr. Stoyan Karakashev for his valuable advice and long discussions through emails. I have never met him but he is without any doubt one of my best friends and I will never forget his kindness.

Thanks to my group members for sharing ideas and providing me helpful feedback during our group meetings. Special thanks to Mr Phong Nguyen for teaching me patiently the micro-interferometric technique and to Dr.Tuan Nguyen for his help in writing the MATLAB code for image processing of interferograms.

I would like to thank Ms Siu-Bit Iball and all the staff of the School of Chemical Engineering for their kind assistance.

I would like to acknowledge the financial support from the University of Queensland (UQ) for the tuition fee and living allowance. Thanks to UQ Graduate School for the Graduate School International Travel Award (GSITA). I would also like to thank Prof. Hans-Jürgen Butt, Dr. Michael Kappl and Prof. Reinhard Miller and all of their group members for hosting my visit to the Max Planck institutes in Mainz and Golm.

Thanks to all my friends and colleagues in the Chemical Engineering postgraduate community for their support and friendship throughout the course of my PhD. Special thanks to Faezeh, Chris, Xiaoyu, Kimia and Amir for being with me, listening to me and for all the happy memories. I am so lucky to have lovely friends like you.

I would also like to thank dear Fiona and Winston, my partner Richard's parents, for their love and kindness.

Last but not least I would like to dedicate this work to my parents and my fiancé, Richard, who have always been supportive throughout the course of this journey. I owe you a lot mother and father for your unconditional love, support and encouragement from a long

distance. Richard, you are a great partner, teacher and advisor. Thanks for listening to me patiently at every stage of this journey.

Keywords

Bubble coalescence, saline liquid films, interface approach speed, colloidal force, air-water interface, critical salt concentration, hydrophobic attraction and dissolved gasses

Australian and New Zealand Standard Research Classifications (ANZSRC)

ANZSRC code: 090499, Chemical Engineering not elsewhere classified, 60%
ANZSRC code: 030306, Chemical Science/Physical Chemistry, 30%
ANZSRC code: 091404, Mineral Processing/Beneficiation, 10%

Fields of Research (FoR) Classification

FoR code: 0904, Chemical Engineering, 60%
FoR code: 0303, Chemical Science/Physical Chemistry, 30%
FoR code: 0914, Resources Engineering and Extractive Metallurgy, 10%

TABLE OF CONTENTS

CONTENTS

Abstract i
Declaration by author iii
Publications during candidature iv
Publications included in this thesis v
Contributions by others to the thesis vii
Statement of parts of the thesis submitted to qualify for the award of another degree vii
Acknowledgements viii
Keywords ix
Australian and New Zealand Standard Research Classifications (ANZSRC) ix
Fields of Research (FoR) Classification ix
Table of Contents x
Chapter 1: Introduction 1
1.1 Background to the Research 2
1.2 Research Aims and Objectives 4
1.3 Hypotheses 4
1.4 Statement of Originality 5
1.5 Structure of the thesis 6
References 6
Chapter 2: A Quantitative Review Of The Transition Salt Concentration For Inhibiting Bubble Coalescence .....
2.1 Abstract 10
2.2 Introduction 10
2.3 Effect of salts on Bubble coalescence 12
2.4 Experimental techniques 15
2.4.1 Bubble column 15
2.4.2 stirred tank 18
2.4.3 Adjacent capillaries 19
2.4.4 Thin liquid film micro-interferometry 23
2.4.5 Comparison of transition concentrations of salts 25
2.5 Reasons for inhibiting bubble coalescence 29
2.5.1 Colloidal forces 29
2.5.2 Gas solubility 31
2.5.3 Gibbs-Marangoni effect 31
2.5.4 Surface Rheology 32
2.5.5 Ion-specific effect 35
2.6 Theoretical models 39
2.7 Summary and conclusion 43
Acknowledgement 43
References 43
Chapter 3: Effects Of Monovalent Anions And Cations On Drainage And Lifetime Of Foam Films At Different Interface Approach Speeds .....
3.1 Abstract 51
3.2 Introduction 51
3.3 Experimental method and material 52
3.4 Results and discussion 54
3.4.1 Film drainage driven by interface approach speed 54
3.4.2 Effect of different air-liquid interface approach speeds 56

3.4.3 Effect of monovalent ions on bubble coalescence 60
3.4.3.1 Effect of colloidal forces 64
3.4.3.1 Ion-specific effect 66
3.4.3.3 Effects of viscosity and surface rheology 69
3.5 Conclusions 70
Acknowledgements 71
References 71
Chapter 4: On the effect of van der Waals attractions on the critical salt concentration for inhibiting bubble coalescence .....
4.1 Abstract 75
4.2 Introduction 75
4.3 Available models for calculatIon OF the critical salt concentration 77
4.4 Uncertainty analysis of numerical values for Hamaker constants for water films between air bubbles 79
4.5 Validation of the availble models using the corrected values for Hamaker constants 83
4.6 Conclusion 85
Acknowledgements 85
References 86
Chapter 5: A Novel Methodology For Predicting Critical Salt Concentration Of Bubble Coalescence Inhibition .....
5.1 Abstract 89
5.2 Introduction 89
5.3 Model development 92
5.4 Further Evaluations and applications 95
5.5 conclusions 101
Acknowledgements 101
References 102
Chapter 6: Critical Salt Concentration In Bubble Coalescence Inhibition: Effect Of Dissolved Gases And Hydrophobic Attraction .....
6.1 Abstract 106
6.2 Introduction 106
6.3 Theoretical analysis 108
6.5.1 Prediction of critical salt concentration 108
6.5.2 Van der Waals force 112
6.5.3 Hydrophobic force 112
6.4 Experimental method 113
6.5 Results and discussion 114
6.5.1 Experimental results 114
6.5.2 Effect of van der Waals attractions 117
6.5.3 Effect of hydrophobic attractions 118
6.5.4 Effect of gas solubility 123
6.6 Conclusion 127
Acknowledgements 128
references 128
Chapter 7: Conclusions and Recommendations .....
7.1 Conclusions 133
7.2 Recommendations for future work 135
Appendices .....
A1. Appendix 1 138
A1.1. Procedure for determining the thickness of foam films 138
A2. Appendix 2 144
A2.1. Model development for determining the critical salt concentration and film thickness 144

A3. Appendix 3 148
A3.1. Surface tension gradient with salt concentration of salts 148
A3.2. Average salting-coefficient of salts 150

List of Figures

Chapter 2……...

Figure 2.1. Sequence of events for formation and thinning of an intervening liquid film between two bubbles (foam film)..... 11

Figure 2.2. Schematic of a bubble column setup to study bubble coalescence in solutions (Nguyen et al., 2012). 16

Figure 2.3. An illustration of salt transition concentration determined at 50% percentage coalescence of bubble population. 17

Figure 2.4. An illustration of salt (KCl) transition concentration determined as the minimum concentration at constant (average) bubble size verses salt concentration (data are taken from (Marrucci and Nicodemo, 1967))..... 17

Figure 2.5. The *CCC95* of salts based on fitting an exponential model to the Sauter mean diameter (D_{32}) and salt concentration data (Quinn et al., 2014b). 19

Figure 2.6. Images of the bubble pair experiment using adjacent capillaries (a) placed side by side (Christenson et al., 2007) (b) facing each other (Tse et al., 1998)..... 20

Figure 2.7. Bubble pair experiments in (a) pure water (b) a high salt concentration solution (Christenson et al., 2007). 21

Figure 2.8. Percentage coalescence of bubbles versus salt concentration for $LaCl_3$ (open squares), $MgSO_4$ (open diamonds), $CaCl_2$ (open triangles) and NaCl (open circles) using adjacent capillaries (bubble pair) method (Christenson et al., 2007). 22

Figure 2.9. Schematic of the bubble-meniscus experiment (Del Castillo et al., 2011)..... 22

Figure 2.10. Experimental interferometric setup with the Scheludko cell (Manev and Nguyen, 2005b). 23

Figure 2.11. Average lifetime of liquid films of aqueous NaCl solutions at interface approach speed of 10 µm/s versus NaCl concentration..... 25

Figure 2.12. Comparison of percentage coalescence of bubbles in NaCl solutions conducted by different experimental techniques..... 27

Figure 2.13. Transition concentration (*TC95*) of NaCl shown in Table 2.2 (points) versus the bubble size. The result from (Quinn et al., 2014b) is excluded. Correlation coefficient of the trend line is equal to 0.92..... 28

Figure 2.14. Drainage of a liquid film of 0.19 M KCl solution between two bubbles. Solid and dashed lines represent the drainage rate predictions with no-slip and fully slip boundary conditions, respectively. The film radius is R_f = 54 µm. 34

Figure 2.15. A typical ordering of cations and anions in Hofmeister series (Kunz, 2009)..... 36

Figure 2.16. Division of group IA cations and VIIA halide anions into kosmotropes and chaotropes (Collins, 1997). The circles show proportional size of the ions. 36
Figure 2.17. Snapshots from molecular dynamics simulations (side and top view of the slabs) and density profiles (i.e., histogramed densities of the electrolyte ions and water molecules in layers parallel to the surface from the centre of the slab across the interface into the gas phase) for 1.2 M aqueous sodium halide salts (Jungwirth and Tobias, 2005)..... 39
Figure 2.18. Comparison of predictions of models proposed by Marrucci (1969) and Prince & Blanch (1990) with the experimental results for the transition concentration (the dotted line represents a perfect match with experimental data) (Prince and Blanch, 1990)..... 41
Figure 2.19. Comparison of the experimental results (Lessard and Zieminski, 1971; Marrucci and Nicodemo, 1967) with the models proposed by Marrucci (1969) and Prince & Blanch (1990) employing the corrected values of Hamaker constants (Firouzi and Nguyen, 2014b). The dotted line represents a perfect match with experimental data. 42
Chapter 3…….
Figure 3.1. Schematic of experimental micro-interferometric setup (Karakashev et al., 2008)..... 53
Figure 3.2. Evolution of 2 M NaCl foam films drainage at an interface approach speed of 10 µm/s (top) and zero approach speed (bottom). 55
Figure 3.3. Significant differences in transient thickness and radius of 2 M NaCl films obtained at interface approach speed of *u* = 10 µm/s and zero interface approach speed..... 56
Figure 3.4. Effect of air-liquid interface approach speed on the film surface morphology for 0.15M NaCl at 100 µm/s (top) and 10 µm/s (bottom)..... 58
Figure 3.5. Effect of air-liquid interface approach speed on the surface morphology of 0.15 M NaCl films at *u* = 100 and 10 µm/s. 59
Figure 3.6. Effect of air-liquid interfacial approach speed on the lifetime of foam films of pure water. 60
Figure 3.7.Comparision of lifetimes of DI water films and halid salt films at (0.01 M) and high (1 M) salt concentrations..... 61
Figure 3.8. Effect of monovalent halide anions and alkali cations on the film lifetime at *u* = 100 and 20 µm/s..... 63
Figure 3.9. Effect of bubble approach velocity on the critical concentration of salts..... 64
Figure 3.10. Disjoining pressures for pure DI water (equivalent to 4µM solution because of CO2 dissolved from the atmosphere) films and 0.01M monovalence salt films, showing significant reductions of DLVO colloidal pressures..... 66
Figure 3.11. Total specific adsorption energy of investigated salts at air-solution interface versus their critical concentrations..... 68

Figure 3.12. Film lifetime (blue) and solution viscosity (red) of LiCl (dotted lines) and KCl (solid lines) vs. salt concentration at u = 10 μm/s. The viscosity data are taken from (Desnoyers and Perron, 1972). 70

Chapter 4……..

Figure 4.1. Numerical results (points) and its short-ranged (non-retarded) limit (green dashed line) and long-ranged (retarded) limit (red solid line) for the van der Waals interaction energy versus film thickness. The black dotted line shows the energy predicted by Prince and Blanch with B=1.5 × 10^{-28} J · m 81

Figure 4.2. Dependence of the retarded Hamaker constant *B* on salt concentration 83

Figure 4.3. Comparison of the experimental results (Lessard and Zieminski, 1971; Marrucci and Nicodemo, 1967) with Marrucci's model described by Eq. (4.2) with with A = 3.979 × 10^{-20} J , and Prince and Blanch's model described by Eq. (4.3) with B = 3.492 × 10^{-29} J.m (Table 2). 85

Chapter 5……..

Figure 5.1. Variation of balance of pressure as described by the left hand side of Eq. (5.4) versus film thickness at three characteristic salt concentrations, i.e., small concentration ($C < C_{cr}$), high concentration ($C > C_{cr}$) and critical concentration ($C = C_{cr}$). The model parameters include: $R = 0.001$ m , $\nu = 2$, $\Pi(h) = -10000 \times \exp(-h/10)$ [Pa] , $C_{cr} = 0.000629$ M $T = 293$ K , $\sigma = 0.072$ N and $\partial\sigma / \partial C = 0.001\ \mathrm{N \cdot m^{-1} \cdot M^{-1}}$ 93

Figure 5.2. Zeta potential of air-NaCl interface versus NaCl concentration. 99

Figure 5.3. Surface tension of NaCl solutions versus concentration up to saturation at 23 ºC (Ozdemir et al., 2009)..... 100

Chapter 6……..

Figure 6.1. Surface tension of monovalent salts versus salt concentration at 20 °C . Data are taken from (Aveyard and Saleem, 1976; Matubayasi et al., 2001). 110

Figure 6.2. Film thickness profile of LiCl 0.125 M at different times and the suction rate of 100 nL/s. 117

Figure 6.3. Transient profiles of film thickness of 0.195 M NaBr solution at suction rates of 100, 120 and 200 nL/s. 117

Figure 6.4. Comparison of the theoretical critical concentrations by considering the long-ranged retarded Casimir-van der Waals attraction $(H = 3.492 \times 10^{-29}\ \mathrm{J.m})$ with the experimental results (Karakashev et al., 2008; Lessard and Zieminski, 1971) (the dashed line represents a perfect match with experimental data)..... 119

Figure 6.5. Comparison of the experimental (filled circles) and the theoretical (empty symbols) critical salt concentration and film thickness versus *K* using the available hydrophobic strengths and decay lengths (1989)·(2009). 121

Figure 6.6. Predicted hydrophobic strength and decay length using the experimental results for h_{cr} and C_{cr} 123

Figure 6.7. Comparison of the theoretical and experimental critical salt concentration of this work and the literature (Karakashev et al., 2008; Lessard and Zieminski, 1971) (the dashed line represents a perfect match with experimental data). 123

Figure 6.8. Change of partial molar volume of salts at infinite dilution and hydrophobic strength with *K*. The partial molar volume data are taken from (Millero, 1972)..... 126

Figure 6.9. Predicted hydrophobic strength and pressure versus gas (oxygen) solubility in salt solutions at critical salt concentrations. 128

Appendices ……...

Figure A1.1.Light intensity and film thickness profile of a dimpled foam film……139

Figure A1.2. Image processing procedure to find the light intensity profile on one strip…..……140

Figure A1.3. Light intensity profile versus radial location for the line shown in Figure A1.2…….141

Figure A1.4. The rotated image to determine the light intensity profile, $\theta = 30^{\circ}$ ……142

Figure A1.5. Light intensity and film thickness profiles of 180 lines, the angular interval = 1º (the red line, represents the average film thickness)……..……..……142

Figure A1.6. Sequential interferograms of a foam film……..……...……143

Figure A1.7. Temporal profile of (a) light intensity and (b) film thickness of a foam film……144

Figure A2.1.Schematic of a liquid film in the film holder in the Scheludko-Exerowa cell……..…..145

List of Tables

Chapter 2…….

Table 2.1. Comparison of transition concentrations (M) of common salts using different techniques. 26

Table 2.2. Bubble radius and the *TC95* of NaCl determined based on the data available in the literature for aqueous NaCl solutions..... 28

Table 2.3. Combining rule for bubble coalescence inhibition in aqueous salt solutions (Henry et al., 2006). 37

Chapter 3…….

Table 3.1. Entropy of hydration and radius of alkali metal and halide ions of interest (Marcus, 1997) 67

Chapter 4…….

Table 4.1. Summary of experimental results (Lessard and Zieminski, 1971; Marrucci and Nicodemo, 1967) and model prediction by fitting with $B = 1.5 \times 10^{-28}\,\mathrm{J \cdot m}$ (Prince and Blanch, 1990) for salts critical concentration. 79

Table 4.2. Summary of results for salts critical concentration as calculated using Eqs. (2) and (3) and the corrected values for the Hamaker constants, and the experimental conditions given in Table 4.1. 84

Chapter 6……..

Table 6.1. Critical concentrations and rupture thicknesses of the saline water films at their critical concentrations at u = 10 μm/s. 118

Appendices ……...

Table A3.1. Average surface tension gradient with respect to the salt concentration …….149

Table A3.2. Average salting-effect coefficient, K_s of different salts at $T = 25\,^{\circ}\mathrm{C}$ and $P = 1\,\mathrm{bar}$ ….150

CHAPTER 1

INTRODUCTION

1.1 BACKGROUND TO THE RESEARCH

Thin liquid films (TLFs) have been the subject of many studies. TLFs are the fundamental element of various colloidal disperse systems including foam films (liquid films between two bubbles), emulsion films (liquid films between two droplets) and wetting films (liquid films between bubbles and solid surfaces). These intervening liquid films have a decisive role in a variety of chemical and biological applications and processes ranging from emulsion systems of food or pharmaceutical products to gas dispersion systems found in chemical reactors (Prud'homme and Khan, 1996). Thin liquid films are also important in froth flotation, in treatment and purification of waste water and de-inking of wastepaper. The efficiency of products is controlled by the stability/instability of intervening liquid films and understanding the behaviour of TLFs is critical to these processes (Manev and Nguyen, 2005).

It is well known that surfactant adsorption at the film surface plays a critical role in stability of TLFs. Many works have been done on investigating the influence of surface properties, the type and concentration of surfactants on the drainage and stability of TLFs (Karakashev et al., 2010; Radoev et al., 1974; Ruckenstein and Sharma, 1987; Valkovska and Danov, 2001). Therefore surfactant – laden films are well understood (Craig, 2004).

In addition to surfactants, salts are believed to significantly affect the stability of foam liquid films and thereby the performance of their applications (Harvey et al., 2002; Paulson and Pugh, 1996). Salt's effect on TLFs has been investigated experimentally but relatively limited research has been done both theoretically and experimentally in this field and it is still poorly understood (Kunz et al., 2004).

Some salts are believed to inhibit bubble coalescence above a specific concentration called the transition concentration. The idea of the stabilizing effect of common salts such as NaCl at concentrations above a critical (transition) concentration on bubble coalescence has stemmed from the comparison of foaminess of the ocean with fresh water. The inhibiting effect of salts on bubble coalescence or stability of foam films has been experimentally investigated utilizing different techniques. These techniques include monitoring bubble population by measuring the solution turbidity in a bubble column (Craig et al., 1993; Marrucci and Nicodemo, 1967; Nguyen et al., 2012), contacting a pair of bubbles and determining the coalescence percentage by counting the number of coalescing bubbles (Christenson et al., 2007; Kirkpatrick and Lockett, 1974; Lessard and Zieminski, 1971) and measuring the lifetime of TLFs of salt solutions between bubbles using an optical interferometric method. The first technique reflects the real flow condition and delivers some

macroscopic information on the effect of salts on bubble coalescence. The other two techniques especially the third one provides microscopic information on the mechanisms responsible for the stability of liquid films in the presence of inhibiting salts. There are few studies on the effect of salts on a single liquid film, however the focus of the majority of the available work is either on the concentration or type of electrolytes at (un-quantified and unknown) interface approach speeds (Christenson et al., 2007; Karakashev et al., 2008; Lessard and Zieminski, 1971), or on the air-solution interface approach speeds but with a single salt (mainly NaCl) (Del Castillo et al., 2011; Wang and Qu, 2012; Yaminsky et al., 2010).

Despite the extensive experimental investigation of the effect of salts on bubble coalescence, there are few models available in the literature (Chan and Tsang, 2005; Marrucci, 1969; Prince and Blanch, 1990) to theoretically describe this complex phenomenon. Although all of these theoretical models follow the same approach proposed by Maruucci (1969), there is no unique and theoretically consistent method to explain the behaviour of saline liquid films. Moreover, there are some uncertainties in the modified models proposed by (Chan and Tsang, 2005; Prince and Blanch, 1990) associated with the values of the Hamaker constants and physics of the models to describe the transition in the behaviour of liquid films in the presence of different salts. Therefore a comprehensive model to describe the stabilizing effect of salts is lacking.

This work aims to illuminate the mechanisms behind the intricate behaviour of saline liquid films. This thesis is composed of published and submitted papers beginning with a review of the literature (chapter 2) concerned with the key parameters and developments in investigation of the inhibiting effect of salts on bubble coalescence both experimentally and theoretically. The focus of chapter 3 is a systematic study on the effect of monovalent anions (F^-, Cl^-, Br^- and I^-) and cations (Li^+, Na^+ and K^+) in a vast range of concentration at different air-interface approach speeds employing an optical interferometric technique. Drainage of liquid films under zero and non-zero interface approach speeds was investigated in terms of drainage rate (temporal thickness profile) and growth rate (temporal radius profile). A MATLAB program was developed for image processing of the recorded interferograms for quantification and off-line analysis.

To develop insight into the mechanisms underlying the effect of salts on bubble coalescence, coalescence of bubbles was also theoretically investigated. In chapter 4 the available models were reviewed and scrutinized for uncertainties. It was shown that none of the available models can predict experimental critical salt concentrations correctly. To modify the models a novel methodology was proposed in chapter 5. The generality of the methodology was validated by applying the theory to the

previous models. Having a generic and consistent method, the models were modified in chapter 6 by incorporating hydrophobic attractions.

1.2 RESEARCH AIMS AND OBJECTIVES

The overall objective of this research program is to investigate the effect of salts on bubble coalescence.

The specific objectives are:

i. To characterise effects of salt ions at different concentrations on the stability of aqueous liquid films at different interface approach speeds.
ii. To evaluate the effect of applied interface speed as an external force on the lifetime and drainage of liquid films of salt solutions.
iii. To understand the mechanisms by which the observed transition in the behaviour of saline liquid films takes place.
iv. To identify the specific ion effect on bubble coalescence and lifetime of foam liquid films.
v. To evaluate the role of colloidal forces specifically van der Waals and hydrophobic attractions on the stability of saline liquid films.
vi. To modify the theoretical models to predict the critical salt concentration.

1.3 HYPOTHESES

Based on a review of the findings available in the current literature and the stated research objectives the following hypotheses are proposed.

i. Inhibiting effect of salts depends on the salt type, concentration and the air-liquid interface approach speed.
ii. Change in the hydrodynamic boundary condition of air-solution interface from mobile to immobile at the critical salt concentration is the main mechanism underlying the inhibiting effect of salts on bubble coalescence.
iii. Van der Waals attractions cannot be responsible for the rupture of the liquid film between two bubbles and stronger attractions in terms of strength and length scale are required.
iv. Electrostatic double layer repulsions are too weak to influence bubble coalescence in the range of critical salt concentration and film thickness.
v. Salts affect bubble coalescence via hydrophobic attractions and disturbing air-water interfaces by reducing concentration of dissolved gasses in salt solutions.

1.4 STATEMENT OF ORIGINALITY

This thesis has not been submitted for a degree in any University, and does not contain material published by another person. The original contributions of this thesis are outlined briefly below:

- A comprehensive and systematic study of the effect of monovalent anions and cations at different concentrations and bubble (air-water interface) approach speeds was precisely carried out on a single liquid film between two bubbles. Drainage of saline liquid films was also investigated under zero and non-zero air-liquid interface approach speeds as an external driving force. The experimental observations for the critical salt concentration and lifetime of liquid film of salt solutions contributed an understanding of the ion-specific effect on bubble coalescence.
- Non-retarded and retarded Hamaker constants of an intervening liquid film between bubbles in pure water and salt solutions were accurately determined by applying the Lifshitz theory on the van der Waals interaction energy and the available spectrum for water dielectric permittivity. Having obtained the Hamaker constants, it was demonstrated that van der Waals attractions as the only disjoining pressures are not sufficient enough to balance the opposing forces due to the Marangoni stress to predict the critical salt concentration and film thickness correctly.
- A novel methodology was proposed for determining the critical salt concentration and film thickness which resolves the mathematical uncertainties in the previous models. This generic approach was successfully validated by applying the method to the available models. This novel approach allows us to examine the influence of any relevant complicated disjoining pressures with non-linear equations.
- The available models were modified incorporating hydrophobic attractions implementing the suggested model by Eriksson et al. (1989) for the hydrophobic force. The parameters including the hydrophobic strength and decay length for evaluating hydrophobic attractions were determined by employing the experimental data for critical concentration and film thickness of salt solutions. An empirical correlation was proposed for the hydrophobic strength of different salts as a function of salting-effect coefficient of salts, K_s which indicates the effect of salts on gas solubility. It was also theoretically demonstrated that the hydrophobic strength of salts increases with increasing the surface hydrophobicity through the effect of dissolved gasses.

1.5 STRUCTURE OF THE THESIS

This thesis has been structured following the format of chapters composed of published or submitted papers. Chapter 1 presents the background to the research, aims and hypotheses, statement of originality and structure of the thesis. Chapter 2 presents a quantitative review of the key factors affecting foam liquid films of salt solutions, the experimental techniques and proposed mechanisms by which salts influence the stability of liquid films (Mahshid Firouzi, Tony Howes and Anh Nguyen, A Quantitative review of the transition salt concentration for inhibiting bubble coalescence, Accepted in Advances in Colloid and Interface Science, July 2014). Chapters 3 to 6 are the candidates own research papers. Chapter 3 presents an inclusive and systematic investigation of the effect of monovalent salts on the drainage and lifetime of liquid films at different bubble approach speeds (Mahshid Firouzi and Anh V. Nguyen, Effects of monovalent anions and cations on drainage and lifetime of foam films at different interfacial approach speeds, Accepted in Advanced Powder Technology, June 2014). Chapter 4 deals with determining the Hamaker constants using the Lifshitz theory to resolve uncertainties in the available models for predicting the critical salt concentration (Mahshid Firouzi and Anh V. Nguyen, On the effect of van der Waals attractions on the critical salt concentration for inhibiting bubble coalescence, Minerals Engineering, 2014, 58:108-112). Chapter 5 focuses on proposing a generic methodology to model saline liquid films to predict the critical salt concentration and film thickness (Mahshid Firouzi and Anh V. Nguyen, A novel methodology for predicting critical salt concentration of bubble coalescence inhibition, The Journal of Physical chemistry C, 2014, 118:1021-1026). Chapter 6 employs the novel methodology proposed in the previous chapter to modify the available models by incorporating hydrophobic attractions and the influence of dissolved gasses (Mahshid Firouzi and Anh V. Nguyen. Critical salt concentration of bubble coalescence inhibition: effect of dissolved gases and hydrophobic attraction, Submitted to The Journal of Physical Chemistry C). Chapter 7 comprises the concluding chapter and includes recommendations for future research.

REFERENCES

Chan, B.S., Tsang, Y.H., A theory on bubble-size dependence of the critical electrolyte concentration for inhibition of coalescence. Journal of Colloid and Interface Science, 2005, **286(1)**, 410-413.

Christenson, H.K., Bowen, R.E., Carlton, J.A., Denne, J.R.M., Lu, Y., Electrolytes that Show a Transition to Bubble Coalescence Inhibition at High Concentrations. The Journal of Physical Chemistry C, 2007, **112(3)**, 794-796.

Craig, V.S.J., Bubble coalescence and specific-ion effects. Current Opinion in Colloid and Interface Science, 2004, **9(1-2)**, 178-184.

Craig, V.S.J., Ninham, B.W., Pashley, R.M., Effect of electrolytes on bubble coalescence. Nature, 1993, **364(6435)**, 317-319.

Del Castillo, L.A., Ohnishi, S., Horn, R.G., Inhibition of bubble coalescence: Effects of salt concentration and speed of approach. Journal of Colloid and Interface Science, 2011, **356(1)**, 316-324.

Eriksson, J.C., Ljunggren, S., Claesson, P.M., A phenomenological theory of long-range hydrophobic attraction forces based on a square-gradient variational approach. Journal of the Chemical Society, Faraday Transactions 2: Molecular and Chemical Physics, 1989, **85(3)**, 163-176.

Harvey, P.A., Nguyen, A.V., Evans, G.M., Influence of electrical double-layer interaction on coal flotation. Journal of Colloid and Interface Science, 2002, **250(2)**, 337-343.

Karakashev, S.I., Ivanova, D.S., Angarska, Z.K., Manev, E.D., Tsekov, R., Radoev, B., Slavchov, R., Nguyen, A.V., Comparative validation of the analytical models for the Marangoni effect on foam film drainage. Colloids and Surfaces A: Physicochemical and Engineering Aspects, 2010, **365(1–3)**, 122-136.

Karakashev, S.I., Nguyen, P.T., Tsekov, R., Hampton, M.A., Nguyen, A.V., Anomalous ion effects on rupture and lifetime of aqueous foam films formed from monovalent salt solutions up to saturation concentration. Langmuir, 2008, **24(20)**, 11587-11591.

Kirkpatrick, R.D., Lockett, M.J., The influence of approach velocity on bubble coalescence. Chemical Engineering Science, 1974, **29(12)**, 2363-2373.

Kunz, W., Lo Nostro, P., Ninham, B.W., The present state of affairs with Hofmeister effects. Current Opinion in Colloid & Interface Science, 2004, **9(1–2)**, 1-18.

Lessard, R.R., Zieminski, S.A., Bubble coalescence and gas transfer in aqueous electrolytic solutions. Ind. Eng. Chem. Fun., 1971, **10(2)**, 260-269.

Manev, E.D., Nguyen, A.V., Critical thickness of microscopic thin liquid films. Advances in Colloid and Interface Science, 2005, **114–115(0)**, 133-146.

Marrucci, G., A theory of coalescence. Chemical Engineering Science, 1969, **24(6)**, 975-985.

Marrucci, G., Nicodemo, L., Coalescence of gas bubbles in aqueous solutions of inorganic electrolytes. Chem. Eng. Sci., 1967, **22(9)**, 1257-1265.

Nguyen, P.T., Hampton, M.A., Nguyen, A.V., Birkett, G., The influence of gas velocity, salt type and concnetration on transition concentration for bubble coalescence inhibition and gas holdup. Chemical Engineering Science, 2012, **90**, 33-39.

Paulson, O., Pugh, R.J., Flotation of Inherently Hydrophobic Particles in Aqueous Solutions of Inorganic Electrolytes. Langmuir, 1996, **12(20)**, 4808-4813.

Prince, M.J., Blanch, H.W., Transition electrolyte concentrations for bubble coalescence. AIChE Journal, 1990, **36(9)**, 1425-1429.

Prud'homme, R., Khan, S.A.E., *Foams:Measurements and Applications*. 1996, Marcel Dekker,New York, NY.

Radoev, B.P., Dimitrov, D.S., Ivanov, I.B., Hydrodynamics of thin liquid films effect of the surfactant on the rate of thinning. Colloid and Polymer Science, 1974, **252(1)**, 50-55.

Ruckenstein, E., Sharma, A., A new mechanism of film thinning: Enhancement of reynolds' velocity by surface waves. Journal of Colloid and Interface Science, 1987, **119(1)**, 1-13.

Valkovska, D.S., Danov, K.D., Influence of ionic surfactants on the drainage velocity of thin liquid films. Journal of Colloid and Interface Science, 2001, **241(2)**, 400-412.

Wang, L., Qu, X., Impact of interface approach velocity on bubble coalescence. Minerals Engineering, 2012, **26(0)**, 50-56.

Yaminsky, V.V., Ohnishi, S., Vogler, E.A., Horn, R.G., Stability of aqueous films between bubbles. Part 1. the effect of speed on bubble coalescence in purified water and simple electrolyte solutions. Langmuir, 2010, **26(11)**, 8061-8074.

CHAPTER 2

A QUANTITATIVE REVIEW OF THE TRANSITION SALT CONCENTRATION FOR INHIBITING BUBBLE COALESCENCE

Mahshid Firouzi, Tony Howes and Anh V. Nguyen

Published in “Advances in Colloid and Interface Science”, July 2014, DOI: 10.1016/j.cis.2014.07.005

2.1 ABSTRACT

Some salts have been proven to inhibit bubble coalescnce above a certain concentration called the transition concentration. The transition concentration of salts has been investigated and determined by using different techniques. Different machanisms have also been proposed to explain the stabilising effect of salts on bubble coalescence. However, as yet there is no consensus on a mechanism which can explain the stabilizing effect of all inhibiting salts. This paper critically reviews the experimental techniques and mechanisms for the coalescence of bubbles in saline solutions. The transition concentrations of NaCl, as the most popularly used salt, determined by using different techniques such as bubble swarm, bubble pairs, thin liquid film micro-interferometry were analysed and compared. For a consistant comparison the concept of *TC95* was defined as a salt concentration at which the "percentage coalescnce" of bubbles reduces by 95% relative to the highest (100% in pure water) and lowest (in high salt concentration) levels. The results show a linear relationship between the *TC95* of NaCl and the reciprocal of the square root of the bubble radius. This relationship holds despite different experimental techniques, salt purities and bubble approach speeds, and highlights the importance of the bubble size in bubble coalescence. The available theoretical models for inhibiting effect of salts have also been reviewed. The failure of these models in predicting the salt transitions concentration commands further theoretical development for a better understanding of bubble coalescence in salt solutions.

Keywords: Salts, transition concentration, colloidal forces, ion-specific, air-water interface

2.2 INTRODUCTION

Bubble coalescence and stability/instability of the liquid film between two bubbles known as a foam film are central to many areas such as surface and colloid chemistry, biology, biochemistry, tertiary oil recovery, foam fractionation, food industry and mineral flotation. Foam stability is controlled by thinning and rupture of the intervening liquid film between air bubbles (Nguyen and Schulze, 2004). The overall process of formation and thinning of a liquid film can be conveniently divided into a number of stages as illustrated in Figure 2.1: They include (a) approaching two bubbles (b) hydrodynamic interaction between approaching bubbles which can cause deformation on bubbles surfaces, called the "dimple" (c) formation of a plane-parallel film by gradual disappearance of the dimples and (d) coalescence of bubbles if attractive pressures overcome negative pressures along the

film surface. The thin liquid film formed between two approaching bubbles initially thins under the influence of the capillary pressure. This capillary pressure arises from the curvature of bubbles and for a small film with a negligible contact angle is defined as $P_\sigma = 2\sigma / R$ where σ is the surface tension and R is the radius of curvature (Manev and Nguyen, 2005a). When the film thickness reduces to 300-200 nm, film drainage owing to the capillary pressure is slowed down and interactions between the film surfaces called the disjoining pressure start affecting the film drainage (Stubenrauch and Klitzing, 2003; Yaminsky et al., 2010). Depending on the balance of the capillary pressure and disjoining pressures, if the film drainage takes longer than the bubbles' contact time, the liquid film is considered to be stable and coalescence does not take place. Otherwise the liquid film between bubbles ruptures at a critical thickness within the range of 200-10 nm, depending on the concentration of chemicals (surfactants or salts), surface impurities and bubble approach speed (Horn et al., 2011; Oolman and Blanch, 1986).

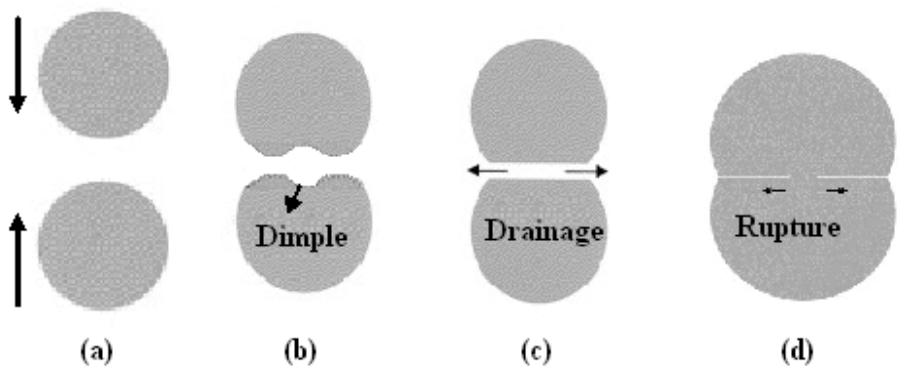

Figure 2.1. Sequence of events for formation and thinning of an intervening liquid film between two bubbles (foam film).

Salts and surfactants influence bubble coalescence by changing the intermolecular forces and surface rheology of liquid films between bubbles. For the case of surfactant-laden films this is relatively well understood (Craig, 2004; Craig et al., 1993a). Saline liquid films have been investigated experimentally but relative to surfactant-laden films, limited work has been done both theoretically and experimentally in this field and is not yet well understood (Kunz et al., 2004). This study reviews the coalescence of bubbles in saline solutions with the focus on mechanisms under

which salts can inhibit bubble coalescence at concentrations above a critical concentration, called the transition concentration.

This review paper was structured as follows. First the background of bubble coalescence in salt solutions is reviewed in section 2. The next section is devoted to a brief review of the experimental techniques followed by a comparison of different methods for determining the transition concentration of common salts. Proposed explanations for the stabilising effect of salts are discussed in section 2.5. Section 2.6 presents a review on the available theoretical models for predicting the transition concentration of salts. A summary and conclusion based on the findings of the reviewed papers are presented in section 2.7.

2.3 EFFECT OF SALTS ON BUBBLE COALESCENCE

It has been known for many years that salts influence bubble coalescence and the stability of thin liquid films (TLFs) between bubbles. The effect of salts on bubble coalescence and TLFs has been investigated experimentally and theoretically (Craig et al., 1993a; Foulk, 1929; Foulk and Hansley, 1932; Foulk and Miller, 1931; Marrucci, 1969; Marrucci and Nicodemo, 1967; Prince and Blanch, 1990). In one study a theory of thin liquid formation was developed (Foulk, 1929; Foulk and Hansley, 1932; Foulk and Miller, 1931) and the effect of salts on bubble coalescence was examined by means of a foam meter and by contacting a pair of bubbles. The results of contacting pairs of bubbles were recorded as “percentage of film formation”, which was defined as the number of times in a hundred that bubbles failed to coalesce and hence liquid films formed. This work showed that bubbles in pure water coalesce spontaneously on contact, and in the presence of salts the percentage of film formation increased and gradually approached 100% with increasing salt concentration. Surface adsorption of the solute and the difference between dynamic and static surface tension were identified as major contributing factors for the formation of foam in salt solutions at specific concentrations. Later, in a systematic study of the effect of salts on the gas holdup and bubble size in a bubble column (Marrucci and Nicodemo,1967), it was observed that increasing the gas flow rate resulted in bubbles with smaller mean diameters. Increasing the salt concentration led to a monotonic decrease in bubble size which asymptotically tended to a constant diameter of 0.41 mm. In addition the concentration at which the bubble size approached the asymptote was different for different salts. The inhibiting effect of salts was related to their valence and the surface tension gradient with respect to salt concentration.

A quantitative study (Lessard and Zieminski,1971) on the effect of different salts and their concentration on coalescence of bubble pairs determined the percentage of the coalescing pairs which, in pure water (double-distilled water), was considered as 100%. A sharp decrease in the percentage of coalescing bubbles at a specific concentration, called the transition concentration, was observed and this transition concentration was found to be unique for each salt. The inhibiting effect of salts was explained on the basis of ion-water interactions. It was argued that ions retard the liquid film drainage and consequently the coalescence of bubbles by affecting the hydrogen bond. A subsequent study (Craig et al., 1993a) determined the transition concentration of an extensive range of salts by focusing on a swarm of bubbles rather than individual bubble-bubble interactions, and also studied the effect of gas flow rate on the transition concentration of NaCl. The transition concentration was found to be independent of the gas flow rate. The effect of gas flow rate in terms of superficial velocity (defined as the gas flow rate per cross-sectional area) was further investigated (Nguyen et al., 2012) for more salt types (NaCl, NaF, NaBr, NaI and CsCl) in a bubble column. These results revealed a significant influence of the gas superficial velocity on the transition concentration of NaI but not on the other investigated salts.

The effect of bubble approach speed on coalescence of bubbles was investigated by measuring the contact time of a bubble of 5 mm diameter rising towards an air-water interface by employing high speed photography (Kirkpatrick and Lockett, 1974). The bubble approach speed was varied by changing the release height of the bubble from the interface. Instant bubble coalescence was observed in distilled and tap water as well as low concentration NaCl solutions at approach speeds less than 1 cm/s. A significant increase in the coalescence time at approach speeds greater than 10 cm/s was observed. This increase was attributed to the bouncing of bubbles, and these critical speeds were found to be specific to the bubble size. In the case of high concentration NaCl solutions (0.6 M) the coalescence times were considerably longer (typically ~ 0.7 s) and found to be independent of the bubble approach speed due to the inhibiting effect of NaCl at this concentration. The effect of bubble approach speed on bubble coalescence in water and NaCl solutions (0.037 and 0.111 M) was investigated (Ribeiro and Mewes, 2007) with the focus on finding the critical speed beyond which bubbles bounce apart. Regardless of the salt concentration, the critical speed was found to decrease with the bubble size for bubble equivalent diameters less than 2.3 mm. For bubbles larger than 2.3 mm in diameter, the critical speed reached a constant value which decreased with increasing the salt concentration.

Drainage and rupture of salt solution liquid films, which usually occurs very rapidly relative to surfactant-laden films, were investigated quantitatively (Cain and Lee, 1985). The changes in film thickness, diameter and lifetime of liquid films of 0.5 and 1 M KCl solutions between two captive air bubbles were simultaneously measured by using an interferometric method. The results showed that the drainage and rupture of these liquid films took 600 and 420 ms respectively. It was also noticed that films could not be formed for 0.1 M KCl solutions, which is below the transition concentration of KCl. Liquid films of salt solutions (NaCl, NaAc, $NaClO_3$ and LiCl) were further investigated (] Karakashev et al., 2008) using an interferometric method to determine the drainage rate, lifetime and transition concentration of liquid films between two bubbles, but it did not explicitly focus on the importance of bubble approach speed. In another experimental study (Yaminsky et al., 2010) the effect of bubble approach speed on the stability of liquid films of deionised (DI) water and NaCl solutions was investigated. Depending on bubble approach speed, three different regimes including stable and transient films and instant coalescence were observed for TLFs of DI water between two bubbles. The behaviour of surfactant-free films at different bubble approach speeds was explained based on surface forces and the Gibbs-Marangoni effect.

Some other studies have also been conducted on the effect of salts on foam liquid films by using different techniques, with the focus on the effects of either salt type or concentration at an un-quantified bubble approach speed, or on the effects of bubble approach speed using a single salt (Christenson et al., 2007; Del Castillo et al., 2011; Henry et al., 2009; Wang and Qu, 2012; Weissenborn and Pugh, 1996). Recently a systematic study considering the combined effects of salt concentration, interface approach speed and salt type on the lifetime, thinning rate (change of the film thickness) and growth rate (change of the radius) of the liquid films of salt solutions was reported (Firouzi and Nguyen, 2014a). The experimental results of the effect of monovalent anions (I^-, Br^-, Cl^- and F^-) and cations (Li^+, Na^+ and K^+) on the lifetime of liquid films showed that film lifetime decreased according to salt type following the order NaF>LiCl>NaCl>KCl>NaBr>NaI. Lifetimes of liquid films for each salt decreased compared to liquid films of DI water upon addition of salt up to a specific concentration. Any further increase in salt concentration resulted in an abrupt increase in the film lifetime for each salt. The specific concentration of salts, called the transition concentration, of salts followed the reverse order of that for film lifetime, and it was shown that the transition concentration was independent of bubble approach speed in the investigated range of 10-300 µm/s. At higher interface approach speeds, the liquid film increased in area and diameter faster than when

they approached at slower speeds. Surface corrugations were observed at higher bubble approach speeds which resulted in a faster rupture of liquid films.

2.4 EXPERIMENTAL TECHNIQUES

There are different techniques for studying the effect of salts on bubble coalescence and determining the transition concentration of salts. The following provides details of the experimental techniques available in the literature.

2.4.1 BUBBLE COLUMN

The experimental setup depicted in Figure 2.2 consists of a cylindrical column or sometimes a square-section column to minimize the light distortion. Gas bubbles are produced in the column containing water or salt solutions by sparging the gas (mainly N_2) from a gas distributer through a porous plate/frit. The porous frit is mounted at the base of the column and the gas flow sweeps any possible surface contamination to the top of the cell which is one of the advantages of this setup. By varying the porosity of the frit, different bubble sizes can be created. An expanded beam of light is passed through the column, condensed by a condensing lens and detected by a photosensor which is connected to a computer. The change in the detected light intensity owing to the change in the turbidity of solutions determines the effect of different salt solutions on bubble coalescence. Assuming 100% bubble coalescence in clean DI water with the lowest turbidity and 0% for high salt concentrations, the "percentage coalescence" of bubbles can be determined from the measured turbidity. Inhibiting salts retard bubble coalescence at salt concentrations above the transition concentration. The inhibition of bubble coalescence results in an increase and a decrease in the number and size of bubbles respectively which increases the solution turbidity. The transition concentration of each salt is defined as the concentration corresponding to 50% bubble coalescence (Craig et al., 1993a). A typical plot of the percentage coalescence of bubbles is shown in Figure 2.3. Gas holdup which is the proportion of gas volume in total volume is another indicator for determining the effect of salts on bubble coalescence. Gas holdup can be defined as $\varepsilon = 1 - H_0 / H$, where H_0 and H are the initial and the aerated heights of the liquid in the column respectively.

A variation comes from monitoring the population and size distribution of bubbles by means of high speed photography. The transition concentration of each salt is defined as the concentration at which the bubble size distribution levels off to reach a constant value (Marrucci and Nicodemo,

1967). Figure 2.4 represents the average bubble size versus concentration for KCl solutions to determine the transition concentration.

In general, bubble column experiments provide useful statistical information on how the flow conditions influence bubble coalescence but give little insight into the mechanisms of bubble coalescence (Horn et al., 2011).

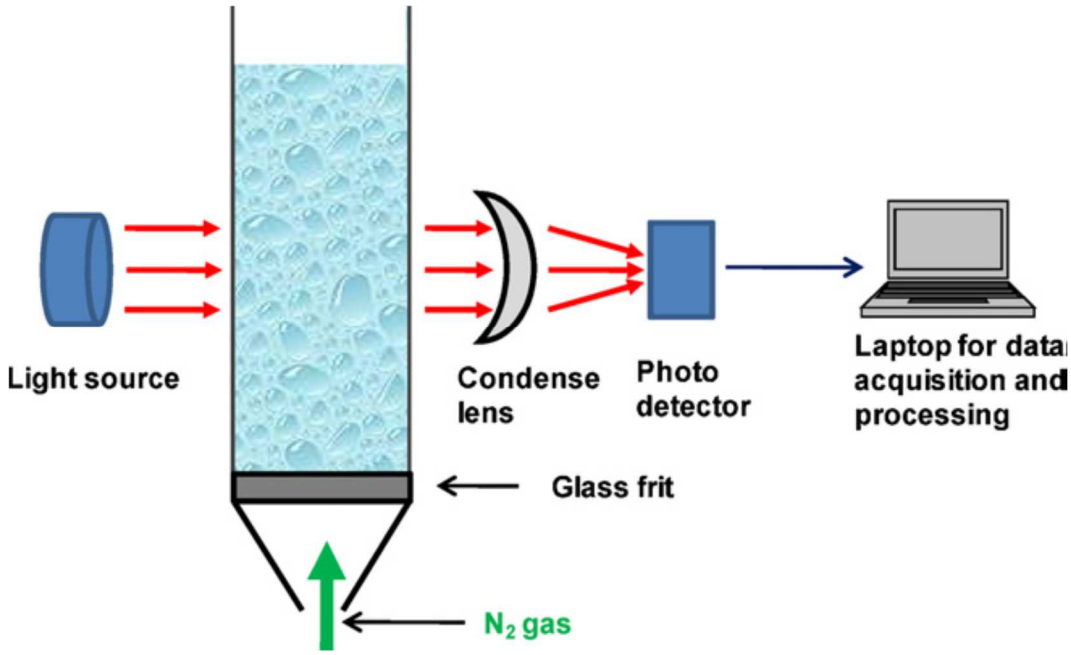

Figure 2.2**.** Schematic of a bubble column setup to study bubble coalescence in solutions (Nguyen et al., 2012).

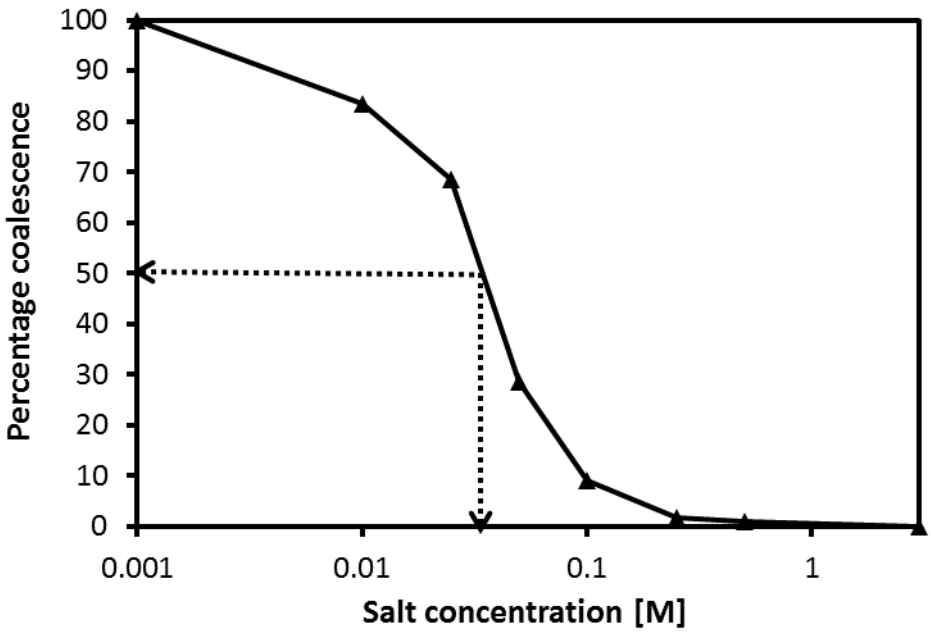

Figure 2.3**.** An illustration of salt transition concentration determined at 50% percentage coalescence of bubble population.

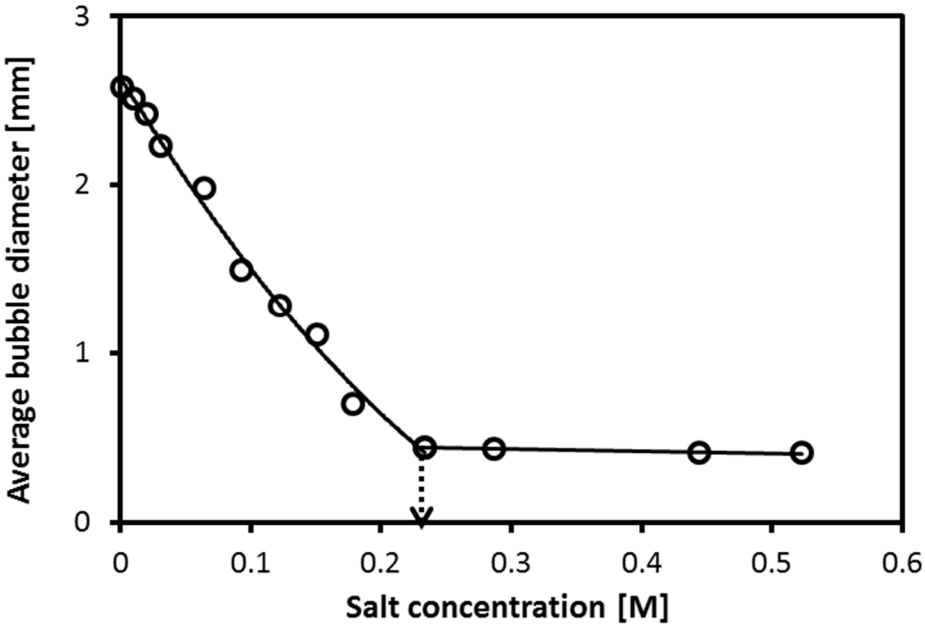

Figure 2.4**.** An illustration of salt (KCl) transition concentration determined as the minimum concentration at constant (average) bubble size verses salt concentration (data are taken from (Marrucci and Nicodemo, 1967)).

2.4.2 STIRRED TANK

Stirred tanks have also been used to investigate the effect of salts on bubble coalescence and breakup with the focus on bubble size distribution. The setup consists of a typical glass tank equipped with impellers and baffles for agitating the liquid in the tank. Bubbles are produced by passing gas through a porous plate placed under the impeller. The main emphasis of investigations employing this technique is to determine the bubble breakup due to the industrial applications of stirred tanks for multiphase processing. Due to difficulties quantifying turbulence intensities throughout the system, little work has been carried out using this experimental technique for studying bubble coalescence (Alves et al., 2002; Machon et al., 1997).

Laboratory-scale flotation machines are another variation of this technique in which effect of salts can be investigated by monitoring the size of bubbles. Fine bubbles are produced by cavitation at the trailing edge of the impeller blade in mechanical flotation cells (Cho and Laskowski, 2002). Castro et al. (2012) and Quinn et al. (2014b) employed the concept of critical coalescence concentration (*CCC*) proposed by Cho and Laskowski (2002) to characterize the effect of different salts on froth stability. The *CCC* is a concentration above which bubbles do not coalesce and reach an almost constant bubble size. Quinn et al. (2014b) defined *CCCX* as the concentration at which the bubble size reduces by *X%* from that in pure water to the constant bubble size at a high salt concentration (Quinn et al., 2014b). The *CCCX* of salts was determined by fitting the bubbles Sauter mean diameter (D_{32}) and salt concentration (C) data to the following model:

$$D_{32} = D_l + A\exp\left(-B \times C\right) \tag{2.1}$$

where D_l is the value of D_{32} as the salt concentration goes to ∞, A is the difference between D_l and D_{32} in pure water and B is the exponential decay constant. The *CCCX* was calculated as $CCCX = -\ln\left(1 - X/100\right)/B$. Figure 2.5 shows the *CCC95* of investigated salts reported by Quinn et al. (2014b), along with the curves and size data used for the fitting of equation (1).

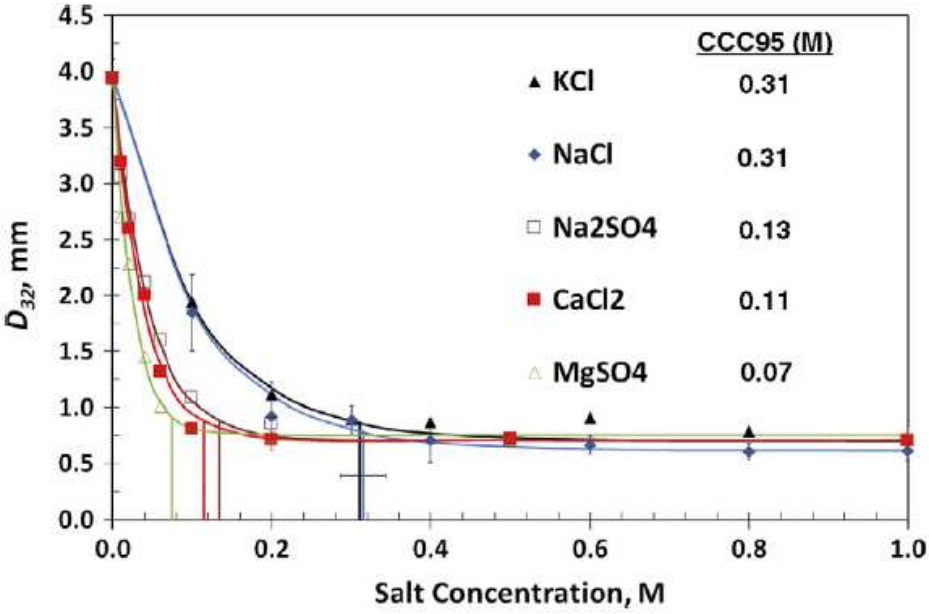

Figure 2.5**.** The *CCC95* of salts based on fitting an exponential model to the Sauter mean diameter (D_{32}) and salt concentration data (Quinn et al., 2014b).

2.4.3 ADJACENT CAPILLARIES

Unlike bubble swarm experiments, the adjacent capillaries or bubble pair method provides direct and precise information on the lifetime, drainage and rupture time of the liquid film between two bubbles. This technique involves producing two bubbles from adjacent capillaries either placed side by side or facing each other in a glass cell as shown in Figure 2.6. Despite the mentioned advantages of this technique relative to the previous ones, surface contamination on bubbles in stagnant solution is an important concern involved in this method.

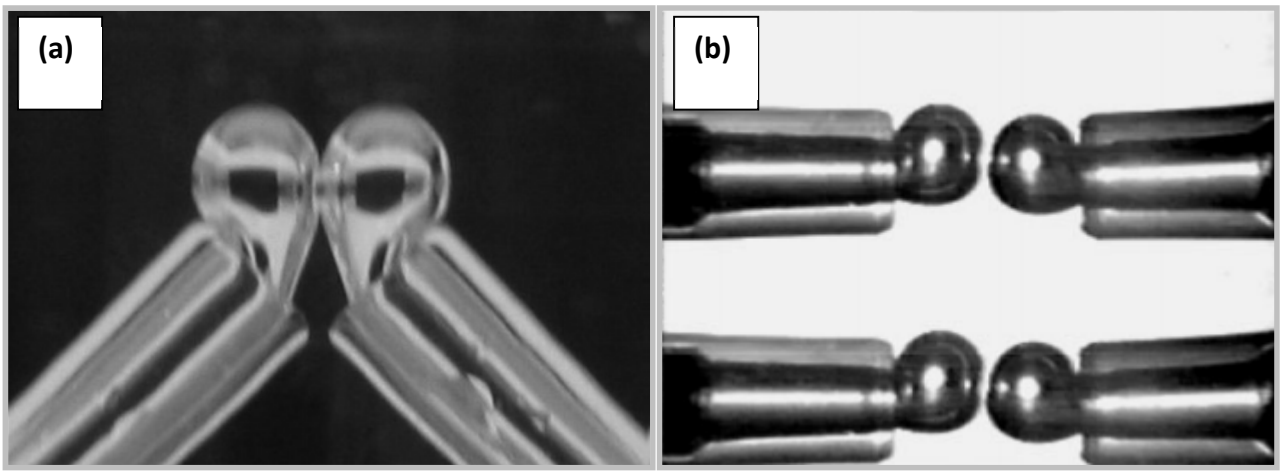

Figure 2.6. Images of the bubble pair experiment using adjacent capillaries (a) placed side by side (Christenson et al., 2007) (b) facing each other (Tse et al., 1998).

Figure 2.7 shows examples of bubble coalescence using adjacent capillaries (a) in pure water in which bubbles coalesce effectively instantly on contact and (b) in a high salt concentration solution. The bubble percentage coalescence is determined by the ratio of the number of coalesced bubbles to the total number of contacted bubbles. The transition concentration of salts is defined as the concentration of the percentage coalescence half way between the percentage of bubble coalescence in pure water (100% coalescence) and the baseline measurement as demonstrated in Figure 2.8 (Lessard and Zieminski, 1971).

Monitoring the coalescence of a single rising bubble to a free surface has been considered as another variation of this technique (Horn et al., 2011). The air above the water surface can be considered to represent a bubble with infinite radius. The effect of salts on bubble coalescence is characterised by measuring the rest time (before coalescence) of air bubbles at the air-liquid interface which significantly increases in the presence of inhibiting salts compared to pure water (Ghosh, 2004).

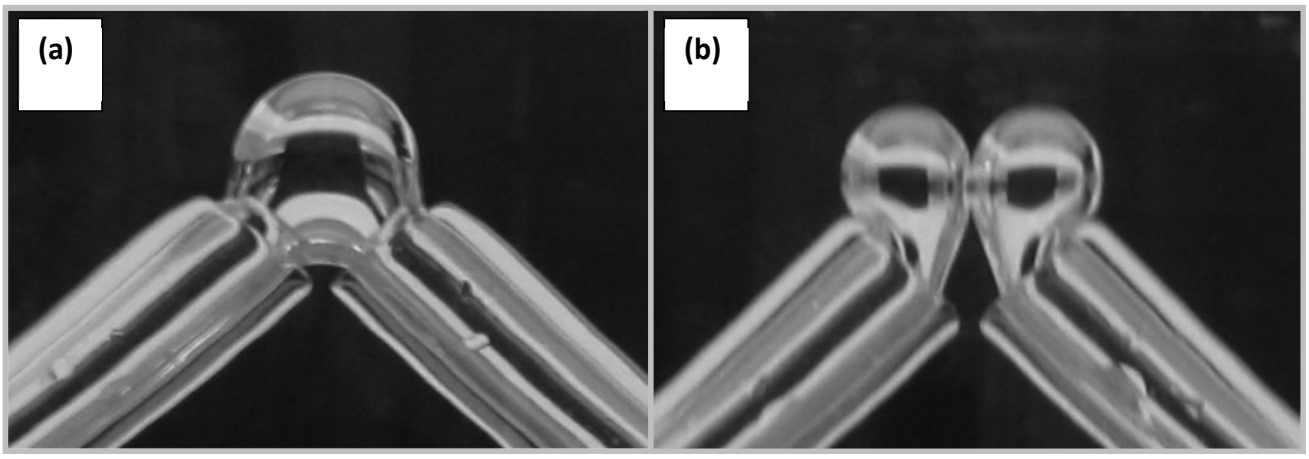

Figure 2.7. Bubble pair experiments in (a) pure water (b) a high salt concentration solution (Christenson et al., 2007).

A slight variation of this technique was described by Del Castillo et al. (2011) in a study of the effect of bubble approach speed on the coalescence of bubbles in pure water and aqueous solutions of 0.1 and 0.5 M KCl. The schematic of the setup is shown in Figure 2.9. An air bubble is formed at the lower end of a glass cylinder using a stainless steel needle. The bubble is allowed to slide up along the inside of the cylinder wall to approach the meniscus of the liquid which mimics the behaviour of a large bubble. Altering the angle of inclination of the glass cylinder provides variation to the bubble approach speed. The authors were able to successfully confirm the importance of bubble approach speed as well as the effect of salt concentration on the coalescence time of bubbles.

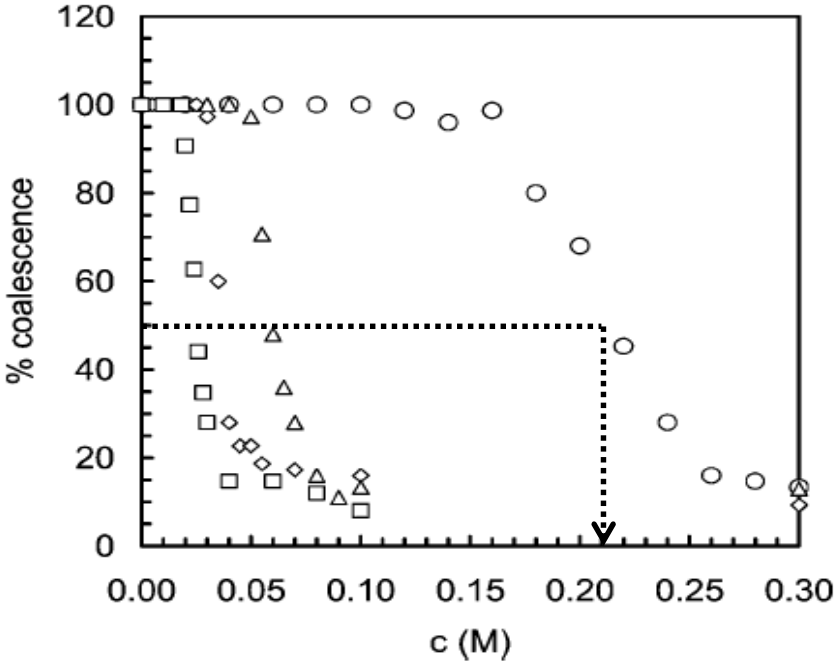

Figure 2.8**.** Percentage coalescence of bubbles versus salt concentration for $LaCl_3$ (open squares), $MgSO_4$ (open diamonds), $CaCl_2$ (open triangles) and NaCl (open circles) using adjacent capillaries (bubble pair) method (Christenson et al., 2007).

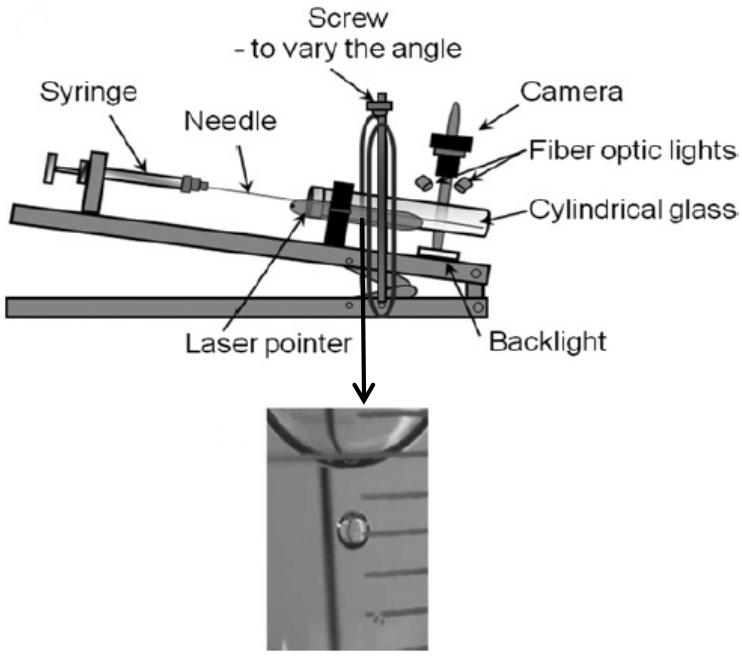

Figure 2.9**.** Schematic of the bubble-meniscus experiment (Del Castillo et al., 2011).

2.4.4 THIN LIQUID FILM MICRO-INTERFEROMETRY

This technique provides very varied and useful information on the mechanisms behind saline liquid films at the microscopic level by allowing detailed analysis of disjoining pressures, thinning and rupture of liquid films. This method works based on the determination of the change in the intensity of the reflected light from a film when illuminated with a parallel, unpolarised, white light beam. As a result of the interference of the reflected light from air-liquid interfaces, a set of colourful fringes (Newton rings) is observed (Karakashev et al., 2008; Nguyen and Schulze, 2004). The following is a brief history of the development of this technique.

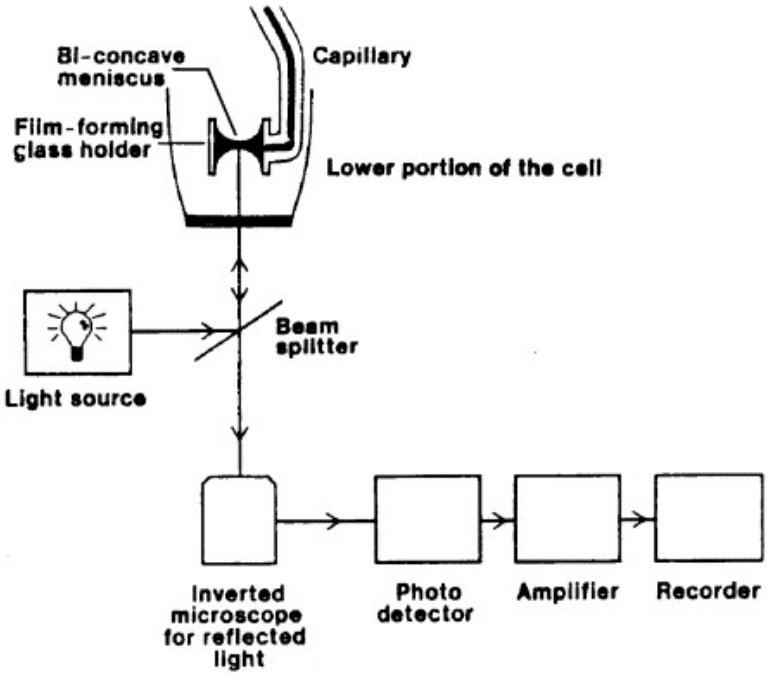

Figure 2.10**.** Experimental interferometric setup with the Scheludko cell (Manev and Nguyen, 2005b).

In 1921, the thickness of particularly thin (so called “black”) soap films were measured by Wells (1921) using a microscope in combination with an interferometer. Later Deryaguin (1954) greatly improved the method by adding an appropriately constructed measuring cell. This part of the apparatus has been further improved and a recording device added to the photo-detector by Scheludko and Exerowa (1959) and now it is referred to as the “Scheludko cell” or “Exerowa cell” in the literature. This technique allows determination of the thickness of thinning films as well as equilibrium films. The setup shown in Figure 2.10 has two major parts; a glass cell (Scheludko cell) in which a liquid film is formed and an optics-electronics system for monitoring the film behaviour.

The liquid film is formed by withdrawing the liquid from the cell by using a syringe or a nano-pump which results in formation of a biconcave meniscus in the glass capillary. The two bounding menisci represent two air bubbles. The Scheludko cell is placed on the stage of an inverted microscope. A beam light is shone onto a small part of the film, and the reflections are viewed through a photometric eyepiece. During the film thinning, a set of colourful interference fringes (Newton rings) is formed, whose colour is dependent on the film thickness. The optical signal is converted to an electrical signal using a fibre optic probe positioned close to the film centre, transmits the signal onto a photomultiplier. This signal is amplified through an electrometer and is recorded on a strip chart recorder. The output of this recorder is photocurrent as a function of time (Rao et al., 1982; Sheludko, 1967).

This method has been successfully applied for the entire range of stability of foam, emulsion and wetting films. Several innovations have been introduced to this technique which one of them is the oscillating photometric probe method proposed by Manev (1985). This technique permits the quantitative estimate of the magnitude of the film non-homogeneity by rapid scanning of a small part of the film surface (ca. < 5% of the total area). Multiple oscillations of the photometric probe along the film diameter at a rate ca. 1 Hz provides a statistical determination of the amplitude of thickness non-uniformity as a function of film size or time in the process of thinning. However this method is useful for small films (with diameters smaller than 0.1 mm), which are usually planar. Larger films exhibit significant corrugations on the film surface which leads to a dimpled film. In these cases the local film thickness profile is important. To solve this problem in the new design of this technique, the light is focused on the whole film instead of just a small part. The interferometric images can be captured by high-speed video CCD microscopy and transferred to a computer for recording and off-line processing. In some cases it can be done by a line scan camera capable of scanning a chosen line through the film and producing a series of interferograms in the suitable digital format.

This method has primarily been applied in the study of surfactant-laden films unlike the case of saline liquid films (Exerowa et al., 1979; Karakashev and Manev, 2003; Manev and Pugh, 1991; Qu et al., 2009). To date few studies have been conducted on saline liquid films using the thin liquid micro-interferometric technique (Firouzi and Nguyen, 2014a; Henry et al., 2009; Karakashev et al., 2008; Yaminsky et al., 2010). The results showed that inhibiting salts increase the lifetime of liquid films at concentrations above the transition. The transition concentration is determined based upon the abrupt increase in the lifetime of saline liquid films from the instant rupture at very dilute salt solutions. Figure 2.11 illustrates the average lifetime of NaCl liquid films between two bubbles using

thin liquid film interferometry in a closed system. The results show a sudden increase in the lifetime of NaCl solutions after 0.1 M.

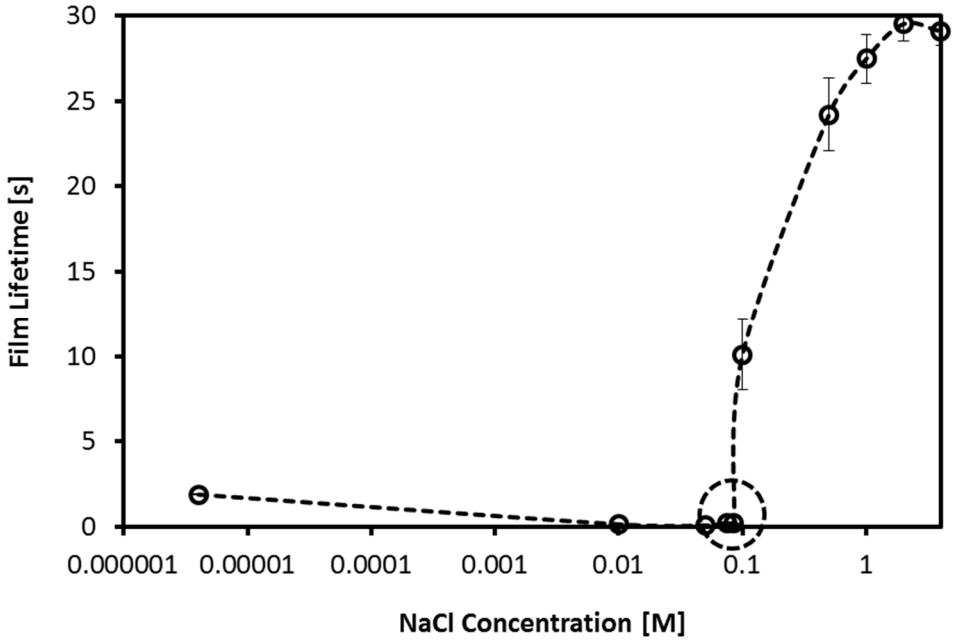

Figure 2.11. Average lifetime of liquid films of aqueous NaCl solutions at interface approach speed of 10 μm/s versus NaCl concentration in a closed system.

2.4.5 COMPARISON OF TRANSITION CONCENTRATIONS OF SALTS

Transition concentration of common salts determined by different techniques described in previous sections was compared in Table 2.1. For consistency, the available data for the bubble size versus salt concentration of aqueous NaCl solutions were converted to the "percentage coalescence" by dividing the bubble size corresponding to each salt concentration by the bubble size in pure water and multiplying by 100. The concept of *TC95* was defined as the concentration at which the percentage coalescence of bubbles is reduced by 95% from 100% in pure water to an asymptotic value of the percentage coalescence at a relatively high salt concentration. Lifetimes of saline liquid films measured by the TLF micro-interferometric method was also converted to the percentage coalescence by dividing the average lifetime of a liquid film at each salt concentration by the average lifetime of liquid films at rapid rupture (ca. 0.2 s) and multiplying by 100. The results for percentage coalescence of bubbles in aqueous NaCl solutions are shown in Figure 2.12. Table 2.2 compares the *TC95* for NaCl based on the experimental data in the literature. Different bubble size, degree of salt

purity and bubble approach speed account for the differences in the transition concentrations of NaCl shown in Table 2.2. The information for the bubble approach speed is not available in the majority of the studies on salt transition concentration. Therefore, it was not possible to study the relationship between the salt transition concentration and bubble approach speed. Purifying salts is challenging since specific techniques are required. Salt purification can be conducted through foam fractionation, roasting salts at temperatures below their melting points following crystallization, calcination or freeze-drying in liquid nitrogen under vacuum to remove excess moisture and possible trace organic contamination (Del Castillo et al., 2011; Henry et al., 2008; Nguyen et al., 2012). The *TC95* of NaCl was plotted versus the reciprocal of the square root of bubble radius ($R^{-1/2}$) in Figure 2.13. The results show a linear relationship (with the correlation coefficient of 0.92) between the *TC95* for NaCl and ($R^{-1/2}$). This trend agrees with the theoretical model for predicting the transition concentration of salts (Prince and Blanch, 1990).

Table 2.1. Comparison of transition concentrations (M) of common salts using different techniques.

Salt	**Experimental technique**			
	Bubble column Light intensity	**Bubble column Size distribution**	**Adjacent capillaries**	**Thin liquid film micro-interferometry**
NaCl	0.078[d], 0.1[e]	0.31[i1] , 0.17[b], 0.15[i2], 0.778[k]	0.175[a], 0.208[h], 0.145[j]	0.1[g,k]
KCl	0.12[d]	0.21[c], 0.31[i1] , 0.14[i2]	0.23[a], 0.202[j]	0.15[k]
LiCl			0.16[a]	0.1[g,k]
NaBr			0.22[a]	0.2[k]
KI		0.62[c]	0.380[j]	
KOH	0.053[d]	0.17[c]		
KNO_3	0.12[d]	0.41[c]		
$MgSO_4$	0.02[d]	0.07[i1],0.03[i2]	0.032[a], 0.017[e], 0.036[h], 0.036[j]	
$CaCl_2$	0.037[d]	0.11[i1] ,0.05[i2]	0.055[a], 0.06[h]	
$MgCl_2$			0.055[a]	
Na_2SO_4		0.13[i1] ,0.06[i2]	0.061[a], 0.051[j]	

a. Lessard and Zieminski (1971)
b. Zieminski et al. (1976)
c. Marrucci and Nicodemo (1967)
d. Craig et al. (1993b)
e. Nguyen et al. (2012)
f. Tsang et al. (2004)
g. Karakashev et al., (2008)
h. Christenson et al. (2007)
i. Quinn et al. (2014b), 1.*CCC95* and 2.*CCC75* the concentration at which D_{32} (the Sauter mean diameter) is reduced by 95% and 75% respectively from that in water to D_{32} as the salt concentration goes to ∞
j. Zahradník et al. (1999)
k. Firouzi and Nguyen (2014a)
l. Castro et al. (2012)

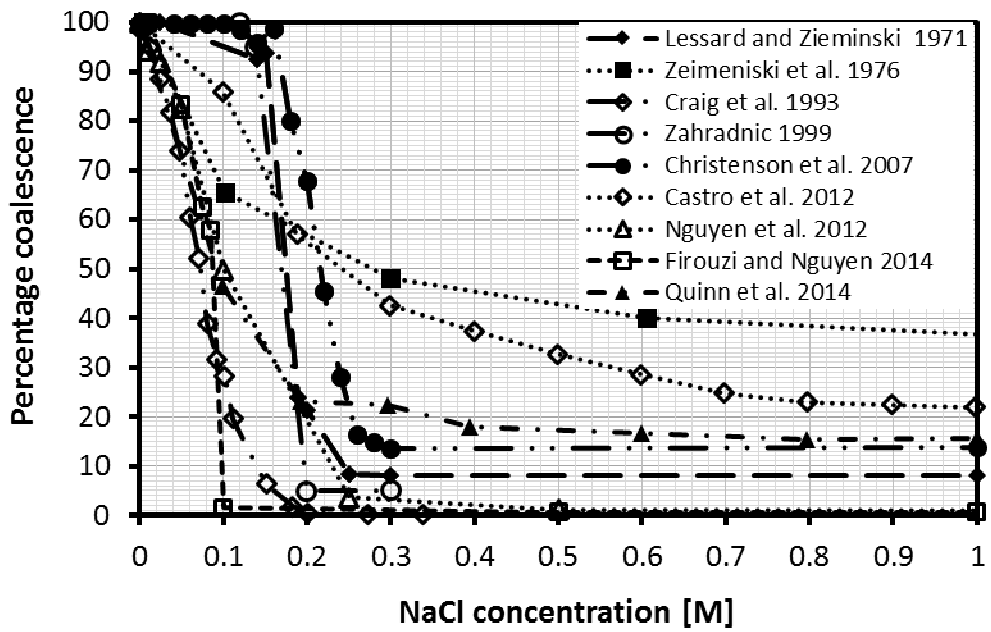

Figure 2.12**.** Comparison of percentage coalescence of bubbles in NaCl solutions conducted by different experimental techniques.

Table 2.2. Bubble radius and the *TC95* of NaCl determined based on the data available in the literature for aqueous NaCl solutions.

Researchers	***TC95* [M]**	**Bubble radius [mm]**
Lessard and Zieminski (1971)	0.25	1.8
Zieminski et al. (1976)	0.54	0.42
Craig et al. (1993b)	0.16	Not available
Zahradník et al. (1999)	0.19	0.8
Christenson et al. (2007)	0.26	1
Castro et al. (2012)	0.78	0.33
Nguyen et al. (2012)	0.24	Not available
Firouzi and Nguyen (2014)	0.1	2
Quinn et al. (2014)	0.30	0.32

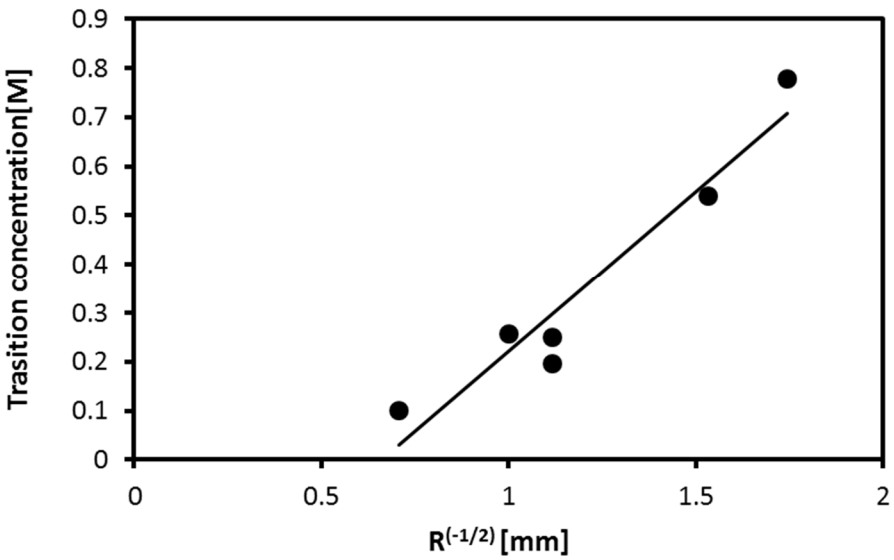

Figure 2.13**.** Transition concentration (*TC95*) of NaCl shown in Table 2.2 (points) versus the bubble size. The result from (Quinn et al., 2014b) is excluded. Correlation coefficient of the trend line is equal to 0.92.

2.5 REASONS FOR INHIBITING BUBBLE COALESCENCE

As yet, there is no definitive agreement on explaining the stabilizing effect of salts on bubble coalescence at salt concentrations above the transition concentration. However, a number of explanations have been proposed concerning the inhibiting effect of salts which are described in the following sections.

2.5.1 COLLOIDAL FORCES

When bubbles approach each other, interfacial forces become significant at small separation distances. Surface forces arise from molecular interactions between charged and uncharged atoms and molecules of the interacting bodies and the surrounding medium (Drelich et al., 2007). Surface forces include van der Waals (electrodynamic) interactions and electrostatic double-layer (EDL) interactions. These interactions form the key components of the celebrated DLVO (Derjagiun-Landau-Verwey-Overbeek) theory of colloid stability. In many cases, the DLVO theory fails to explain the direct measured surface forces in a liquid medium. Under these circumstances, further non-DLVO disjoining pressures are introduced into the surface forces. The non-DLVO pressures include the (repulsive) hydration pressure (between hydrophilic surfaces) and the (attractive) hydrophobic pressure (between hydrophobic surfaces). Steric pressure is another component of the non-DLVO pressure and arises from confinement and layering of macromolecular reagents used as depressants or flocculants (Nguyen and Firouzi, 2012).

Van der Waals attractions which arise from molecular interactions are attractive in the case of bubble-bubble interactions which enhance the drainage of liquid films rather than stabilizing the liquid films to inhibit bubble coalescence. Van der Waals attractions are considered as non-retarded London and retarded Casimir van der Waals attractions. The non-retarded London-van der Waals attraction is very short-ranged, i.e., shorter than 10 nm (Israelachvili, 2005) which is much shorter than the average thickness of saline liquid films at which coalescence of gas bubbles occurs. Furthermore, the Hamaker constants in Van der Waals attractions do not specifically depend on specific properties of salt ions. Therefore, van der Waals attractions cannot explain the inhibiting effect of different salts on bubble coalescence.

Air-liquid interfaces are known to be negatively charged (Creux et al., 2007). The approach of two negatively charged surfaces results in repulsive EDL interactions, which keep air-liquid interfaces away from each other and thereby inhibit bubble coalescence. However, the EDL

repulsions become vanishingly small at salt concentrations greater than 0.01 M which is almost one order of magnitude smaller than the range of the transition concentration of salts (Nguyen et al., 2012; Yaminsky et al., 2010). Therefore, EDL repulsions cannot explain the stabilizing effect of salts at concentrations beyond transition concentrations. In addition, the DLVO theory excludes any ion-specific effect (Craig, 2004). Thus, it cannot explain the effect of different types of salts and ions on bubble coalescence.

The repulsive hydration pressure/force has been suggested as a reason for the inhibiting effect of salts (Chan and Tsang, 2005; Tsao and Koch, 1994). The hydration or structural force is believed to arise from the strongly bound and oriented first layer of water molecules on surfaces which may prevent two surfaces or macromolecules from approaching any closer than 5-6 Å (the size of two water molecules) (Israelachvili and Wennerstrom, 1996) . Therefore, they cannot significantly influence liquid films in salt solutions with an average rupture thickness of tens of nanometres (Cain and Lee, 1985; Weissenborn and Pugh, 1996).

Hydrophobic surfaces are inert to water as they are unable to interact or bind with water either by electrostatic means or via hydrogen bonds. Air-water interfaces are strongly hydrophobic and the hydrophobic force between air-water interfaces which is believed to be appreciably stronger than van der Waals attractions can derive the interfaces to coalesce (Pugh and Yoon, 1994). There is evidence in the literature that salts reduce the decay length and strength of the hydrophobic attractions and thereby retards the drainage of liquid films and consequently inhibit bubble coalescence (Craig et al., 1993a; Pugh and Yoon, 1994). However, in 1998, this hypothesis was abandoned after measuring the hydrophobic interaction between silica surfaces since hydrophobic attractions did not decrease in the presence of concentrated electrolytes (Craig et al.,1998). Later, it was shown that adding salts resulted in reducing hydrophobic attractions, and it was explained that the observed increase in foam stability can be partially attributed to the diminishing effect of salts on these interactions (Wang and Yoon, 2004). Further to that, the effect of dissolved gasses on the lifetime of DI water was studied (Nguyen and Nguyen, 2010) whose results emphasized the existence of long-ranged hydrophobic attractions. These attractions were attributed to the disturbing effect of the present dissolved gases on the hydrogen bond of the water molecule network.

Despite so many studies on the measurement of forces between hydrophobic surfaces, there is still no consensus on the origin, magnitude and length of hydrophobic attractions.

2.5.2 GAS SOLUBILITY

There is ample evidence in the literature showing that salts reduce the solubility of gas molecules in salt solutions (Cramer, 1980; Geffcken, 1904; Millero et al., 2002; Sherwood et al., 1991; Shoor et al., 1969; Weissenborn and Pugh, 1996). This phenomenon has been proposed as an alternative mechanism by which salts inhibit bubble coalescence.

Decreasing hydrophobic interactions (Craig et al., 1999; Stevens et al., 2005; Yaminsky and Ninham, 1993), influencing the properties of air-solution interfaces such as surface tension and viscosity (Nguyen and Nguyen, 2010; Weissenborn and Pugh, 1996), affecting drainage and rupture of thin liquid films by migration of dissolved gases in the solution (Horn et al., 2011; Nguyen and Nguyen, 2010; Weissenborn and Pugh, 1996) are a number of explanations have been proposed to link the solubility of gas molecules to bubble coalescence in salt solutions.

The role of gas solubility in stability/instability of saline liquid films is discussed in more details in section 2.5.4.

2.5.3 GIBBS-MARANGONI EFFECT

Rapid stretching of the interface of a liquid film of salt solutions between two bubbles during its thinning and drainage causes a non-uniform distribution of ions at the interface by moving the ions along the interface. The resultant surface concentration gradient leads to a surface tension gradient along the air-solution interface. This tension gradient creates a tangential stress which opposes the film drainage and immobilizes the interface. This phenomenon is referred to as the Gibbs-Marangoni effect which has been considered as an effective contributor in explaining bubble coalescence inhibition in salt solutions (Christenson et al., 2007; Marrucci and Nicodemo, 1967; Yaminsky et al., 2010). Marrucci and Nicodemo (1967) theoretically demonstrated the significance of the Gibbs-Marangoni effect in determining the transition concentration of salts. However, Weissenborn and Pugh (1996) ruled out this mechanism by relying on the “mediocre correlation coefficient” for the Gibbs-Marangoni factor defined as the inverse square of surface tension gradient versus transition concentration of salts, $(d\sigma/dc)^{-2}$. Further to that, the experimental observations of Henry et al. (2006) rejected the correlation between $(d\sigma/dc)^{-2}$ and the transition concentration of mixed electrolytes. They concluded that the Gibbs-Marangoni effect cannot solely be taken into account as the responsible

mechanism for inhibition of bubble coalescence in salt solutions. Ion-specificity and prevention of film rupture owing to the short-ranged double layer repulsion arising from the location of ions at the interface were suggested as alternative mechanisms. However, despite the recent considerable progress in understanding the basic of ion-specificity, its origin and effect on bubble coalescence remain contentious. Moreover, the question that how these short-ranged and weak EDL repulsions can inhibit bubble coalescence at transition concentrations in the order of 0.1 M and rupture thicknesses of tens of nanometres remains un-answered. Later the possible mechanisms by which a surface tension gradient can be established were comprehensively discussed (Yaminsky et al., 2010). It was shown that the Gibbs-Marangoni effect is very effective even at very small surface tension gradients to alter the air-bubble interface from a mobile to partially mobile or immobile interface (Klaseboer et al., 2000; Yaminsky et al., 2010).

2.5.4 SURFACE RHEOLOGY

Salts are known to inhibit bubble coalescence by affecting the dynamic interfacial properties and consequently the hydrodynamic boundary condition of the air-solution interface of a thin liquid film between two bubbles. There is sufficient evidence in the literature indicating that boundary conditions of the flow between two bubbles will dramatically affect the drainage of liquid films (Barnocky and Davis, 1989; Chesters and Hofman, 1982). In the case of mobile surfaces the velocity profile is uniform (the plug flow), unlike the immobile surfaces with the velocity profile having a parabolic shape (the Poiseuille flow). The latter case is associated with a large hydrodynamic resistance which retards the drainage rate and enhances the film stability (Horn et al., 2011). The rapid coalescence of bubbles in pure DI water is ascribed to the mobile air-water interface of the liquid film between two bubbles (Li and Liu, 1996). Pure water contains clusters of dissolved gases with a typical diameter of around 15-20 nm termed “nanobubbles” (Vinogradova et al., 1995). Nanobubbles in a thin liquid film between two bubbles migrate towards the air-liquid interfaces which lead to increasing the local disruption of hydrogen bonding and decrease of the effective viscosity of the water film. Therefore the water liquid film drains faster due to this increase in surface mobility (Nguyen and Nguyen, 2010).

Salts are believed to stabilize bubble coalescence by changing the hydrodynamic boundary condition from mobile to immobile at the transition concentration (Henry et al., 2006; Marrucci, 1969; Prince and Blanch, 1990). This stabilizing effect of salts on bubble coalescence is attributed to the slow drainage (less surface mobility) of liquid films owing to factors such as surface tension gradient

(Marrucci, 1969; Prince and Blanch, 1990), decreasing the gas solubility and consequently the gas migration (Nguyen and Nguyen, 2010) or repulsive EDL forces (Henry et al., 2006) at the interface . The mobility of an air-liquid interface in saline solutions was experimentally investigated by measuring the terminal rise velocity of fine bubbles towards a free surface (Henry et al., 2008). The results indicated that the terminal rise velocity of bubbles in pure water and aqueous salt solutions follows Hadamard-Rybczynski's model which corresponds to a mobile surface. These observations were considered as strong evidence against immobilizing effect of salts despite admitting that there are differences between the rise of a single bubble in a quiescent liquid and the thinning of a liquid film between two colliding bubbles. It is noted that the evidence that the bubble rise velocity in solutions of bubble coalescence inhibiting and non-inhibiting salts is the same as that in pure water is contradictory to the experimental results of Quinn et al. (2014a). These contradictory evidences can be attributed to the salts purity since bubbles smaller than 1 mm in diameter show little effect of contamination on bubble size and velocity, while larger bubbles can undergo surface deformation affected by impurities via surface tension and surface viscoelastic properties of the air-water interface (Quinn et al., 2014a). Later the boundary condition of a liquid film between a rising bubble and a TiO_2 solid surface during drainage was studied (Parkinson and Ralston, 2010). The results confirmed the immobile (no-slip) boundary condition at the interface of the air bubble as it approached the solid surface in KCl solutions. The viscous (immobile) drainage of liquid films was assigned to the influence of ion redistribution at the interface during drainage. The terminal rise velocity of each bubble prior to interaction with the solid surface was also determined which indicated a fully mobile surface.

Figure 2.14 represents the result for the drainage rate of a thin liquid film of 0.19 M KCl solution between two bubbles using the thin liquid micro-interferometric method. The experimental data were compared with the Stefan-Reynolds drainage models for immobile $-dh/dt = 2h^3/(3\mu R_f^{\,2})\times(P_\sigma - \Pi)$ and mobile $-dh/dt = 8h^3/(3\mu R_f^{\,2})\times(P_\sigma - \Pi)$ boundary conditions. Here h and R_f are the film thickness and radius respectively, μ is the viscosity of liquid, P_σ is the capillary pressure due to the curvature of bubbles and Π is the disjoining pressure which includes the retarded van der Waals attraction. The results confirm the immobile air-liquid interface of the draining thin liquid film of KCl solution at its transition concentration (~0.19 M). It should be noted that the instant rupture of thin liquid films of pure water and salt solutions at concentrations

below the transition concentration as well as the traditional shake test rule out any possible contamination in the system.

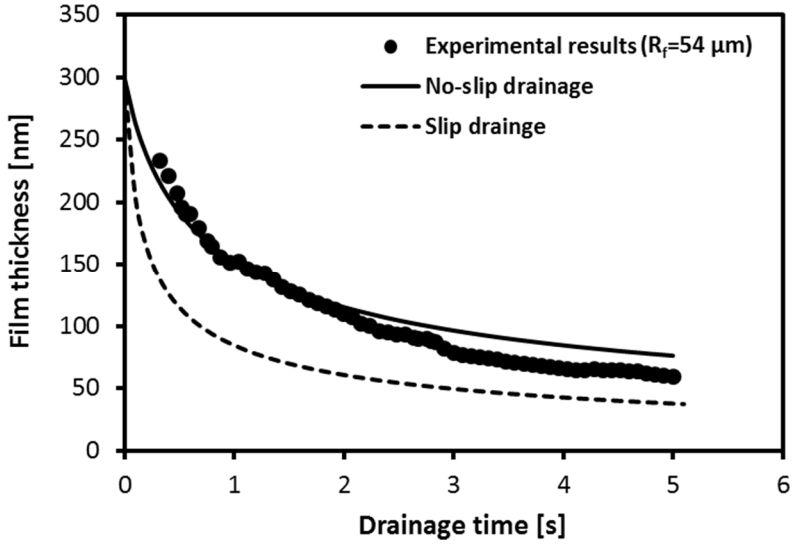

Figure 2.14**.** Drainage of a liquid film of 0.19 M KCl solution between two bubbles. Solid and dashed lines represent the drainage rate predictions with no-slip and fully slip boundary conditions, respectively. The film radius is R_f = 54 µm.

Further to the mentioned experimental evidence, it was suggested that a surface tension gradient can be established during drainage of a thin liquid film even in the case of very clean air-water interface (2010). It was also demonstrated that the tangential stress created is sufficient enough to inhibit bubble coalescence in saline solutions.

Salts can alternatively inhibit bubble coalescence by influencing the rupture of a liquid film rather than its drainage (Craig, 2004; Henry et al., 2006; Nguyen and Nguyen, 2010). The growth of surface waves or capillary waves due to thermal disturbances and the nucleation of holes in a liquid film are known as the rupture mechanisms of thin liquid films (Derjaguin and Prokhorov, 1981; Vrij, 1966). Salts can hinder the rupture of liquid films by making the liquid film resistant to local deformation as well as retarding any spatial variations and the growth of capillary waves at the interface of the liquid film by affecting its surface mobility and viscosity.

2.5.5 ION-SPECIFIC EFFECT

Hofmeister was the first who did a revolutionary study on ion-specific effect which is beyond the effect of different charges and for a long time it is still the reference for the effect of salts (Kunz, 2009). Salts were ordered based on their effect on the solubility of proteins (Collins, 2004). Figure 2.15 represents the typical ordering of the Hofmeister series. Over the decades it turned out that depending on the system the Hofmeister series order varies and in some cases some common ions are difficult to incorporate into the series. The change in the effect of salts on the precipitation of proteins by heavy metals with the salt concentration is an example (Kunz, 2009). Furthermore, anions appear to have a dominant effect in Hofmeister interactions. However recent studies reveal that in such cases in which ion-ion interactions are stronger than ion-water interactions, specific-cation effects can be as significant as specific-anion effects (Collins, 2004; Kunz, 2010).

Collins (1997) introduced the concept of “matching water affinities” to elucidate the Hofmeister interactions. Collins showed that the effect of an ion on the structure of water depends to a large extent on its charge density and whether the water-water interactions in bulk solutions are comparable to ion-water interactions. In Collins’ concept, each ion is considered as a sphere with a point charge in its centre. Adjacent water molecules are tightly bound around small ions owing to the high charge density of ions. These ions are referred to as kosmotropic or hard ions. Large ions have a loose hydration shell and are referred to as chaotropic or soft ions. Owing to the strong electrostatic attraction between two small hydrated ions of opposite charge, ions pair and expel the water molecules between them. In the case of two oppositely charged large ions, despite their weak electrostatic attraction, they tend to pair due to their loose hydration shells. The situation is different when it comes to a small-large pair of ions of opposite charge. In this case, the electrostatic attraction by the large ion is not sufficient enough that the hard ion loses its hydration shell. Therefore, a small-large or (kosmotropic-chaotropic) ion pair tends to remain apart in aqueous solutions (Collins, 1997; Kunz, 2009).

Figure 2.16 illustrates the Collins’ classification for group IA cations and group VIIA halide anions into strongly hydrated kosmotropes and weakly hydrated chaotropes.

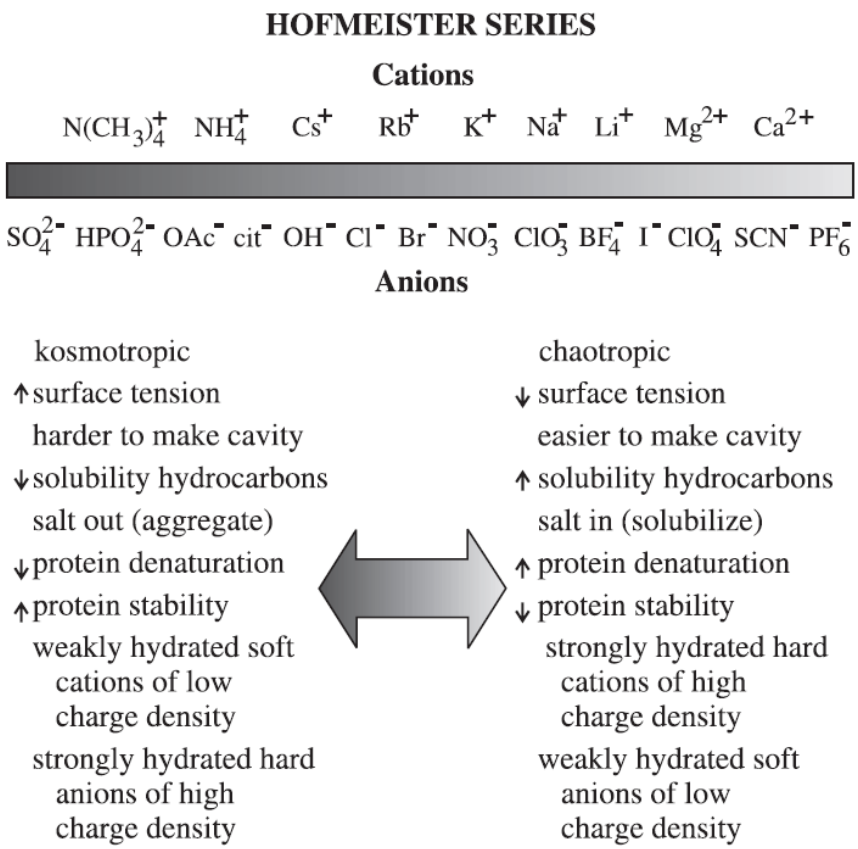

Figure 2.15**.** A typical ordering of cations and anions in Hofmeister series (Kunz, 2009).

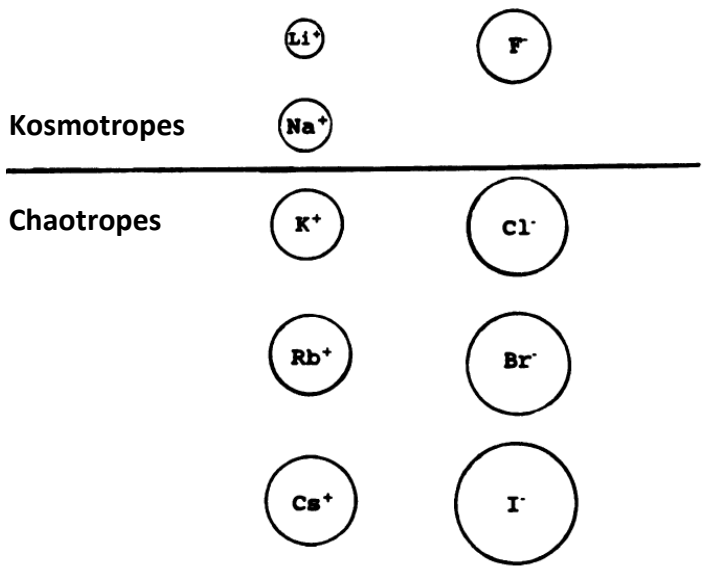

Figure 2.16**.** Division of group IA cations and VIIA halide anions into kosmotropes and chaotropes (Collins, 1997). The circles show proportional size of the ions.

Although Collins' concept of "matching water affinities" allows one to understand the general effect of salts on bubble coalescence, it does not align with the observations concerning the inhibiting effect of all salts on bubble coalescence. For example, NaF as a kosmotrope–kosmotrope salt with matching affinities has a strong effect on bubble coalescence compared to NaI or NaCl as kosmotrope-chaotrope salts. NaF and KI are kosmotrope–kosmotrope and chaotrope-charotrope salts respectively. Based on the concept of matching affinities they both should have a stronger effect than kosmotrope-chaotrope salts such as NaI or NaCl. However, this contrasts with experimental observations for the effect of these salts on bubble coalescence.

Craig et al. (1993a) investigated the ion-specific effect particularly in bubble coalescence and proposed a combining rule based on their experimental observations. They assigned the property α or β to each anion and cation. The combination of $\alpha\alpha$ or $\beta\beta$ salts inhibit bubble coalescence whereas the $\alpha\beta$ or $\beta\alpha$ salts do not affect bubble coalescence. Table 2.3 presents the combining rule for single salts in water. The ion empirical assignments can be different in different solvents as demonstrated by Henry and Craig (2008).

Table 2.3. Combining rule for bubble coalescence inhibition in aqueous salt solutions (Henry et al., 2006).

Ions		Li^+	Na^+	K^+	Cs^+	Mg^{2+}	Ca^{2+}	NH_4^+	H^+	$(CH_3)NH_3^+$	$(CH_3)_2NH_2^+$	$(CH_3)_3NH^+$	$(CH_3)_4N^+$
Assignment		α	α	α	α	α	α	α	β	β	β	β	β
OH^-	α		✓	✓					×				
Cl^-	α	✓	✓	✓		✓	✓		×	×	×	×	×
Br^-	α		✓	✓	✓				×				×
NO_3^-	α	✓	✓	✓			✓		×				
SO_4^{2-}	α	✓	✓	✓		✓			×				
$(COO_2)^{2-}$	α			✓					×				
IO_3^-	α		✓										
ClO_3^-	β		×										
ClO_4^-	β		×			×		×	✓				
CH_3COO^-	β		×	×	×	×		×	✓				✓
SCN^-	β		×										

✓=inhibit coalescence ×=no inhibition
αα, ββ = ✓
αβ βα = ×

As mentioned previously, the combining rule proposed by Craig et al. is purely empirical and the origin of their ion assignment is obscure. Useful information from molecular dynamic simulations (Jungwirth and Tobias, 2001, 2002, 2005) and sum frequency generation spectroscopy (Brown et al., 2005; Liu et al., 2004; Mucha et al., 2005) has provided a better understanding of ions at the air-liquid interface. The results show that ions in salt solutions have a varying propensity for the interface.

Depending on the ion polarizability and size and hence interfacial forces, ions are attracted or repelled from the interface. Expressed in other words, larger and more polarizable ions like I^- are preferentially adsorbed to the interface whereas smaller ions like F^- have a strong propensity for staying in the bulk. Figure 2.17 illustrates the simulation results of 1.2 M aqueous solutions of the sodium halide salts for the average distribution of ions and water molecules from the bulk region to the interface (Jungwirth and Tobias, 2005). In the case of NaF solution, both ions are strongly repelled from the surface, leaving an ion-free layer. In contrast, Cl^- and especially Br^- and I^- favour the air/water interface (Jungwirth and Tobias, 2001).

Later, the origin of the α and β assignments to different ions in bubble coalescence was explained based on different ion affinities to the air-liquid interface (2004). It was suggested that α cations and β anions are repelled from the free surface (air-liquid interface) while β cations and α anions are attracted to the surface. Therefore, salts in which, one of the ions has the propensity for the interface and the other one for the bulk, inhibit bubble coalescence. This group of salts is assigned as $\alpha\alpha$ or $\beta\beta$ salts in the combining rule of Craig et al. (Henry et al., 2006).

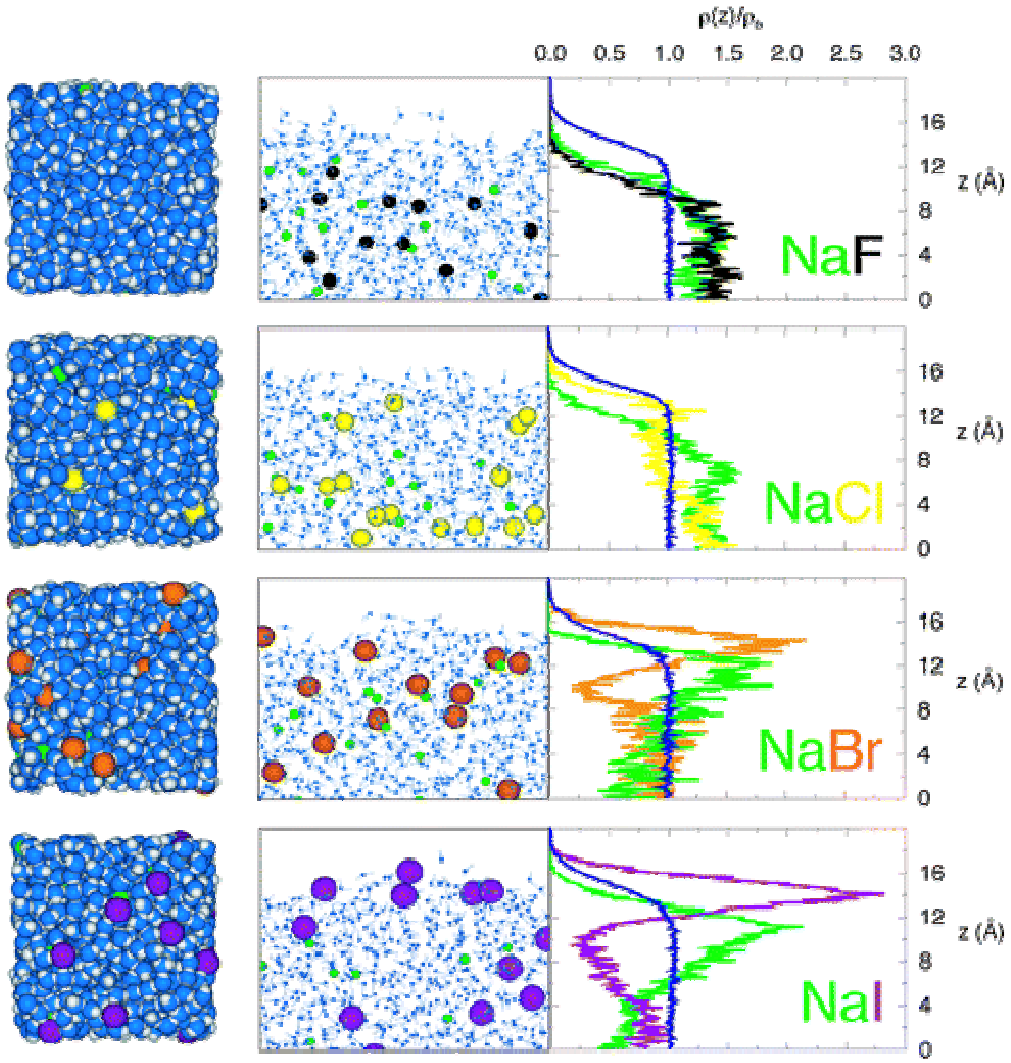

Figure 2.17. Snapshots from molecular dynamics simulations (side and top view of the slabs) and density profiles (i.e., histogramed densities of the electrolyte ions and water molecules in layers parallel to the surface from the centre of the slab across the interface into the gas phase) for 1.2 M aqueous sodium halide salts (Jungwirth and Tobias, 2005).

2.6 THEORETICAL MODELS

Despite the maturity of experimental techniques and evidence, a full theoretical understanding of inhibition of bubble coalescence in salt solutions is still lacking. So far, there are few models available in the literature to predict the transition concentration of salts. Marrucci (1969) was the first to theoretically describe the transition concentration of salts based on balancing the driving and opposing forces of the drainage of thin films between bubbles. These forces (pressures) include the capillary pressure and (non-retarded) London-van der Waals attraction balanced with an opposing force owing to the Gibbs-Marangoni stress. This theoretical model relies on the competence of Gibbs-

Marangoni stress in immobilizing the film surfaces at high salt concentration. As a result, a transition from the inertial (at low salt concentration) to viscous (at high salt concentration) liquid drainage inside the thin film occurs at the transition salt concentration. Therefore, the transition concentration (C_{tr}) can be described as follows (Marrucci, 1969; Prince and Blanch, 1990):

$$C_{tr} = 0.084 \upsilon R_g T \left(\frac{\sigma A^2}{R} \right)^{1/3} \left(\frac{\partial \sigma}{\partial c} \right)^{-2} \tag{2.2}$$

where υ is the number of ions produced upon dissociation, R_g is the gas constant, T is the absolute temperature, R is the bubble radius, and σ and $\partial\sigma / \partial c$ are the surface tension and the surface tension gradient with salt concentration, respectively. A is the non-retarded Hamaker constant which has been considered as $A = 2.5 \times 10^{-20}\,\mathrm{J}$ for saline liquid films between two bubbles (Prince and Blanch, 1990).

Prince and Blanch (1990) argued that the short-ranged non-retarded London-van der Waals attraction is insufficient considering the range of the film thickness encountered during coalescence of bubbles in salt solutions. Therefore, they modified Marrucci's model by replacing the non-retarded London-van der Waals attraction with the retarded Casimir-van der Waals attraction and also taking into account the effect of inertia. These modifications led to the following expression for the transition concentration:

$$C_{tr} = 1.18 \upsilon R_g T \left(\frac{\sigma B}{R} \right)^{1/2} \left(\frac{\partial \sigma}{\partial c} \right)^{-2} \tag{2.3}$$

where B is the retarded Hamaker constant and it has been assigned a value of $B = 1.5 \times 10^{-28}\,\mathrm{J \cdot m}$ based on the best fit of the model to the experimental results of Marrucci and Nicodemo (1967) and Lessard and Zieminski (1971). Figure 2.18 compares the predictions of the models for the transition salt concentration with the experimental data. To resolve the uncertainty of the reported Hamaker constants, Firouzi and Nguyen (2014b) applied the advanced Lifshitz theory to calculate the van der Waals interaction energy per unit area, E, for an intervening water film between gas bubbles. Calculating the van der Waals energy, non-retarded and retarded Hamaker constants were determined as A=3.979$\times 10^{-20}\,\mathrm{J}$ and B=5.397 $\times 10^{-29}\,\mathrm{J \cdot m}$ respectively. They also demonstrated that in the case of saline liquid films, the retarded Hamaker constant reduces to B=3.492 $\times 10^{-29}\,\mathrm{J \cdot m}$ owing to the screening effect of salts on the zero-frequency term. Figure 2.19 shows a comparison of the

predictions of Eqs. (2.2) and (2.3) using the corrected Hamaker constants relative to the same experimental data used by Prince and Blanch (1990) in Table 1 in their paper. The significant difference between the model predictions and experimental data shown in Figure 2.19 indicates that van der Waals attractions as the disjoining pressure are not strong enough to counterbalance the opposing force owing to the Gibbs-Marangoni stress to correctly predict the experimental transition concentration of salts. Furthermore, stronger attractions than van der Waals attractions are required to correctly explain the available experimental results for the critical salt concentration (Firouzi and Nguyen, 2014b).

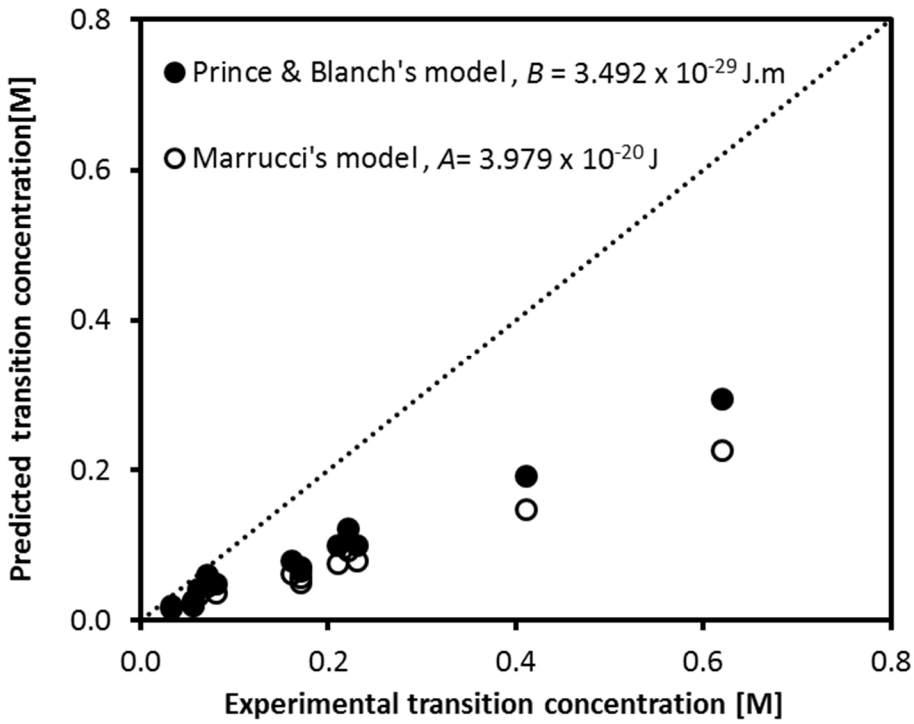

Figure 2.18**.** Comparison of predictions of models proposed by Marrucci (1969) and Prince & Blanch (1990) with the experimental results for the transition concentration (the dotted line represents a perfect match with experimental data) (Prince and Blanch, 1990).

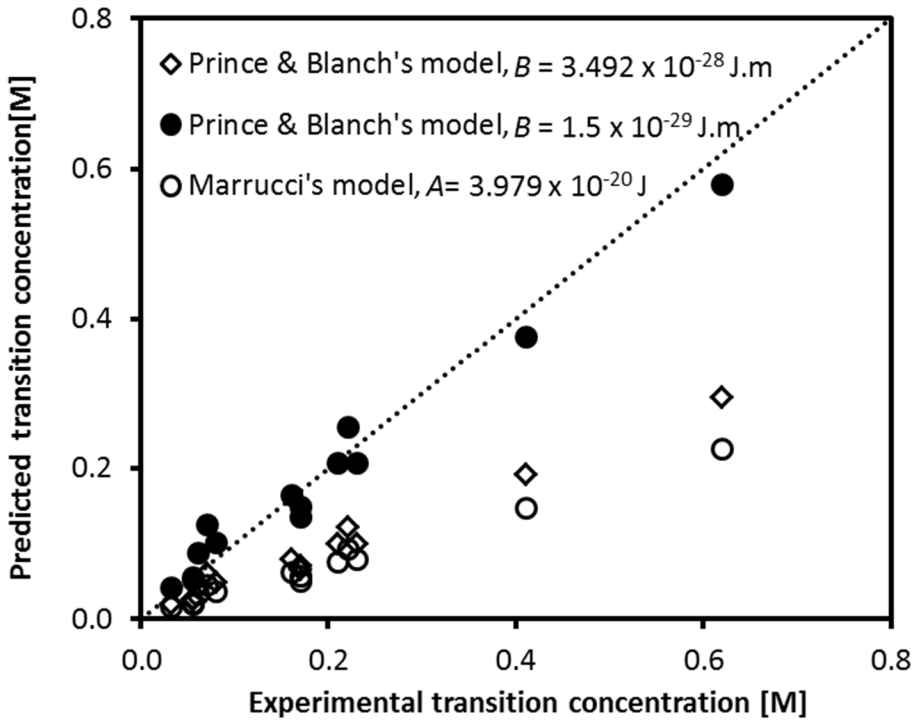

Figure 2.19**.** Comparison of the experimental results (Lessard and Zieminski, 1971; Marrucci and Nicodemo, 1967) with the models proposed by Marrucci (1969) and Prince & Blanch (1990) employing the corrected values of Hamaker constants (Firouzi and Nguyen, 2014b). The dotted line represents a perfect match with experimental data.

Later Chan and Tsang (2005) argued that the opposing force owing to the Gibbs-Marangoni effect is insufficient to immobilize the air-solution interface of saline liquid films to inhibit bubble coalescence. Therefore, they modified the previous models by replacing van der Waals attractions with hydration repulsions (as opposing forces) which resulted in the following formula for predicting the transition concentration of salts

$$C_{tr} = \upsilon R_g T \left(\frac{\sigma h_{rup}^2}{2R} \right) \left(\frac{\partial \sigma}{\partial C} \right)^{-2} \tag{2.4}$$

where h_{rup} is the thickness of the liquid film just before the rupture which is usually unknown and requires further experimental work to be determined. Further to that, Firouzi and Nguyen (2013) demonstrated that replacing van der Waals attractions with the hydration repulsions is physically inconsistent and cannot be justified (the decay length of the hydration force is shorter than 2 nm and cannot inhibit film rupture between two bubbles which occurs within a range of tens of nano-meters). Therefore, none of the available models can predict experimental transition concentrations of salts in

inhibiting bubble coalescence. This failure demands an urgent need of revising the available theories on bubble coalescence in salt solutions.

2.7 SUMMARY AND CONCLUSION

Bubble coalescence and the stability of a liquid film between two bubbles known as a foam film are central to many natural and industrial activities. Some salts are known to inhibit bubble coalescence via retarding the drainage and rupture of the liquid films between bubbles above a critical salt concentration called the transition concentration. The inhibiting effect of salts is not yet well understood. Here, the current literature regarding the inhibiting effect of salts on bubble coalescence at salt concentrations above the transition concentrations has been critically reviewed. The experimental transition concentrations of common inhibiting salts obtained by different techniques were compared. For a consistent comparison, the available data for the average bubble size and liquid film lifetimes versus NaCl concentrations were converted to the “percentage coalescence” of bubbles. The transition concentration of NaCl was determined as the concentration at which the bubble percentage coalescence reduced by 95% from 100% in pure water to a constant value in a relatively high concentration salt solution. The transition concentrations obtained (called *TC95*) were compared versus the bubble radius of each experimental technique which resulted in a linear relationship between *TC95* and the reciprocal of the square root of the bubble radius. This relationship indicates the pronounced effect of bubble size on bubble coalescence despite different experimental techniques, bubble approach speeds and salt purities.

The theoretical models for predicting the transition concentration of salts were also reviewed. The significant difference between the model predictions and experimental transition concentrations for salts highlights the demand for modification of the available models.

ACKNOWLEDGEMENT

This research is supported under Australian Research Council's DP Projects funding scheme (project number DP140101089).

REFERENCES

Alves, S.S., Maia, C.I., Vasconcelos, J.M.T., Serralheiro, A.J., Bubble size in aerated stirred tanks. Chemical Engineering Journal, 2002, **89(1–3)**, 109-117.

Barnocky, G., Davis, R.H., The lubrication force between spherical drops, bubbles and rigid particles in a viscous fluid. International Journal of Multiphase Flow, 1989, **15(4)**, 627-638.

Brown, E.C., Mucha, M., Jungwirth, P., Tobias, D.J., Structure and Vibrational Spectroscopy of Salt Water/Air Interfaces: Predictions from Classical Molecular Dynamics Simulations. The Journal of Physical Chemistry B, 2005, **109(16)**, 7934-7940.

Cain, F.W., Lee, J.C., A technique for studying the drainage and rupture of unstable liquid films formed between two captive bubbles: Measurements on KCl solutions. Journal of Colloid and Interface Science, 1985, **106(1)**, 70-85.

Castro, S., Toledo, P., Laskowski, J.S., 2012. Foaming properties of flotation frothers at high electrolyte concentrations, pp. 51-60.

Chan, B.S., Tsang, Y.H., A theory on bubble-size dependence of the critical electrolyte concentration for inhibition of coalescence. Journal of Colloid and Interface Science, 2005, **286(1)**, 410-413.

Chesters, A.K., Hofman, G., Bubble coalescence in pure liquids. Appl. Sci. Res., 1982, **38**, 353-361.

Cho, Y.S., Laskowski, J.S., Bubble coalescence and its effect on dynamic foam stability. The Canadian Journal of Chemical Engineering, 2002, **80(2)**, 299-305.

Christenson, H.K., Bowen, R.E., Carlton, J.A., Denne, J.R.M., Lu, Y., Electrolytes that Show a Transition to Bubble Coalescence Inhibition at High Concentrations. The Journal of Physical Chemistry C, 2007, **112(3)**, 794-796.

Collins, K.D., Charge density-dependent strength of hydration and biological structure. Biophysical Journal, 1997, **72(1)**, 65-76.

Collins, K.D., Ions from the Hofmeister series and osmolytes: effects on proteins in solution and in the crystallization process. Methods, 2004, **34(3)**, 300-311.

Craig, V.S.J., Bubble coalescence and specific-ion effects. Current Opinion in Colloid and Interface Science, 2004, **9(1-2)**, 178-184.

Craig, V.S.J., Ninham, B.W., Pashley, R.M., Effect of electrolytes on bubble coalescence. Nature, 1993a, **364(6435)**, 317-319.

Craig, V.S.J., Ninham, B.W., Pashley, R.M., The effect of electrolytes on bubble coalescence in water. The Journal of Physical Chemistry, 1993b, **97(39)**, 10192-10197.

Craig, V.S.J., Ninham, B.W., Pashley, R.M., Study of the long-range hydrophobic attraction in concentrated salt solutions and its implications for electrostatic models. Langmuir, 1998, **14(12)**, 3326-3332.

Craig, V.S.J., Ninham, B.W., Pashley, R.M., Direct Measurement of Hydrophobic Forces: A Study of Dissolved Gas, Approach Rate, and Neutron Irradiation. Langmuir, 1999, **15(4)**, 1562-1569.

Cramer, S.D., The Solubility of Oxygen in Brines from 0 to 300 °C. Industrial & Engineering Chemistry Process Design and Development, 1980, **19(2)**, 300-305.

Creux, P., Lachaise, J., Graciaa, A., Beattie, J.K., Specific Cation Effects at the Hydroxide-Charged Air/Water Interface. The Journal of Physical Chemistry C, 2007, **111(9)**, 3753-3755.

Del Castillo, L.A., Ohnishi, S., Horn, R.G., Inhibition of bubble coalescence: Effects of salt concentration and speed of approach. Journal of Colloid and Interface Science, 2011, **356(1)**, 316-324.

Derjaguin, B.V., Prokhorov, A.V., On the theory of the rupture of black films. Journal of Colloid and Interface Science, 1981, **81(1)**, 108-115.

Derjaguin, B.V., Titijevskaia, A.S., Abricossova, I.I., Malkina, A.D., Investigations of the forces of interaction of surfaces in different media and their application to the problem of colloid stability. Discussions of the Faraday Society, 1954**(18)**, 24-41.

Drelich, J., Long, J., Yeung, A., Determining Surface Potential of the Bitumen-Water Interface at Nanoscale Resolution using Atomic Force Microscopy. The Canadian Journal of Chemical Engineering, 2007, **85(5)**, 625-634.

Exerowa, D., Zacharieva, M., Cohen, R., Platikanov, D., Dependence of the equilibrium thickness and double layer potential of foam films on the surfactant concentration. Colloid & Polymer Sci, 1979, **257(10)**, 1089-1098.

Firouzi, M., Nguyen, A.V., Novel Methodology for Predicting the Critical Salt Concentration of Bubble Coalescence Inhibition. The Journal of Physical Chemistry C, 2013, **118(2)**, 1021-1026.

Firouzi, M., Nguyen, A.V., Effects of monovalent anions and cations on drainage and lifetime of foam films at different interface approach speeds Advanced Powder Technology, 2014a, **Accepted**.

Firouzi, M., Nguyen, A.V., On the effect of van der Waals attractions on the critical salt concentration for inhibiting bubble coalescence. Minerals Engineering, 2014b, **58(0)**, 108-112.

Foulk, C.W., Theory of liquid film formation. Ind. Eng. Chem., 1929, **21**, 815-817.

Foulk, C.W., Hansley, V.L., Solid matter in boiler-water foaming. I. Experiments at atmospheric pressure. Ind. Eng. Chem., 1932, **24**, 277-281.

Foulk, C.W., Miller, J.N., Experimental evidence in support of the balancedlayer theory of liquid film formation. Ind. Eng. Chem., 1931, **23**, 1283-1288.

Geffcken, G., Comparative solubility of gases, etc., in water and in aqueous solutions. Zeit. Physical. Chem., 1904, **49**, 257-302.

Ghosh, P., Coalescence of Air Bubbles at Air–Water Interface. Chemical Engineering Research and Design, 2004, **82(7)**, 849-854.

Henry, C.L., Craig, V.S.J., Ion-Specific Influence of Electrolytes on Bubble Coalescence in Nonaqueous Solvents. Langmuir, 2008, **24(15)**, 7979-7985.

Henry, C.L., Dalton, C.N., Scruton, L., Craig, V.S.J., Ion-Specific Coalescence of Bubbles in Mixed Electrolyte Solutions. The Journal of Physical Chemistry C, 2006, **111(2)**, 1015-1023.

Henry, C.L., Karakashev, S.I., Nguyen, P.T., Nguyen, A.V., Craig, V.S.J., Ion Specific Electrolyte Effects on Thin Film Drainage in Nonaqueous Solvents Propylene Carbonate and Formamide. Langmuir, 2009, **25(17)**, 9931-9937.

Henry, C.L., Parkinson, L., Ralston, J.R., Craig, V.S.J., A Mobile Gas−Water Interface in Electrolyte Solutions. The Journal of Physical Chemistry C, 2008, **112(39)**, 15094-15097.

Horn, R.G., Del Castillo, L.A., Ohnishi, S., Coalescence map for bubbles in surfactant-free aqueous electrolyte solutions. Advances in Colloid and Interface Science, 2011, **168(1–2)**, 85-92.

Israelachvili, J., Wennerstrom, H., Role of hydration and water structure in biological and colloidal interactions. Nature, 1996, **379(6562)**, 219-225.

Israelachvili, J.N., *Intermolecular and Surface Forces*. 2005, Academic Press, London.

Jungwirth, P., Tobias, D.J., Molecular Structure of Salt Solutions: A New View of the Interface with Implications for Heterogeneous Atmospheric Chemistry. The Journal of Physical Chemistry B, 2001, **105(43)**, 10468-10472.

Jungwirth, P., Tobias, D.J., Ions at the Air/Water Interface. The Journal of Physical Chemistry B, 2002, **106(25)**, 6361-6373.

Jungwirth, P., Tobias, D.J., Specific Ion Effects at the Air/Water Interface. Chemical Reviews, 2005, **106(4)**, 1259-1281.

Karakashev, S.I., Manev, E.D., Correlation in the properties of aqueous single films and foam containing a nonionic surfactant and organic/inorganic electrolytes. Journal of Colloid and Interface Science, 2003, **259(1)**, 171-179.

Karakashev, S.I., Nguyen, P.T., Tsekov, R., Hampton, M.A., Nguyen, A.V., Anomalous ion effects on rupture and lifetime of aqueous foam films formed from monovalent salt solutions up to saturation concentration. Langmuir, 2008, **24(20)**, 11587-11591.

Kirkpatrick, R.D., Lockett, M.J., The influence of approach velocity on bubble coalescence. Chemical Engineering Science, 1974, **29(12)**, 2363-2373.

Klaseboer, E., Chevaillier, J.P., Gourdon, C., Masbernat, O., Film Drainage between Colliding Drops at Constant Approach Velocity: Experiments and Modeling. J. Colloid Interface Sci., 2000, **229(1)**, 274-285.

Kunz, W., 2009. Specific Ion Effects. World Scientific Publishing, p. 347.

Kunz, W., Specific ion effects in colloidal and biological systems. Current Opinion in Colloid & Interface Science, 2010, **15(1–2)**, 34-39.

Kunz, W., Lo Nostro, P., Ninham, B.W., The present state of affairs with Hofmeister effects. Current Opinion in Colloid & Interface Science, 2004, **9(1–2)**, 1-18.

Lessard, R.R., Zieminski, S.A., Bubble coalescence and gas transfer in aqueous electrolytic solutions. Ind. Eng. Chem. Fun., 1971, **10(2)**, 260-269.

Li, D., Liu, S., Coalescence between Small Bubbles or Drops in Pure Liquids. Langmuir, 1996, **12(21)**, 5216-5220.

Liu, D., Ma, G., Levering, L.M., Allen, H.C., Vibrational Spectroscopy of Aqueous Sodium Halide Solutions and Air−Liquid Interfaces: Observation of Increased Interfacial Depth. The Journal of Physical Chemistry B, 2004, **108(7)**, 2252-2260.

Machon, V., Pacek, A.W., Nienow, A.W., Bubble Sizes in Electrolyte and Alcohol Solutions in a Turbulent Stirred Vessel. Chemical Engineering Research and Design, 1997, **75(3)**, 339-348.

Manev, E., Study of thickness non-homogeneity and rate of thinning of free microscopic liquid films. God. Sofii. Univ, 1985, **75**, 174-183.

Manev, E.D., Nguyen, A.V., Critical thickness of microscopic thin liquid films. Advances in Colloid and Interface Science, 2005a, **114–115(0)**, 133-146.

Manev, E.D., Nguyen, A.V., Effects of surfactant adsorption and surface forces on thinning and rupture of foam liquid films. International Journal of Mineral Processing, 2005b, **77(1)**, 1-45.

Manev, E.D., Pugh, R.J., Diffuse layer electrostatic potential and stability of thin aqueous films containing a nonionic surfactant. Langmuir, 1991, **7(10)**, 2253-2260.

Marčelja, S., Short-range forces in surface and bubble interaction. Current Opinion in Colloid & Interface Science, 2004, **9(1–2)**, 165-167.

Marrucci, G., A theory of coalescence. Chemical Engineering Science, 1969, **24(6)**, 975-985.

Marrucci, G., Nicodemo, L., Coalescence of gas bubbles in aqueous solutions of inorganic electrolytes. Chem. Eng. Sci., 1967, **22(9)**, 1257-1265.

Millero, F.J., Huang, F., Laferiere, A.L., Solubility of oxygen in the major sea salts as a function of concentration and temperature. Marine Chemistry, 2002, **78(4)**, 217-230.

Mucha, M., Frigato, T., Levering, L.M., Allen, H.C., Tobias, D.J., Dang, L.X., Jungwirth, P., Unified Molecular Picture of the Surfaces of Aqueous Acid, Base, and Salt Solutions. The Journal of Physical Chemistry B, 2005, **109(16)**, 7617-7623.

Nguyen, A.V., Firouzi, M., 2012. Collision and attachment interactions of single air bubbles with flat surfaces in aqueous solutions, In *Drops and bubbles in contact with solid surfaces*, eds. Ferrari, M., Liggerie, L., Miller, R. CRC Press, Boca Raton, FL, U.S.A., pp. 211-240.

Nguyen, A.V., Schulze, H.J., *Colloidal science of flotation*. 2004, Marcel Dekker, New York.

Nguyen, P.T., Hampton, M.A., Nguyen, A.V., Birkett, G., The influence of gas velocity, salt type and concnetration on transition concentration for bubble coalescence inhibition and gas holdup. Chem. Eng. Res. Des., 2012, **90**, 33-39.

Nguyen, P.T., Nguyen, A.V., Drainage, rupture, and lifetime of deionized water films: Effect of dissolved gases. Langmuir, 2010, **26(5)**, 3356-3363.

Oolman, T.O., Blanch, H.W., BUBBLE COALESCENCE IN STAGNANT LIQUIDS. Chemical Engineering Communications, 1986, **43(4-6)**, 237-261.

Parkinson, L., Ralston, J., The Interaction between a Very Small Rising Bubble and a Hydrophilic Titania Surface. The Journal of Physical Chemistry C, 2010, **114(5)**, 2273-2281.

Prince, M.J., Blanch, H.W., Bubble coalescence and break-up in air-sparged bubble columns. AIChE Journal, 1990, **36(10)**, 1485-1499.

Pugh, R.J., Yoon, R.H., Hydrophobicity and Rupture of Thin Aqueous Films. Journal of Colloid and Interface Science, 1994, **163(1)**, 169-176.

Qu, X., Wang, L., Karakashev, S.I., Nguyen, A.V., Anomalous thickness variation of the foam films stabilized by weak non-ionic surfactants. Journal of Colloid and Interface Science, 2009, **337(2)**, 538-547.

Quinn, J.J., Maldonado, M., Gomez, C.O., Finch, J.A., Experimental study on the shape–velocity relationship of an ellipsoidal bubble in inorganic salt solutions. Minerals Engineering, 2014a, **55(0)**, 5-10.

Quinn, J.J., Sovechles, J.M., Finch, J.A., Waters, K.E., Critical coalescence concentration of inorganic salt solutions. Minerals Engineering, 2014b, **58(0)**, 1-6.

Rao, A.A., Wasan, D.T., Manev, E.D., FOAM STABILITY—EFFECT OF SURFACTANT COMPOSITION ON THE DRAINAGE OF MICROSCOPIC AQUEOUS FILMS. Chemical Engineering Communications, 1982, **15(1-4)**, 63-81.

Ribeiro Jr, C.P., Mewes, D., The effect of electrolytes on the critical velocity for bubble coalescence. Chemical Engineering Journal, 2007, **126(1)**, 23-33.

Sheludko, A., Thin liquid films. Advances in Colloid and Interface Science, 1967, **1(4)**, 391-464.

Sherwood, J.E., Stagnitti, F., Kokkinn, M.J., Williams, W.D., Dissolved oxygen concentrations in hypersaline waters. Limnol. Oceanogr., 1991, **36(2)**, 235-250.

Shoor, S.K., Walker, R.D., Gubbins, K.E., Salting out of nonpolar gases in aqueous potassium hydroxide solutions. The Journal of Physical Chemistry, 1969, **73(2)**, 312-317.

Stevens, H., Considine, R.F., Drummond, C.J., Hayes, R.A., Attard, P., Effects of Degassing on the Long-Range Attractive Force between Hydrophobic Surfaces in Water. Langmuir, 2005, **21(14)**, 6399-6405.

Stubenrauch, C., Klitzing, R.v., Disjoining pressure in thin liquid foam and emulsion films—new concepts and perspectives. Journal of Physics: Condensed Matter, 2003, **15(27)**, R1197–R1232.

Tsang, Y.H., Koh, Y.-H., Koch, D.L., Bubble-size dependence of the critical electrolyte concentration for inhibition of coalescence. Journal of Colloid and Interface Science, 2004, **275(1)**, 290-297.

Tsao, H.K., Koch, D.L., Collisions of slightly deformable, high Reynolds number bubbles with short-range repulsive forces. Physics of Fluids (1994-present), 1994, **6(8)**, 2591-2605.

Tse, K., Martin, T., McFarlane, C.M., Nienow, A.W., Visualisation of bubble coalescence in a coalescence cell, a stirred tank and a bubble column. Chemical Engineering Science, 1998, **53(23)**, 4031-4036.

Vinogradova, O.I., Bunkin, N.F., Churaev, N.V., Kiseleva, O.A., Lobeyev, A.V., Ninham, B.W., Submicrocavity Structure of Water between Hydrophobic and Hydrophilic Walls as Revealed by Optical Cavitation. Journal of Colloid and Interface Science, 1995, **173(2)**, 443-447.

Vrij, A., Possible mechanism for the spontaneous rupture of thin, free liquid films. Discussions of the Faraday Society, 1966, **42(0)**, 23-33.

Wang, L., Qu, X., Impact of interface approach velocity on bubble coalescence. Minerals Engineering, 2012, **26(0)**, 50-56.

Wang, L., Yoon, R.-H., Hydrophobic Forces in the Foam Films Stabilized by Sodium Dodecyl Sulfate: Effect of Electrolyte. Langmuir, 2004, **20(26)**, 11457-11464.

Weissenborn, P.K., Pugh, R.J., Surface tension of aqueous solutions of electrolytes: Relationship with ion hydration, oxygen solubility, and bubble coalescence. Journal of Colloid and Interface Science, 1996, **184(2)**, 550-563.

Wells, P.V., Thickness of stratified films. Annalen der Physik, 1921, **16**, 69-110.

Yaminsky, V.V., Ninham, B.W., Hydrophobic force: lateral enhancement of subcritical fluctuations. Langmuir, 1993, **9(12)**, 3618-3624.

Yaminsky, V.V., Ohnishi, S., Vogler, E.A., Horn, R.G., Stability of aqueous films between bubbles. Part 1. The effect of speed on bubble coalescence in purified water and simple electrolyte solutions. Langmuir, 2010, **26(11)**, 8061-8074.

Zahradník, J., Fialová, M., Linek, V., The effect of surface-active additives on bubble coalescence in aqueous media. Chemical Engineering Science, 1999, **54(21)**, 4757-4766.

Zieminski, S.A., Hume Iii, R.M., Durham, R., Rates of oxygen transfer from air bubbles to aqueous NaCl solutions at various temperatures. Marine Chemistry, 1976, **4(4)**, 333-346.

CHAPTER 3

EFFECTS OF MONOVALENT ANIONS AND CATIONS ON DRAINAGE AND LIFETIME OF FOAM FILMS AT DIFFERENT INTERFACE APPROACH SPEEDS

Mahshid Firouzi and Anh V. Nguyen

Published in “Advanced Powder Technology”, July 2014, 25, 1212-1219

3.1 ABSTRACT

Ions of inorganic salts are known to affect bubble coalescence via ion charge density and polarizability. In this paper, a systematic study of the effect of monovalent anions (F^-, Cl^-, Br^- and I^-) and cations (Li^+, Na^+ and K^+) on the lifetime of liquid films between two bubble surfaces is carried out by applying the thin film micro-interferometric method. To mimic realistic conditions of bubble coalescence in a bubble column, drainage and stability of saline water films driven by different interface approach speeds (10-300 μm/s) using a nano-pump were investigated. The results show significant effects of the interface approach speed on the transient film thickness, radius, film stability and lifetime of saline water films. The experiments also indicate that there is a critical approach speed of 35 μm/s for pure deionized water above which water films instantly coalesce, i.e., no water film can be obtained. High interface approach speeds create corrugation on saline water film surfaces, which rapidly increases the rates of film radial expansion and drainage, and shortens the film lifetime. There is a critical salt concentration above which the saline water film lifetime abruptly increases. This critical concentration is independent of the interface approach speed in the range of 10-300 μm/s. Our experimental results show a decreasing trend of film lifetime with increasing the size of either the cation or anion (NaF>LiCl>NaCl>KCl>NaBr>NaI). The order of the critical salt concentrations is the opposite of the order of lifetimes. The experimental results highlight the ion-specific effect of salt ions on the water structure and hence the behaviour of saline liquid films. These results are relevant to a number of chemical engineering processes taking place in salt solutions, including mineral separation by flotation using air bubbles in saline water.

Keywords: saline water, liquid film, bubble coalescence, ion-specificity, critical concentration, colloidal forces

3.2 INTRODUCTION

The stability of bubbles and foams is important in many scientific and technological fields, such as surface and colloid chemistry, biology, biochemistry, tertiary oil recovery, foam fractionation and mineral flotation. Salts and surfactants are known to affect bubble coalescence and foam stability. The case of surfactant-laden films is relatively well understood (Craig, 2004; Craig et al., 1993a). The effect of salts on liquid film drainage and rupture has been studied experimentally. However, the

majority of the experiments on bubble coalescence were conducted using bubble columns (Craig et al., 1993a; Henry et al., 2006; Liu et al., 2009; Marrucci and Nicodemo, 1967; Nguyen et al., 2012b).

Bubble size and rise velocity, salt type and concentration can affect the stability of liquid films and hence bubble coalescence and foam stability. There are few papers devoted to the effect of approach velocity between bubbles (interface approach speed), compared to other effective factors, such as surfactant and salt types and concentrations (Nguyen et al., 2012 ; Yaminsky et al., 2010). It is reported in the literature that there is little experimental information on the behaviour of single (foam) films between two bubbles in the presence of different salts at different interface approach speeds (Karakashev et al., 2008; Ozdemir et al., 2011). Moreover, the focus of the majority of the available literature is on either the concentration or type of salts at (unquantified and unknown) interface approach speeds (Christenson et al., 2007; Karakashev et al., 2008; Lessard and Zieminski, 1971a), or on the air-solution interface approach speeds but with a single salt (mainly NaCl) (Del Castillo et al., 2011; Wang and Qu, 2012; Yaminsky et al., 2010). Therefore, this paper aims to fill this gap to develop a better understanding of the combined effect of salt type, concentration and interface approach speed on the stability of saline liquid films. In particular, this study provides further microscopic evidence of the important role displayed by halide anions and alkali cations during interactions between two air-saline water interfaces at very small separation distances. The remainder of this paper is arranged as follows. The next section outlines the experimental method applied in this work. It is followed by a discussion of the findings. The discussion highlights the significant effect of the interface approach speed, salt concentration and ion types on the lifetime and drainage of saline liquid films between two air-saline water interfaces. Finally, the conclusion part summarises the main findings presented in this work.

3.3 EXPERIMENTAL METHOD AND MATERIAL

Light micro-interferometry with the experimental setup shown in Figure 3.1 was used to investigate the drainage and lifetime of aqueous (foam) films between two air-water interfaces (two bubbles). It involves the determination of film thickness from the change in intensity because of the phase lag of light reflected from the film interfaces illuminated by a white light. As a result of the interference of the light reflected from the interfaces, a set of fringes with different colours (the Newton rings) was observed and recorded using the ImageJ software. The interferograms were analysed using the available theory (Nguyen and Schulze, 2004) and MATLAB code developed in our laboratory. The setup consists of (1) a film holder with an inner diameter of 4 mm for producing

the foam film, (2) a glass (Scheludko-Exerowa) cell to enclose the film holder, the aqueous solution and the gas phase, (3) a motorized nano-pump for controlling the liquid suction rate, (4) a light source, (5) an inverted metallurgical microscope (Nikon, Japan) for illuminating and observing the film as well as the interference fringes in the reflected light, (6) a CCD video camera (Canon PSA640) for registering the transient interferometric images and (7) a computer for recording the transient interferometric images for further off-line processing and analysis. The film holder remained at a fixed position in the field of view of a reflection video microscope. The nano-pump was used to control the interface approach speeds between 10 and 300 μm/s.

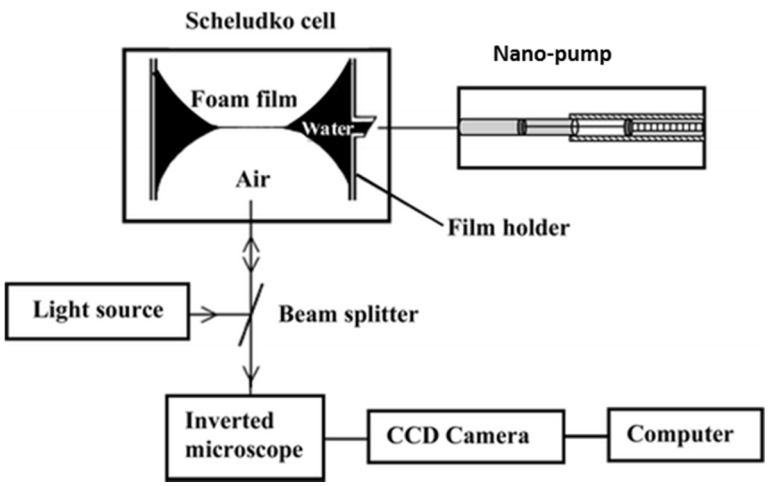

Figure 3.1. Schematic of experimental micro-interferometric setup (Karakashev et al., 2008)

All the glassware and tubes were thoroughly cleaned in a laminar flow cabinet by soaking in alkaline cleaning solution prepared from potassium hydroxide, water and ethanol (12.5:16:80 mass ratio), and vigorously rinsed many times with pure deionized (DI) water purified using an Ultrapure Academic Milli-Q system (Millipore, USA). The glassware and tubes were then soaked in a dilute hydrochloric acid solution and flushed thoroughly with DI water. This cleaning method ensured all the equipment was free from contamination. All the salts were purchased from Sigma-Aldrich (Australia) with purity higher than 99.5% and further purified by either roasting at 500 ^{o}C for 4 hours or foam fractionation by bubbling the solutions with nitrogen for 2-3 minutes. Initially, the film holder was flushed with the salt solutions before each experiment. A double-concave droplet of the salt solution of interest was created inside the film holder and a small amount was kept in the cell to saturate the environment inside the glass cell. The setup was left for about one hour to reach thermal equilibrium so as to avoid film thinning due to evaporation. Film drainage was obtained by utilizing

the nano-pump. To mimic realistic conditions of bubble coalescence in a bubble column, the liquid within the film holder was continuously pumped out until the film ruptured. The suction rate was changed over a wide range (100-4000 nL/s) in order to see the dynamic effect of interface approach speed on the film drainage. For comparison, drainage experiments at a zero air-liquid interface approach speed were also conducted by stopping the pump when the first film was observed. Each experiment for a particular salt type and concentration at a particular suction rate was repeated at least 20 times to obtain statistically reliable data. The film lifetime was measured from the instant of film formation (the first interferogram) until film disappearance by rupture. All the experiments were conducted at a constant room temperature (22 °C).

The suction rate was converted to interface approach speed by dividing the rate by the cross-section area of the film holder. This interface approach speed is approximately equal to the approach speed of the film surfaces at the beginning of film drainage when effects of colloidal forces and micro-hydrodynamics on film drainage are weak.

3.4 RESULTS AND DISCUSSION

3.4.1 FILM DRAINAGE DRIVEN BY INTERFACE APPROACH SPEED

It was observed that owing to the applied external driving force by the pump suction, the liquid films rapidly expanded during drainage until reaching a critical thickness at which the film rupture occurred. Depending on the applied interface approach speed, the film lifetime, expansion rate and critical thickness could differ significantly. Figure 3.2 shows the significant effect of the applied interface approach speed on the evolution of saline water films. In the case of the non-zero interface approach speed, the liquid film expanded very rapidly because of the continuous work of the nano-pump. In contrast, in the case of the zero interface approach speed, the radius of the film did not change significantly. Figure 3.3 shows the transient film thickness and radius obtained for the saline water films in Figure 3.2. (Details of calculation of film thickness and radius are available in Appendix).

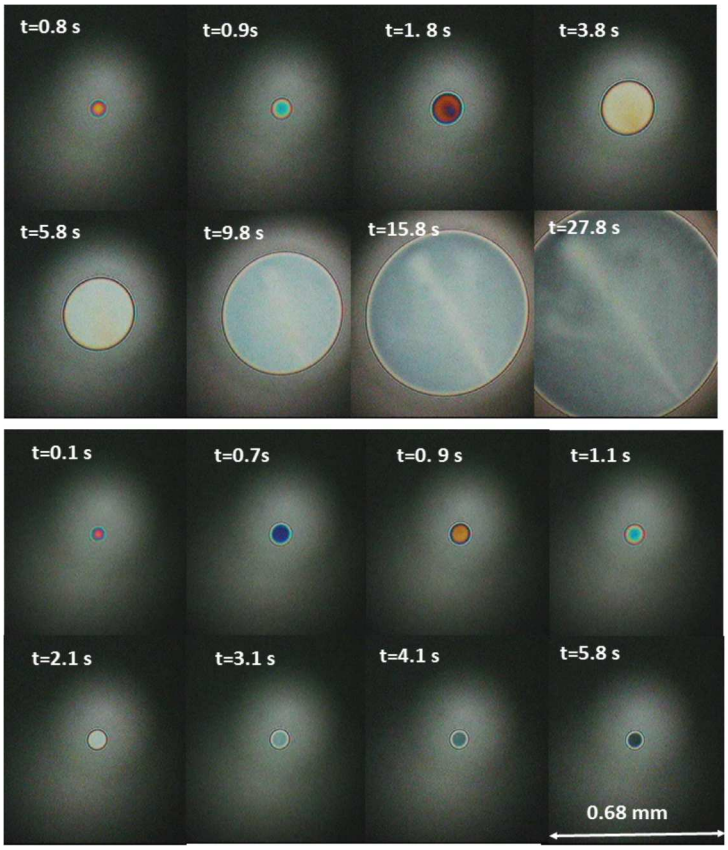

Figure 3.2**.** Evolution of 2 M NaCl foam films at an interface approach speed of 10 µm/s (top) and zero approach speed (bottom).

According to the classical theory of Stefan-Reynolds (Nguyen, 2000) and the other improved drainage models (Radoëv et al., 1974; Ruckenstein and Sharma, 1987; Tsekov, 1998), the drainage rate is inversely proportional to the film radius. Therefore, increasing the film radius would decrease the film drainage rate which supports our experimental results shown in Figure 3.3. Liquid films driven by an external pressure of the pump suction could last considerably longer than the films drained under the condition of no externally applied pressure (at the zero interface approach speed).

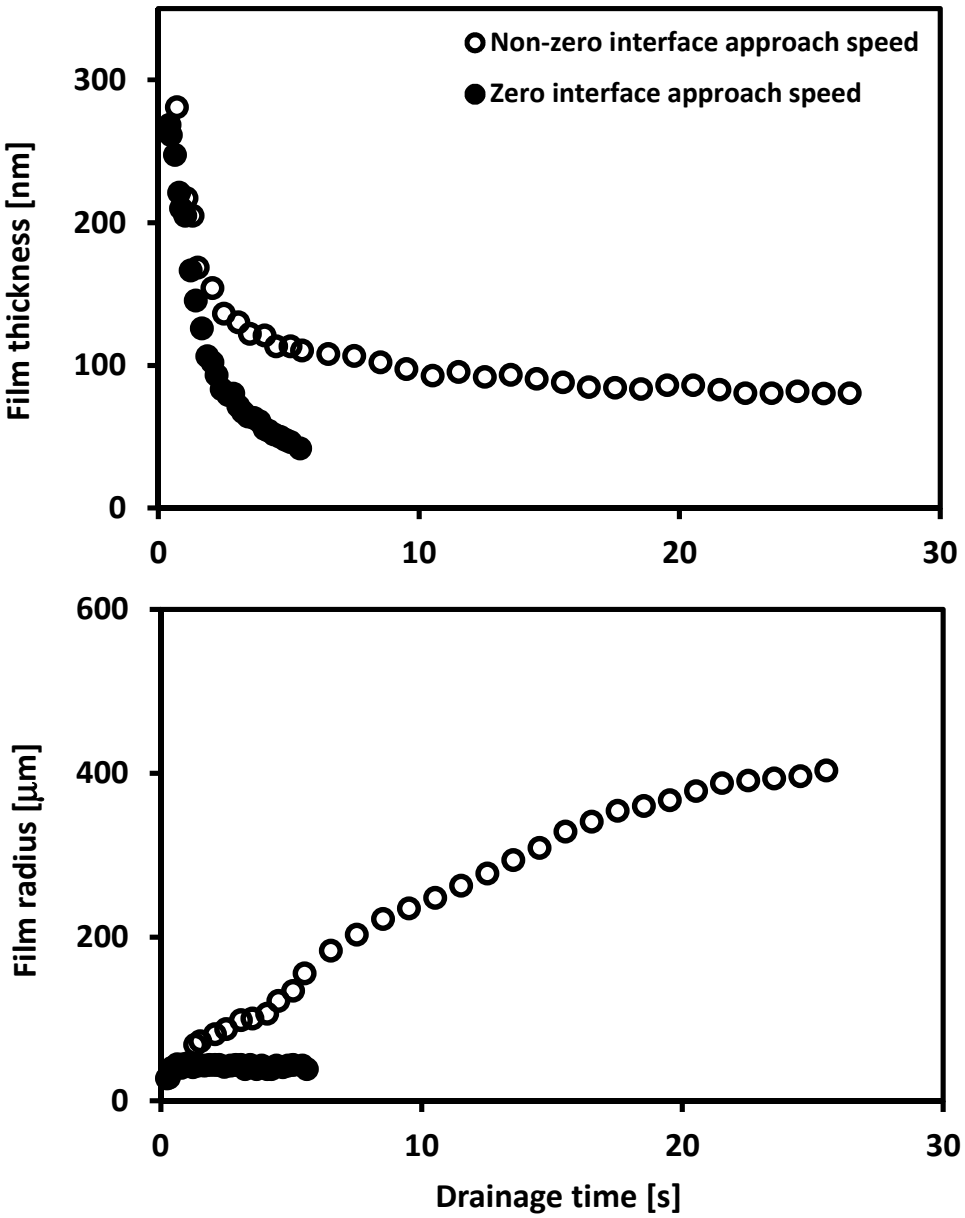

Figure 3.3**.** Significant differences in transient thickness and radius of 2 M NaCl films obtained at the interface approach speed of u = 10 µm/s and zero interface approach speed.

3.4.2 EFFECT OF DIFFERENT AIR-LIQUID INTERFACE APPROACH SPEEDS

Film instability and bubble coalescence are quantified by two parameters: film drainage time and film rupture time, which can be influenced by surface mobility and surface hydrodynamic

inhomogeneity (corrugation). In the case of highly mobile film surfaces the water velocity profile is uniform (plug flow) inside the film, unlike immobile surfaces with the velocity profile having a parabolic shape (Poiseuille flow). The latter case is associated with large hydrodynamic resistance which decreases the drainage rate and large surface corrugation which causes the film rupture at large thickness (Yaminsky et al., 2010). Figure 3.4 shows the effect of interface approach speed on film surface topology in 0.15 M NaCl solutions at two speeds: 100 and 10 µm/s. When bubbles approach at the higher speed, the film surface area and diameter increase faster than when approaching at a slow speed. As shown in Figure 3.4, the film expanded up to a radius of 0.287 mm in just 1.8 s at the high interface approach speed (100 µm/s), while it took 15.4 s to expand up to almost that radius at the slow approach speed (10 µm/s). It is shown for surfactant-laden films that at relatively high approach speeds, the hydrodynamic pressure can be sufficiently large to cause the film surfaces to be dimpled with film thickness being thinner at the barrier rim than at the film centre. As a result, the rim (barrier) impedes the flow from the centre and causes an inward flow towards the dimple which accelerates thinning the film thickness at the rim (Frankel and Myseis, 1962; Klaseboer et al., 2000a). This behaviour of the surfactant-stabilised films is also applied to saline water films shown in Figure 3.4, where many small hydrodynamic domains can be seen at a high approach speed. The foam film at the high interface approach speed (100 µm/s) ruptured at about 5.5 s which was significantly shorter than the rupture time of the case of the slow interface approach speed (15.5 s).

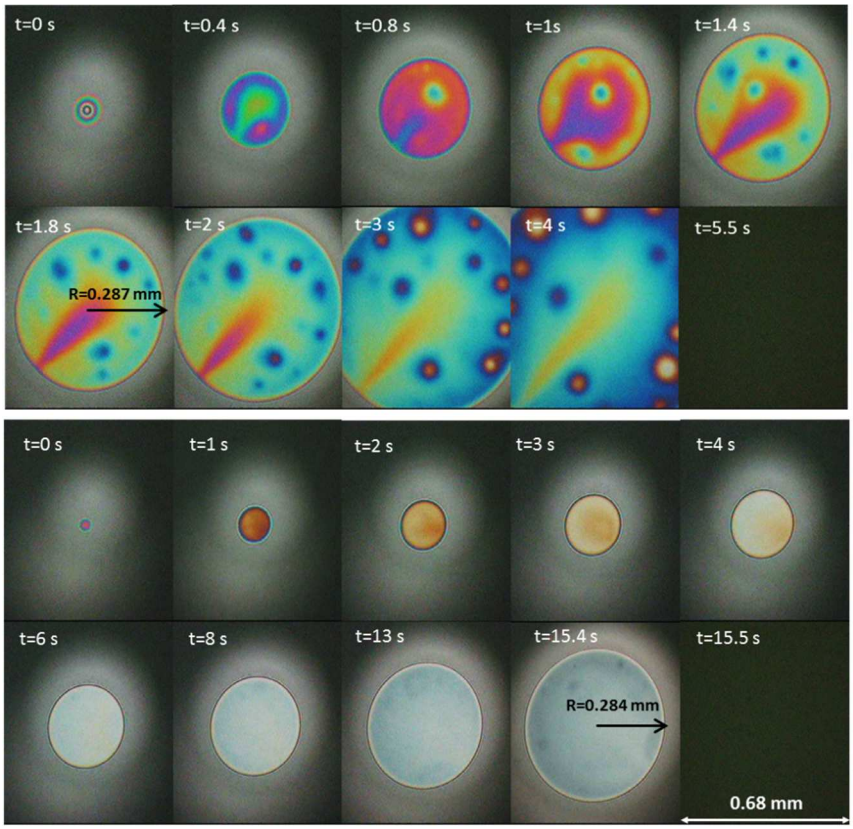

Figure 3.4**.** Effect of air-liquid interface approach speed on the film surface morphology for 0.15M NaCl at 100 µm/s (top) and 10 µm/s (bottom).

Figure 3.5 shows the effect of interface approach speed on the surface morphology of the films of similar size taken at 1.8 s and 15.4 s from Figure 3.4. Fast interface approach causes surface inhomogeneity due to the hydrodynamic effect, which can lead to dimple formation. Unlike the non-uniform surface film observed at the high interface approach speed, the film is relatively uniform and planar when the air-liquid interfaces approach at the slow speed (10 µm/s).

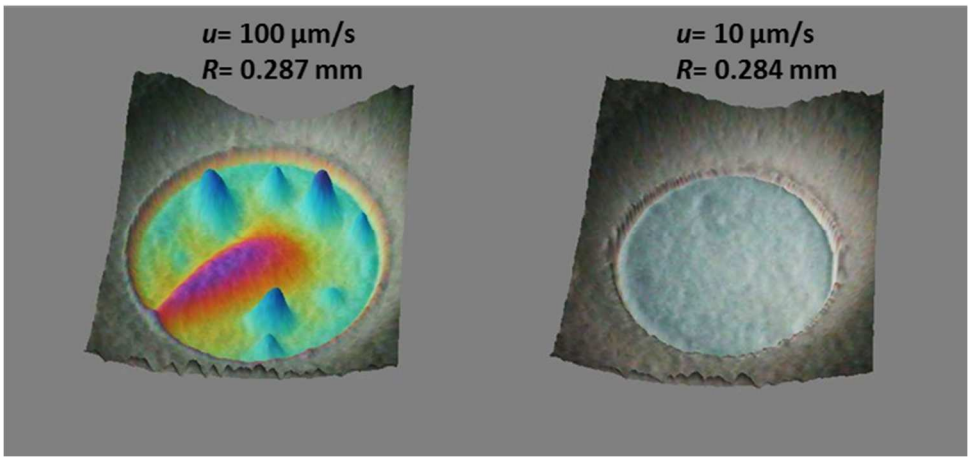

Figure 3.5**.** Effect of the air-liquid interface approach speed on the surface morphology of 0.15 M NaCl films at u = 100 and 10 µm/s.

Figure 3.6 illustrates the effect of the interface approach speed on the lifetime of foam films of DI water. The results in this figure indicate that there is a critical approach speed of ~ 35 µm/s above which foam films rupture instantly. For speeds smaller than this critical value, films can form and last for a few seconds. Yaminsky et al. (2010) estimated this critical velocity by equating the predicted critical separations at which surfaces of a liquid film become mobile and flat, which gives

$$u_c = \left(\frac{4}{3}\right)^3 \frac{\Delta\sigma^2}{\eta\sigma} \tag{3.1}$$

where σ is the surface tension, $\Delta\sigma$ is the required surface tension difference to fully immobilize the film interfaces and η is the solution viscosity. Considering $\Delta\sigma = 0.07$ mN/m as the required surface tension difference to fully immobilize the interfaces, σ = 72 mN/m and η = 1 mPa.s for pure water the authors estimated a critical approach speed of 160 µm/s . As discussed by Yaminsky et al. (2010), the local variations in the structure of the electrical double layer because of the presence of hydroxyl and hydronium ions of water can generate a surface tension gradient through an electrokinetic phenomenon. This very small surface tension difference can change the surface mobility of the air-liquid interfaces. The predicted critical speed of 160 µm/s by Yaminsky et al. (2010) is larger by a factor of 4 compared to our critical value of 35 µm/s. Yaminsky et al. noted that they likely

overestimated the value of $\Delta\sigma$ by ignoring the effect of bubble deformation and partial mobility. Substituting our critical speed for DI water films (35 μm/s) into Eq. (3.1) results in $\Delta\sigma = 0.033$ mN/m. This value is in agreement with the reported value of $\Delta\sigma \approx 0.03$ mN/m by Lin and Slattery (1982) who accounted for the surface deformation of a rising bubble towards a solid surface by the hydrodynamic pressure. We noted that a trace amount of impurities from an old N_2 gas used in drying the glassware can change this critical speed to values higher than 100 μm/s and the liquid films can be stable for minutes.

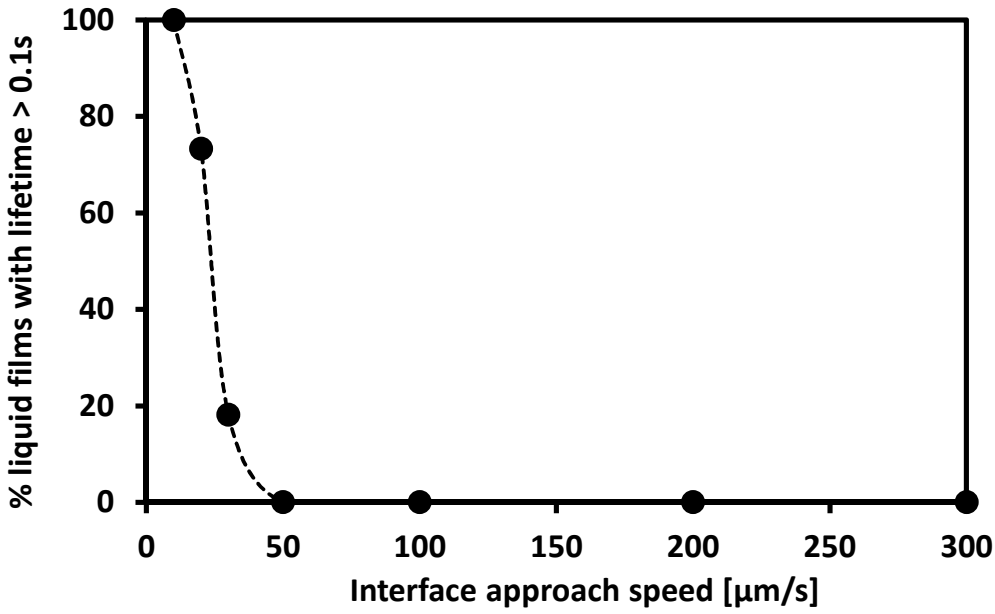

Figure 3.6**.** Effect of air-liquid interfacial approach speed on the lifetime of foam films of pure water.

3.4.3 EFFECT OF MONOVALENT IONS ON BUBBLE COALESCENCE

Figure 3.7 shows the effect of monovalent ions on the lifetime of DI water and saline water films of low (0.01 M) and high (1 M) salt concentrations. Sodium fluoride is not included in Figure 3.7 (1 M) because its saturation concentration is around 1 M and the interferograms were not visible for quantification. The results show that at very small concentrations, sodium halide films have a shorter lifetime than the lifetime of DI water films and therefore do not inhibit bubble coalescence at low concentrations. However, at high concentrations (> 0.01 M), saline liquid films can last significantly longer than DI water films.

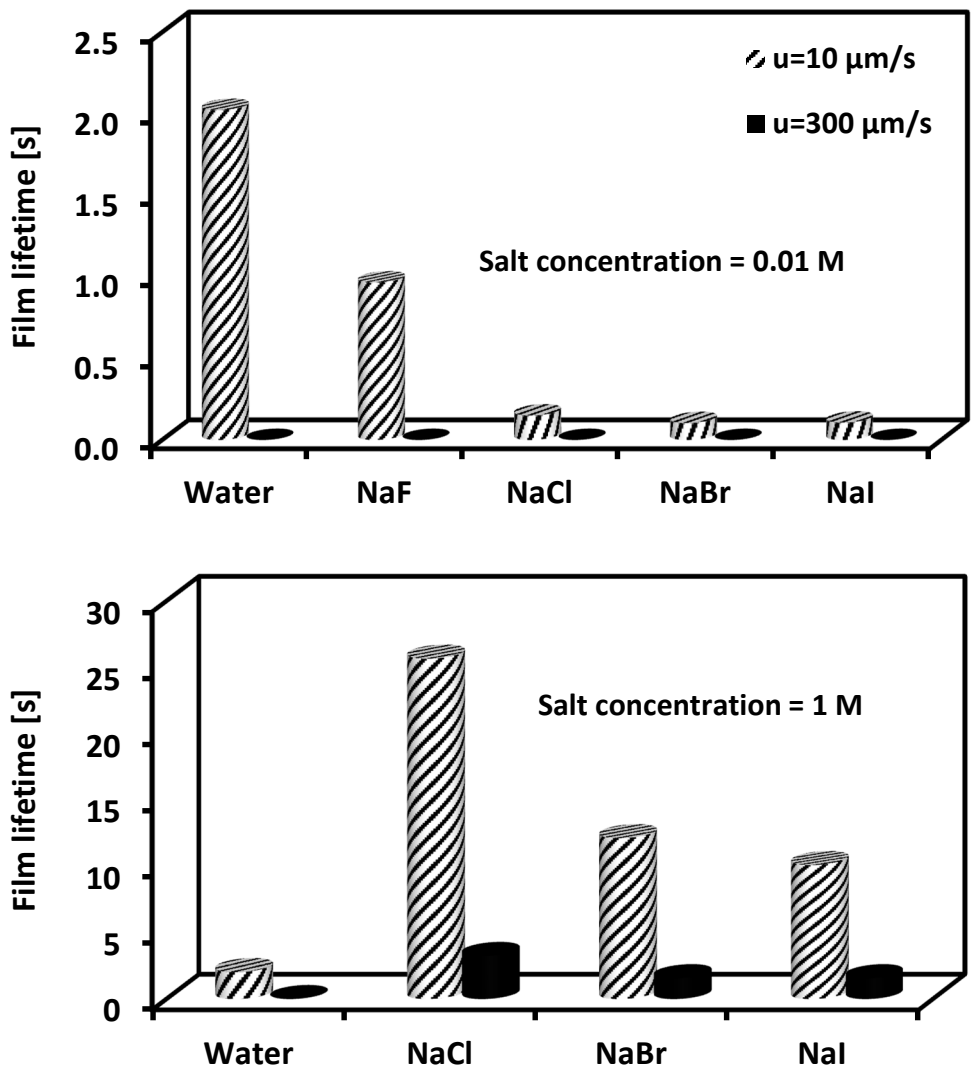

Figure 3.7.Comparison of lifetimes of DI water films and halid salt films at (0.01 M) and high (1 M) salt concentrations.

Figure 3.8 compares the effect of halide anions and alkali cations on the lifetime of saline water film (bubble coalescence) at two interface approach speeds of 20 and 100 µm/s. The results indicate that for each salt there is a critical concentration beyond which the film lifetime abruptly increases and the liquid film can last for 2-50 seconds depending on the salt type, concentration and approach speed of air-liquid interfaces. This critical concentration is also referred to as the “transition concentration” since bubbles (liquid films) in saline solutions undergo a transition from coalescence (instant rupture) to non-coalescence (stable film). This transition is attributed to a change in the

hydrodynamic boundary condition of the bubble-solution interface from mobile to immobile (Firouzi and Nguyen, 2013; Marrucci, 1969; Prince and Blanch, 1990).

The insets in Figure 3.8 represent film lifetime versus salt concentration in the logarithmic scale. In the case of slower approach of bubbles, u = 10 µm/s (Figure 3.7) and 20 µm/s (Figure 3.8), the results show a decrease in the film lifetime of DI water (equivalent to the salt solution of 4 µM because of the presence of CO_2 dissolved from the atmosphere as well as hydronium and hydroxyl ions) with increasing salt concentration up to the critical concentrations. Further increasing salt concentration results in an abrupt increase in the lifetime of saline water films. In contrast, when the film interfaces (bubbles) approach each other at the speed of 100 µm/s, which is above the critical approach speed of DI water (35 µm/s), bubbles coalesce instantly in pure DI water. The results also indicate that further increase of salt concentration up to the critical concentration does not stabilize the saline water films relative to the pure DI water films, owing to high drainage rate and screening of the electrical double-layer (EDL) repulsion. As in the case of the slow approach of bubbles, increasing the salts concentration above the critical concentration enhances the stability of liquid films, as a result of the stabilizing effect of opposing forces such as the tangential stress owing to the Gibbs-Marangoni effect.

Film lifetime of the investigated salts follows the following order: NaF> LiCl> NaCl > KCl> NaBr> NaI. These results reveal that the cation-specific and anion-specific effects are equally important, as opposed to the general principle that the anion-specific effect is more pronounced than the cation effect. Although anions have strong interactions with water molecules compared to cations, ion-water interactions are strongly affected by the counter-ions in their vicinity.

Figure 3.9 shows the effect of interface approach speed on the critical salt concentration. The critical concentrations are similar for LiCl, KCl and NaI. A slight increase in the critical concentration with increasing approach speed was observed for NaF, NaCl and NaBr. This slight increase is within the experimental error (± 0.01 M), since we cannot observe a consistent trend for all the salts of interest. Therefore, the critical concentration of salts can be considered independent of the approach speed of bubbles at the investigated range of low approach speeds (10-300 µm/s).

So far, a number of mechanisms have been proposed concerning the inhibiting effect of salts and are described in the following sections.

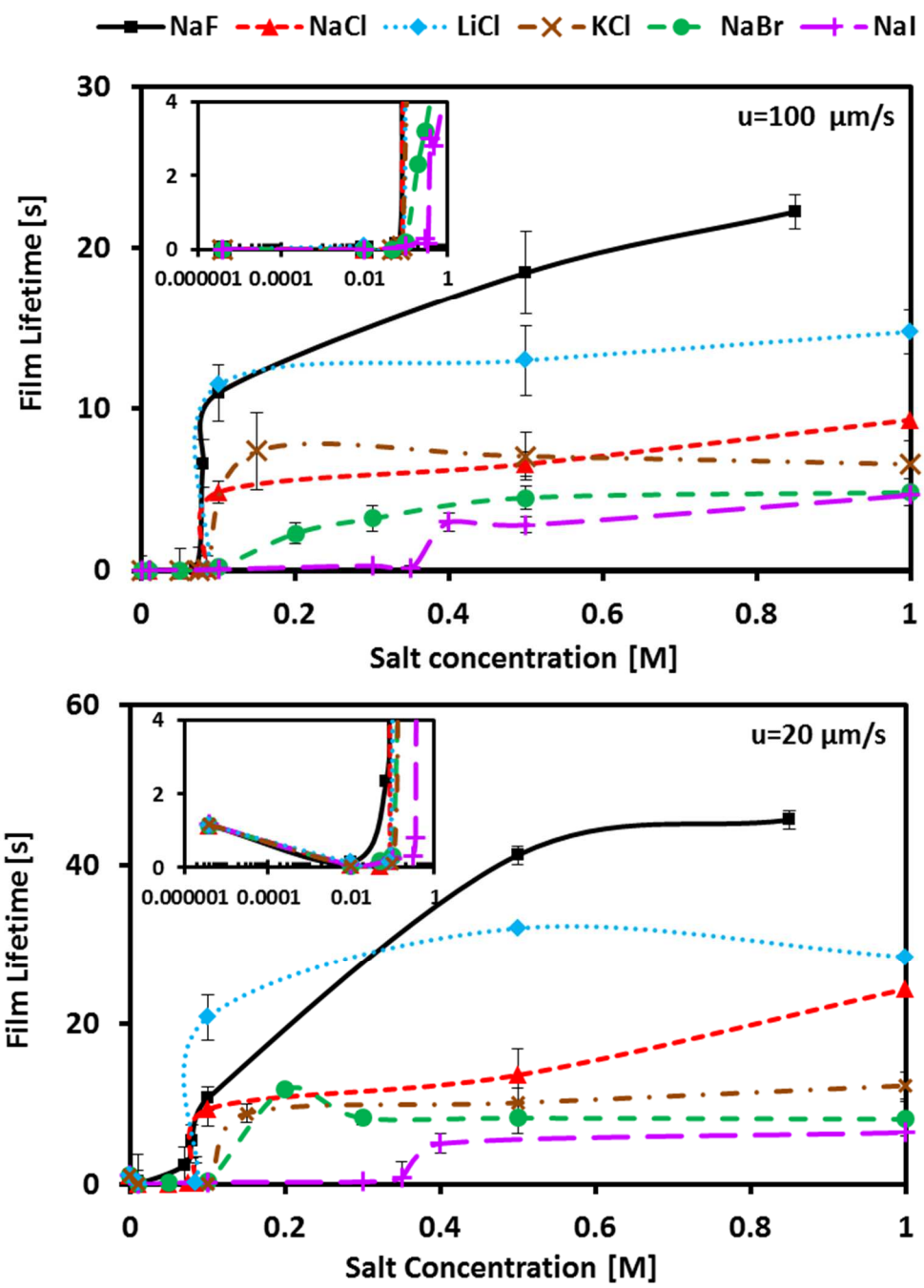

Figure 3.8**.** Effect of monovalent halide anions and alkali cations on the film lifetime at u = 100 and 20 µm/s.

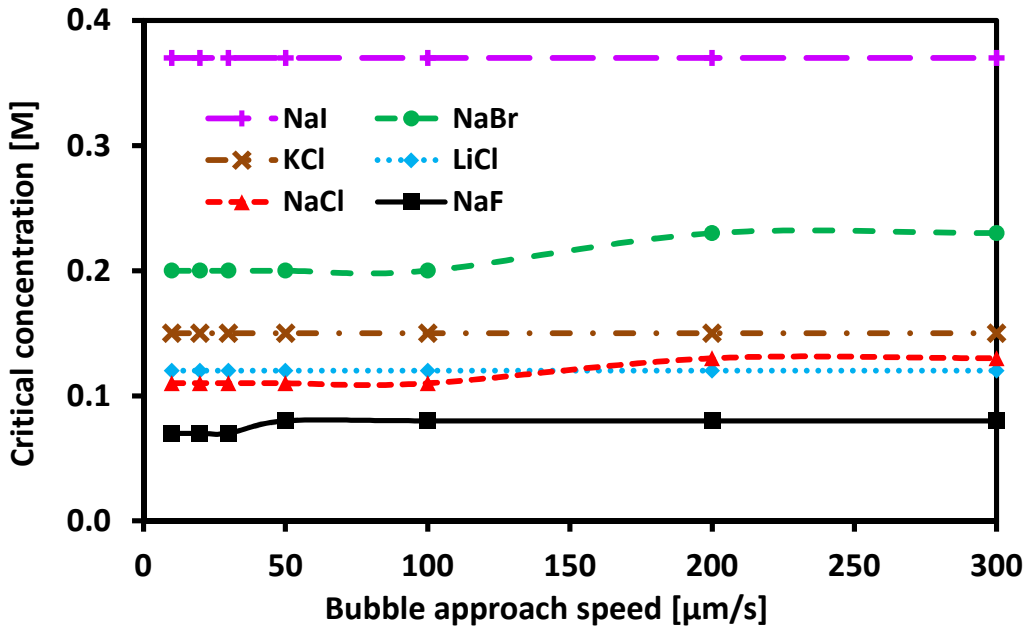

Figure 3.9**.** Effect of bubble approach velocity on the critical concentration of salts

3.4.3.1 EFFECT OF COLLOIDAL FORCES

Surface forces can affect bubble coalescence significantly, as exemplified by the film drainage rate, *V*, predicted by the classical Stefan-Reynolds theory (Nguyen, 2000) as follows: $V = -dh/dt = -\frac{2h^3}{3\eta R_f^{\,2}}\left(\frac{2\sigma}{R_c} - \Pi\right)$, where *h* is the film thickness, η is the viscosity, σ is the surface tension, R_f and R_c are the radii of the film and film holder (bubble), respectively, and Π is the (disjoining) pressure of surface forces. These forces consist of DLVO and non-DLVO components. The DLVO interactions include van der Waals attractions and electrostatic double layer (EDL) interactions which are repulsive in the case of air-water interfaces. Van der Waals attractions are very weak and the Hamaker constant in the van der Waals force is not significantly influenced by properties of salt ions. Since the air-water interface is negatively charged (-63 ±2 mV) (Creux et al., 2007), the approach of two negatively charged bubbles results in a sufficiently large repulsive EDL force (as shown by solid blue line in Figure 3.10[1]) which outweighs the van der Waals attractive forces and keeps the air-water interfaces separated. At high salt concentrations EDL forces normally become

[1] The Hamaker constant in the van der Waals force was calculated based on the approximate formula for the Hamaker constant at each separation (Nguyen and Schulze, 2004). Surface potentials of air- liquid interface was calculated as explained in section 5.4.

vanishingly small (dashed blue line in Figure 3.10) and therefore they cannot explain the inhibiting effect of salts (Nguyen et al., 2012b; Yaminsky et al., 2010). At this stage the DLVO theory fails to consistently explain the behavior of saline water films. The effect of the ion type is explicitly excluded in this theory and it cannot explain the ion-specific effect on bubble coalescence (Craig, 2004). Therefore, a consistent mechanism is required.

Non-DLVO forces include the (repulsive) hydration force (between hydrophilic surfaces) and the (attractive) hydrophobic force (between hydrophobic surfaces). The hydration force arising from the strongly bound and oriented layers of water molecules is short-ranged. This force may prevent two surfaces or macromolecules from approaching closer than 0.5-0.6 nm (the size of two water molecules) (Israelachvili and Wennerstrom, 1996), but cannot stabilize saline water films thicker than 40 nm (Nguyen et al., 2012b). Hydrophobic attractions are known to be 10-100 times stronger than van der Waals attractions (Craig et al., 1993a; Henry et al., 2006). Such strong interactions have a significant effect on film stability and can affect bubble coalescence. The literature data show that salts reduce the solubility of gases, which results in inhibition of bubble coalescence via the hydrophobic force (Craig et al., 1993a; Henry et al., 2006; Weissenborn and Pugh, 1996). Therefore, at relatively high salt concentrations, adding salts is expected to inhibit bubble coalescence by screening hydrophobic attractions. It can to some extent explain the noticeably longer lifetime of liquid films of sodium halide salts at higher concentration in Figure 3.7. However, there is no unique quantitative measurement to illustrate the effect of different salts of different concentrations on the hydrophobic force between two bubbles.

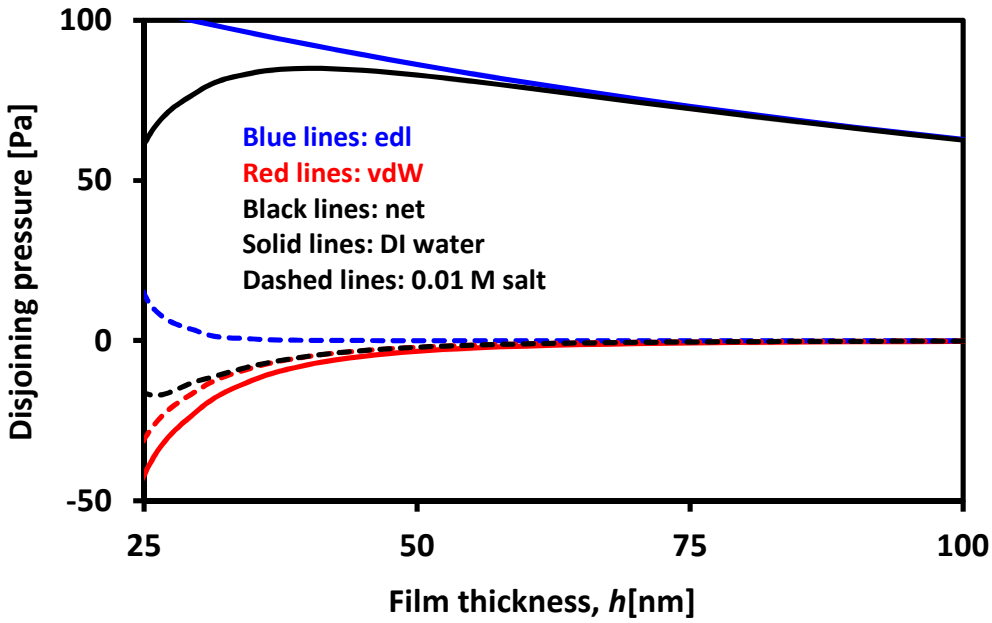

Figure 3.10**.** Disjoining pressures for pure DI water (equivalent to 4μM solution because of CO_2 dissolved from the atmosphere as well as hydronium and hydroxyl ions) films and 0.01M monovalence salt films, showing significant reductions of DLVO colloidal pressures.

3.4.3.2 ION-SPECIFIC EFFECT

The general behaviour of salt solutions is attributed to the ion-specific effect which depends on the interplay of ion-ion, ion-solvent and solvent-solvent interactions. Specifically, the specific-ion effect depends on the nature of the cation and anion species in a solution and their interactions with the solvent molecules (Ninham and Nostro, 2010). Indeed the water structure or the perturbations of the hydrogen-bonding network are very decisive and they are believed to strongly depend on the size and polarizability of the hydrated ions. Collins (1985) has shown that the effect of an ion on the structure of water depends to a large extent on ion charge density and whether the water-water interactions in bulk solutions are comparable to ion-water interactions. Based on this competition, ions are defined as structure-makers (kosmotropes) with high charge density that bind the immediately adjacent water molecules tightly and structure-breakers (chaotropes) with low charge density that are loosely bound to the adjacent water molecules. The entropy of hydration, ΔS, which is the difference between the entropy of water molecules in the bulk and the water molecules adjacent to ions, is one of the parameters that can describe the effect of ions on water structure quantitatively (Collins and Washabaugh, 1985; Marcus, 1997). Table 3.1 shows the ΔS value and radius of the alkali metal and halide ions. Positive ΔS values indicate the strong ordering effect of ions owing to the

strong ion-water interaction. Negative ΔS values are associated with larger ions, which reflect the disordering effect and greater mobility of a water molecule in the vicinity of the ion compared to the water molecule in the bulk. The former and latter groups of ions are referred to as kosmotropes (Li^+, Na^+ and F^-) and chaotropes (K^+, Cl^-,Br^- and I^-) respectively.

Table 3.1. Entropy of hydration and radius of alkali metal and halide ions of interest (Marcus, 1997)

Ion name	Li^+	Na^+	K^+	F^-	Cl^-	Br^-	I^-
ΔS [$JK^{-1}mol^{-1}$]	+56	+5	-34	+70	-6	-28	-55
Radius [pm]	69	102	138	133	181	196	220

Ion adsorption energy (the change in the energy of an ion from the bulk water to an interface) is a function of ion size, polarizability and ionization potential. It can manifest the ion-specific effect on the water structure. Figure 3.11 shows a linear relationship between the non-dimensional specific adsorption energy of salts of interest and their critical concentrations. The details of the calculations are available in the literature (Slavchov et al., 2012). The general trend of the specific adsorption energy is towards a larger $-U / K_B T$ when increasing the size of either the cation or anion. Salts with lower specific adsorption energy affect bubble coalescence at lower concentrations owing to their strong ion-water interactions. This trend is consistent with our observations shown in Figure 3.9 in which NaF and NaI have the smallest and greatest critical concentration, respectively.

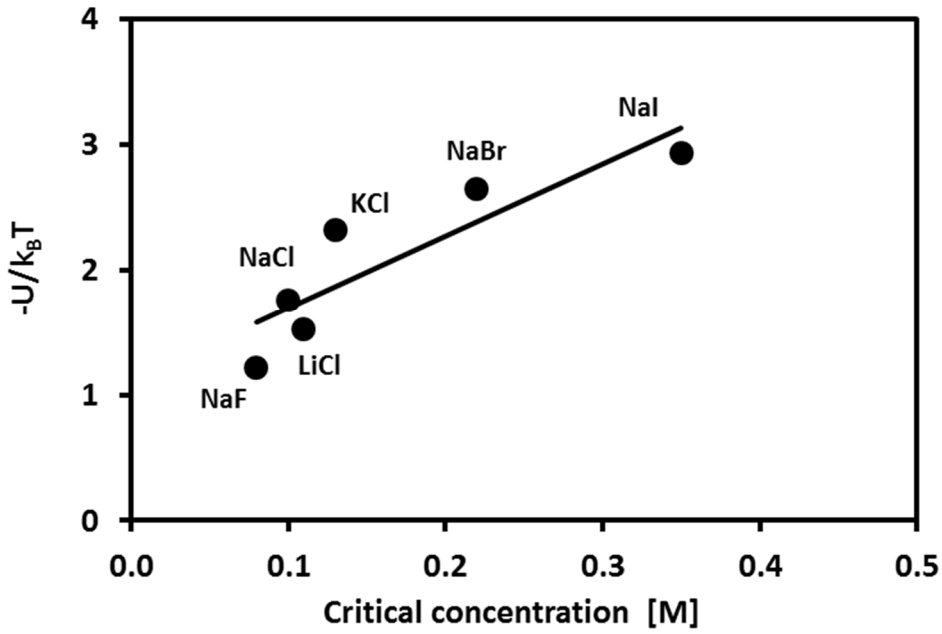

Figure 3.11. Total specific adsorption energy of investigated salts at air-solution interface versus their critical concentrations.

The above-described classification of ions helps explain many experimental results if they are considered as a pair of salt ions. This concept is known as Collins' concept of matching water affinities of salt ions (Collins and Washabaugh, 1985; Kunz, 2010; Ozdemir et al., 2011). The concept generally aligns with the observations concerning the effect of salts on bubble coalescence, but not for all salts. For example, the kosmotrope–kosmotrope and chaotrope–chaotrope pairs of salt ions, such as in the case of NaF and KCl, are matched in water affinity, the partitions of the ion pair at the water–air interface layer are similar and the ions capability of inhibiting bubble coalescence is strong. Conversely, if pair ions are not matched in water affinity (kosmotrope–chaotrope), such as in the case of NaI, the salt ion partitions at the water–air interface layer are significantly different and the salt capability of inhibiting bubble coalescence in water is weak. Collins' concept agrees with the combining rule postulated for the ion-specific effect on bubble coalescence by Craig et al. (1993) for some salts. The combining rule and Collins' concept indicate that taking into account the individual effect of each ion alone is not sufficient to fully explain the inhibiting effect of salts on bubble coalescence.

3.4.3.3 EFFECTS OF VISCOSITY AND SURFACE RHEOLOGY

Salts can make liquid films resistant to local deformation and rupture during thinning by affecting the dynamic properties. Salts can decrease the drainage rate substantially at concentrations beyond critical concentrations by changing the surface mobility (Chesters and Hofman, 1982; Davis et al., 1989; Marrucci, 1969; Prince and Blanch, 1990). Small ions like F^- and Li^+ are tightly bound by the surrounding water molecules and substantially confine the water molecules. Unlike the small ions, the hydration shells of large ions like I^- are loosely bound and therefore the water molecules can move freely towards the interface, leading to the deformation of hydration shells. In LiCl solutions the strong cation-water interactions result in a very viscous system with low surface mobility and increasing the salt concentration significantly increases the viscosity. For larger ions like K^+, the water-ion electrostatic interactions are not strong enough to influence the viscosity/mobility of the water molecules and unlike LiCl, increasing the salt concentration does not alter the viscosity appreciably (Du et al., 2006). These trends are consistent with our observations in our experiments. Figure 3.12 shows the effect of salt concentration on the film lifetime and viscosity of LiCl and KCl solutions up to 4 M. Increasing the LiCl concentration results in a considerable increase in film lifetime and the solution viscosity. However, in the case of KCl films, the lifetime first increases and then decreases with increasing KCl concentration, but the solution viscosity remains almost constant. Therefore, solution viscosity alone cannot be used to explain the inhibiting effect of salts on bubble coalescence.

Salts can affect bubble coalescence by changing the surface tension and mobility of the bubble-liquid interface. The rapid stretch of the saline liquid film during thinning and drainage causes a non-uniform distribution of ions at the air-liquid interface and a surface tension gradient which changes the tangential stress along the interface. The Gibbs-Marangoni stress arising from the surface tension gradient with respect to the salt concentration retards the film thinning by causing the backward interface flow radially towards the film centre and thereby immobilizing the interface. This stabilizing phenomenon, known as the Marangoni effect, has been considered as a mechanism for inhibiting bubble coalescence by salts at concentrations above transition concentrations (Christenson et al., 2007; Marrucci, 1969b; Yaminsky et al., 2010). This inhibiting effect of salts was first theoretically described by Marrucci (1969) and was later supported by Prince and Blanch (Prince and Blanch, 1990b). In 2005 Chan and Tsang (2005) argued that the Marangoni effect of salt solutions cannot be large enough to inhibit bubble coalescence. Therefore, they incorporated the short-range repulsive hydration force to explain the stabilizing effect of salts. We recently mathematically proved

the inconsistency of this model (Firouzi and Nguyen, 2013a). Yaminsky et al. (Yaminsky et al., 2010) and Kalseboer et al. (Klaseboer et al., 2000b) also demonstrated that that the Marangoni effect is very effective even at very small surface tension gradients to alter the air-bubble interface from mobile to partially mobile or immobile interface.

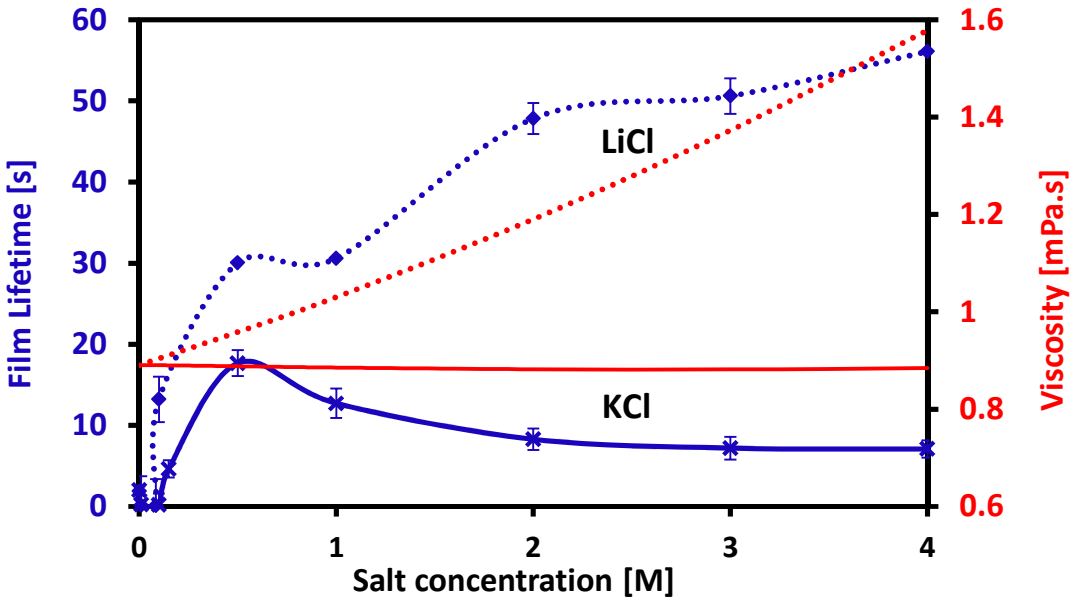

Figure 3.12. Film lifetime (blue) and solution viscosity (red) of LiCl (dotted lines) and KCl (solid lines) vs. salt concentration at u = 10 µm/s. The viscosity data are taken from (Desnoyers and Perron, 1972).

3.5 CONCLUSIONS

A systematic study of the effect of halide anions and alkali cations on bubble coalescence at different air-interface approach speeds was conducted over an interface approach speed range of 10-300 µm/s. The film drainage experiments showed significant difference between zero and non-zero interface approach speeds. In the former case, the nano pump was stopped as soon as the first interferometric image of the film was observed. In the latter case, the nano-pump was used to continuously pump out the liquid until the film ruptured and disappeared. The film lifetime was measured from the instance of film formation (the first interferometric image of a film) until the film disappearance by rupture. The vital role of interface approach speed was demonstrated and the results reconfirmed that the inhibiting effect of salts on film stability and rupture (bubble coalescence) depends not only on the salt type and concentration but also on the interface approach speed. The

results also demonstrated that pure DI water films can be formed and last for a few seconds at interface approach speeds smaller than a critical speed of 35 µm/s. For the interface approach speeds greater than the critical speed, the water films rupture instantly. All the salts examined inhibited bubble coalescence above a critical concentration, called the transition concentration. The results indicated the important role of cations as well as anions on bubble coalescence.

ACKNOWLEDGEMENTS

The authors gratefully acknowledge the financial support from the Australian Research Council (Grant DP0985079). The assistance of Drs Tuan AH Nguyen and Stoyan Karakashev is warmly acknowledged.

REFERENCES

Chan, B.S., Tsang, Y.H., A theory on bubble-size dependence of the critical electrolyte concentration for inhibition of coalescence. Journal of Colloid and Interface Science, 2005, **286(1)**, 410-413.

Chesters, A.K., Hofman, G., Bubble coalescence in pure liquids. Appl. Sci. Res., 1982, **38**, 353-361.

Christenson, H.K., Bowen, R.E., Carlton, J.A., Denne, J.R.M., Lu, Y., Electrolytes that Show a Transition to Bubble Coalescence Inhibition at High Concentrations. The Journal of Physical Chemistry C, 2007, **112(3)**, 794-796.

Collins, K.D., Washabaugh, M.W., The Hofmeister effect and the behaviour of water at interfaces. Quarterly Reviews of Biophysics, 1985, **18(04)**, 323-422.

Craig, V.S.J., Bubble coalescence and specific-ion effects. Current Opinion in Colloid and Interface Science, 2004, **9(1-2)**, 178-184.

Craig, V.S.J., Ninham, B.W., Pashley, R.M., Effect of electrolytes on bubble coalescence. Nature, 1993, **364(6435)**, 317-319.

Creux, P., Lachaise, J., Graciaa, A., Beattie, J.K., Specific Cation Effects at the Hydroxide-Charged Air/Water Interface. The Journal of Physical Chemistry C, 2007, **111(9)**, 3753-3755.

Davis, R.H., Schonberg, J.A., Rallison, J.M., The lubrication force between two viscous drops. Physics of Fluids A: Fluid Dynamics (1989-1993), 1989, **1(1)**, 77-81.

Del Castillo, L.A., Ohnishi, S., Horn, R.G., Inhibition of bubble coalescence: Effects of salt concentration and speed of approach. Journal of Colloid and Interface Science, 2011, **356(1)**, 316-324.

Desnoyers, J.E., Perron, G., The viscosity of aqueous solutions of alkali and tetraalkylammonium halides at 25°C. J. Solution Chem., 1972, **1(3)**, 199-212.

Du, H., Rasaiah, J.C., Miller, J.D., Structural and Dynamic Properties of Concentrated Alkali Halide Solutions: A Molecular Dynamics Simulation Study. J. Phys. Chem. B, 2006, **111(1)**, 209-217.

Firouzi, M., Nguyen, A.V., Novel Methodology for Predicting the Critical Salt Concentration of Bubble Coalescence Inhibition. The Journal of Physical Chemistry C, 2013, **118(2)**, 1021-1026.

Frankel, S.P., Myseis, K.J., ON THE "DIMPLING" DURING THE APPROACH OF TWO INTERFACES1. The Journal of Physical Chemistry, 1962, **66(1)**, 190-191.

Henry, C.L., Dalton, C.N., Scruton, L., Craig, V.S.J., Ion-Specific Coalescence of Bubbles in Mixed Electrolyte Solutions. The Journal of Physical Chemistry C, 2006, **111(2)**, 1015-1023.

Israelachvili, J., Wennerstrom, H., Role of hydration and water structure in biological and colloidal interactions. Nature, 1996, **379(6562)**, 219-225.

Karakashev, S.I., Nguyen, P.T., Tsekov, R., Hampton, M.A., Nguyen, A.V., Anomalous ion effects on rupture and lifetime of aqueous foam films formed from monovalent salt solutions up to saturation concentration. Langmuir, 2008, **24(20)**, 11587-11591.

Klaseboer, E., Chevaillier, J.P., Gourdon, C., Masbernat, O., Film Drainage between Colliding Drops at Constant Approach Velocity: Experiments and Modeling. J. Colloid Interface Sci., 2000a, **229(1)**, 274-285.

Klaseboer, E., Chevaillier, J.P., Gourdon, C., Masbernat, O., Film Drainage between Colliding Drops at Constant Approach Velocity: Experiments and Modeling. J. Colloid Interface Sci., 2000b, **229(1)**, 274-285.

Kunz, W., 2010. Specific ion effects. World Scietific, p. 325.

Lessard, R.R., Zieminski, S.A., Bubble Coalescence and Gas Transfer in Aqueous Electrolytic Solutions. Ind. Eng. Chem. Fundam., 1971, **10(2)**, 260-269.

Lin, C.Y., Slattery, J.C., Thinning of a liquid film as a small drop or bubble approaches a solid plane. AIChE Journal, 1982, **28(1)**, 147-156.

Liu, G., Hou, Y., Zhang, G., Craig, V.S.J., Inhibition of Bubble Coalescence by Electrolytes in Binary Mixtures of Dimethyl Sulfoxide and Propylene Carbonate. Langmuir, 2009, **25(18)**, 10495-10500.

Marcus, Y., *Ion Properties*. 1997, Marcel Dekker, New York.

Marrucci, G., A theory of coalescence. Chemical Engineering Science, 1969, **24(6)**, 975-985.

Marrucci, G., Nicodemo, L., Coalescence of gas bubbles in aqueous solutions of inorganic electrolytes. Chem. Eng. Sci., 1967, **22(9)**, 1257-1265.

Nguyen, A.V., Historical Note on the Stefan–Reynolds Equations. J. Colloid Interface Sci., 2000, **231(1)**, 195.

Nguyen, A.V., Schulze, H.J., *Colloidal science of flotation*. 2004, Marcel Dekker, New York.

Nguyen, P.T., Hampton, M.A., Nguyen, A.V., Birkett, G.R., The influence of gas velocity, salt type and concentration on transition concentration for bubble coalescence inhibition and gas holdup. Chem. Eng. Res. Des., 2012, **90(1)**, 33-39.

Ninham, B.W., Nostro, P.L., *Molecular Forces and Self Assembly : In Colloid, Nano Sciences and Biology*. 2010, Cambridge University Press.

Ozdemir, O., Du, H., Karakashev, S.I., Nguyen, A.V., Celik, M.S., Miller, J.D., Understanding the role of ion interactions in soluble salt flotation with alkylammonium and alkylsulfate collectors. Adv. Colloid Interface Sci., 2011a, **163(1)**, 1-22.

Prince, M.J., Blanch, H.W., Transition electrolyte concentrations for bubble coalescence. AIChE Journal, 1990, **36(9)**, 1425-1429.

Radoëv, B.P., Dimitrov, D.S., Ivanov, I.B., Hydrodynamics of thin liquid films effect of the surfactant on the rate of thinning. Colloid Polym. Sci., 1974, **252(1)**, 50-55.

Ruckenstein, E., Sharma, A., A new mechanism of film thinning: Enhancement of reynolds' velocity by surface waves. Journal of Colloid and Interface Science, 1987, **119(1)**, 1-13.

Slavchov, R.I., Karakashev, S.I., Ivanov, I.B., 2012. Ionic surfactants and ion-specific effects: adsorption, micellization, thin liquid films, In *In Surfactant Science and Technology: Retrospects and Prospects*. Romsted, L.S. (Ed.),Taylor & Francis Group.

Tsekov, R., The R4/5-problem in the drainage of dimpled thin liquid films. Colloids and Surfaces A, 1998, **141(2)**, 161-164.

Wang, L., Qu, X., Impact of interface approach velocity on bubble coalescence. Minerals Engineering, 2012, **26(0)**, 50-56.

Weissenborn, P.K., Pugh, R.J., Surface tension of aqueous solutions of electrolytes: Relationship with ion hydration, oxygen solubility, and bubble coalescence. Journal of Colloid and Interface Science, 1996, **184(2)**, 550-563.

Yaminsky, V.V., Ohnishi, S., Vogler, E.A., Horn, R.G., Stability of aqueous films between bubbles. Part 1. the effect of speed on bubble coalescence in purified water and simple electrolyte solutions. Langmuir, 2010, **26(11)**, 8061-8074.

CHAPTER 4

ON THE EFFECT OF VAN DER WAALS ATTRACTIONS ON THE CRITICAL SALT CONCENTRATION FOR INHIBITING BUBBLE COALESCENCE

Mahshid Firouzi and Anh V. Nguyen

Published in “Minerals Engineering”, April 2014, 58, 108-112

4.1 ABSTRACT

The coalescence of gas bubbles in many salt solutions such as NaCl is significantly inhibited if the salt concentration exceeds a critical concentration which is unique for each salt. It has been predicted as a function of the Hamaker constants of van der Waals attractions between two bubbles. In this paper, the Lifshitz theory on the van der Waals interaction energy and the available spectrum for water dielectric permittivity are applied to determine the Hamaker constants for liquid films between bubbles in pure water and salt solutions. Using the new values for Hamaker constants for thin films of saline solutions, we show that the effect of van der Waals attractions on the critical salt concentration is significantly weaker than previously hypothesized. The predictions based on van der Waals attractions significantly under-estimate the experimental critical concentrations. The failure of the van der Waals attraction in predicting the critical salt concentration highlights the urgent need of revising the available theories on bubble coalescence in salt solutions and saline water.

Keywords: bubble coalescence, saline water, van der Waals attractions, Hamaker constants, flotation

4.2 INTRODUCTION

The effect of inorganic salts on bubble coalescence, froth stability and flotation performance is well known and documented (Klassen and Mokrousov, 1963; Kracht and Finch, 2009; Kurniawan et al., 2011; Laskowski, 2001; Nguyen et al., 2003; Ozdemir et al., 2011; Quinn et al., 2007). Bubble coalescence in many salt solutions and saline water can be inhibited if the salt concentration exceeds a concentration, called the transition concentration (Craig et al., 1993; Hofmeier et al., 1995; Marrucci and Nicodemo, 1967; Nguyen et al., 2012). Bubbles undergo a transition from coalescence to non-coalescence at a critical moment at which the opposing forces are balanced. Therefore, this concentration is referred to as a critical concentration in this paper. The transition and critical concentrations can be different in many cases as discussed below.

The inhibiting effect of salts on bubble coalescence has been investigated experimentally using three techniques. The first technique is to monitor the population of bubbles in a swarm in a bubble column by measuring the solution turbidity (the gas holdup) or bubbles size distribution (Craig et al., 1993; Marrucci and Nicodemo, 1967; Nguyen et al., 2012). The transition concentration is the concentration halfway between 100% (the invariable result in pure water) of solution turbidity and the baseline measurement. Likewise, it is the concentration at 50% of cumulative distribution of bubble size. The second one is to contact pairs of bubbles and determine the coalescence percentage

of the pairs by dividing the number of coalescing bubbles by the total number of contacted pairs (Christenson et al., 2007; Kirkpatrick and Lockett, 1974; Lessard and Zieminski, 1971). The transition concentration is determined in the same way for solution turbidity. The third method is to create thin liquid films of salt solutions in a small cylindrical cell, called the Scheludko-Exerowa cell (Karakashev et al., 2008; Nguyen and Nguyen, 2010). Bubble coalescence and film lifetime can be determined by optical interferometry (Karakashev et al., 2008; Yaminsky et al., 2010). There is an abrupt increase in film lifetime with increasing salt concentration. The salt concentration at this rapid change in film lifetime is the critical concentration. In general, the first method can provide some statistical information on the change of bubbles population in saline solutions, but the flow condition can influence the transition concentration. On contrary, the second and third methods provide more direct information on the mechanisms at the microscopic level (Horn et al., 2011).

So far different mechanisms have been proposed to explain the inhibiting effect of salts on bubble coalescence. Craig et al. (1993) show that the inhibiting effect of salts follows a combining rule. This rule assigns each cation or anion a tag α or β. Salts comprising an $\alpha\alpha$ or $\beta\beta$ combination exhibit inhibition of coalescence while the combinations $\alpha\beta$ and $\beta\alpha$ have no effect on the coalescence. For example, NaCl is an $\alpha\alpha$ salt but $NaClO_3$ is an $\alpha\beta$ salt. Typical critical salt concentration for bubble coalescence inhibition is salt-specific, but about 0.1 M for monovalent salts. Christenson and Yaminsky (1995) showed that salts can increase the stability of liquid films by increasing the interface elasticity which determines the interface response to mechanical disturbances such as changes in film thickness. Salts are also known to inhibit bubble coalescence via hydrophobic attractions by reducing gas solubility, especially at high salt concentrations (Craig et al., 1993; Henry et al., 2006; Weissenborn and Pugh, 1996). Furthermore, salts make the liquid film resistant to local deformation and rupture during thinning by affecting the dynamic interfacial properties and consequently altering the hydrodynamic boundary condition of air-solution interface (Henry et al., 2006; Marrucci, 1969). Affecting film rupture rather than drainage is an alternative mechanism to explain the inhibiting effect of salts (Henry et al., 2006). All of the mentioned mechanisms have been argued and challenged alongside with the research into the so-called ion-specific effect on bubble coalescence which is strongly believed to be related to the effect of ions on water structure and hydrogen-bonding network (Henry and Craig, 2010; Kunz, 2010; Ozdemir et al., 2011). Many of the discussions remain qualitative rather than quantitative, but there are at least two models for predicting the critical or transition salt concentration for inhibiting bubble coalescence which are based on attractive van der Waals forces.

In this paper we aim to quantify the effect of van der Waals attractions on bubble coalescence in saline solutions. The main question to be addressed in this paper is whether or not van der Waals attractions are strong enough to balance the opposing forces to inhibit bubble coalescence. Therefore, we first review the two mathematical models proposed by Marrucci (1969), and Prince & Blanch (1990) to predict the critical salt concentration. We will then critically examine the certainty of available values for Hamaker constants of van der Waals attractions. It is followed by assessing the model predictions for salt critical concentrations using the correct Hamaker constants.

4.3 AVAILABLE MODELS FOR CALCULATION OF THE CRITICAL SALT CONCENTRATION

The first theoretical model to predict the critical salt concentration was proposed by Marrucci (1969). The model is based on balancing the driving forces of the drainage and rupture of thin films between bubbles, which includes the capillary pressure and (non-retarded) London-van der Waals attraction with an opposing force owing to the change in the surface excess of salts. This surface excess creates a surface tension gradient by tangential stress, called the Gibbs-Marangoni stress, which is capable of immobilizing the film surfaces at high salt concentration. Thus, the transition from the inertial (at low salt concentration) to viscous (at high salt concentration) liquid drainage inside the thin film occurs at the critical salt concentration. We would have the following pressure balance equation at the transition concentration (Marrucci, 1969; Prince and Blanch, 1990):

$$\frac{4C}{h^2 \upsilon R_g T}\left(\frac{\partial \sigma}{\partial C}\right)^2 - \frac{2\sigma}{R} + \Pi(h) = 0 \tag{4.1}$$

where $\Pi(h)$ is the disjoining pressure, h is the average film thickness, υ is the number of ions produced upon dissociation (i.e. $\upsilon = 2$ for most of inorganic salts), R_g is the universal gas constant, T is the absolute temperature, R is the bubble radius, and σ and $\partial\sigma / \partial C$ are the surface tension and the surface tension gradient with salt concentration, respectively. The first and second terms on the left hand side of Eq. (4.1) describe the pressure due to the Gibbs-Marangoni stress and the capillary pressure, respectively.

The non-retarded London-van der Waals disjoining pressure was first considered in modelling the disjoining pressure in Eq. (4.1), giving $\Pi = -A / 6\pi h^3$, where A is the non-retarded Hamaker constant. Then the critical salt concentration, C_{cr}, is described as follows (Marrucci, 1969; Prince and Blanch, 1990):

$$C_{cr} = 0.084 \upsilon R_g T \left(\frac{\sigma A^2}{R} \right)^{1/3} \left(\frac{\partial \sigma}{\partial c} \right)^{-2} \tag{4.2}$$

An exact value for the Hamaker constant in Eq. (4.2) is difficult to determine with precision. However, a value of $A = 2.5 \times 10^{-20}\,\mathrm{J}$ has been suggested and used in the literature (Prince and Blanch, 1990).

Prince and Blanch (1990) argued that the bubble coalescence would occur at the film thickness greater than the range of magnetically non-retarded London-Waals attraction used by Marrucci and therefore the long-ranged, magnetically retarded Casimir-van der Waals attraction should be used in modelling the critical salt concentration. The disjoining pressure of the Casimir-van der Waals attraction was defined by the authors as $\Pi = -B / h^4$, where B is the retarded Hamaker constant. They modified the Marrucci model by incorporating the effect of inertia and the retarded Casimir-van der Waals attraction into the force balance. These modifications have led to the following expression for the critical concentration:

$$C_{cr} = 1.18 \upsilon R_g T \left(\frac{\sigma B}{R} \right)^{1/2} \left(\frac{\partial \sigma}{\partial c} \right)^{-2} \tag{4.3}$$

Again, an exact value for the magnetically retarded Hamaker constant in Eq. (4.3) is difficult to obtain and a value of $B = 1.5 \times 10^{-28}\,\mathrm{J \cdot m}$ has been assigned to best fit the model with the experimental results (Prince and Blanch, 1990). Table 1 summarises the available experimental results and the best fitted results of Eq. (3) with $B = 1.5 \times 10^{-28}\,\mathrm{J \cdot m}$. The comparison between the experimental and best fitted results is quite favourable. It is noted that the critical concentrations reported by Marrucci and Nicodemo (1967), and Lessard and Zieminski (1971) were determined by the bubble swarm and bubble pair methods, respectively. However, the similar experimental results highlight that the two experimental techniques used by the two groups were compatible.

It is noted that Eq. (4.2) could be used to best fit the data presented in Table 1, giving a best fitted value for $A = 2 \times 10^{-19}\,\mathrm{J}$ which is one order of magnitude higher than the value $A = 2.5 \times 10^{-20}\,\mathrm{J}$ quoted by Prince and Blanch (Prince and Blanch, 1990). Since both Eqs. (4.2) and (4.3) can be best fitted to the experimental results, further analysis of Hamaker constants is critical to a better understanding of the underlying physics governing bubble coalescence in salt solutions. The numerical values for the two Hamaker constants are scrutinised below.

Table 4.1. Summary of experimental results (Lessard and Zieminski, 1971; Marrucci and Nicodemo, 1967) and model prediction by fitting with $B = 1.5 \times 10^{-28}$ J·m (Prince and Blanch, 1990) for salts critical concentration.

Salt	$\partial\sigma / \partial C$ (mN/mM)	Bubble radius R (mm)	Critical salt concentration, C_{cr} [M]	
			Eq. (4.3) with $B = 1.5 \times 10^{-28}$ J·m	Experimental results
$MgSO_4$*	3.2	1.8	0.042	0.032
$MgCl_2$*	3.4	1.8	0.056	0.055
$CaCl_2$*	3.5	1.8	0.053	0.055
Na_2SO_4*	2.7	1.8	0.089	0.061
LiCl*	1.62	1.8	0.165	0.160
NaCl*	1.7	1.8	0.150	0.170
NaBr*	1.3	1.8	0.257	0.220
KCl*	1.44	1.8	0.209	0.230
KCl**	1.44	2.05	0.196	0.210
K_2SO_4**	2.52	2.05	0.096	0.080
KOH**	1.78	2.05	0.128	0.170
$CuSO_4$**	1.85	2.05	0.120	0.070
KI**	0.84	2.05	0.580	0.630
KNO_3**	1.04	2.05	0.376	0.410

* Lessard and Zieminski (1971)

**Marrucci and Nicodemo (1967).

4.4 UNCERTAINTY ANALYSIS OF NUMERICAL VALUES FOR HAMAKER CONSTANTS FOR WATER FILMS BETWEEN AIR BUBBLES

The uncertainty of assigning the values for the Hamaker constants in determining the critical salt concentration using Eqs. (4.2) and (4.3) has to be analysed to ascertain whether or not the critical salt concentration is governed by the van der Waals attraction. In this analysis, we use the advanced Lifshitz theory based on quantum mechanics to calculate the van der Waals interaction energy per

unit area, E, for the intervening liquid film between gas bubbles. The Lifshitz theory gives (Nguyen and Schulze, 2004):

$$E(h) = \frac{k_B T}{8\pi h^2} \sum_{n=0}^{\infty}{}' \int_{x_n}^{\infty} \ln\left\{\left[1-\left(\frac{x-s\varepsilon}{x+s\varepsilon}\right)^2 e^{-x}\right]\left[1-\left(\frac{x-s}{x+s}\right)^2 e^{-x}\right]\right\} x\mathrm{d}x \tag{4.4}$$

where h is the film thickness and the prime on the summation symbol indicates that the zero-frequency (n = 0) term is divided by 2. The other symbols and terms are defined as follows:

$$s^2 = x^2 + x_n^2 \frac{1-\varepsilon}{\varepsilon} \tag{4.5}$$

$$x_n = 2h\xi_n \sqrt{\varepsilon} / c \tag{4.6}$$

where c is the speed of light in vacuum, $\xi_n = 2n\pi k_B T / \hbar$ is the sampling frequency (with $\hbar$ being the Planck constant divided by 2π) and $\xi_n = \varepsilon(i\xi_n)$ is the spectrum of water dielectric permittivity (with $i\xi_n$ being the discrete equally spaced imaginary frequencies). Since the water permittivity is experimentally known, the Lifshitz theory can be used to quantify the van der Waals attractions with high certainty.

The experimental data for complete spectrum of $\varepsilon(i\xi)$ for water is described by the following equation (Nguyen and Schulze, 2004):

$$\varepsilon(i\xi) = 1 + \frac{d_m}{1+\xi\tau_m} + \sum_{j=1}^{10} \frac{f_i}{\omega_j^2 + g_j\xi + \xi^2} \tag{4.7}$$

Therefore, the accurate representation of $\varepsilon(i\xi)$ by Eq. (4.7) requires 12 terms in total which describe a Debye-type microwave relaxation of water molecules with frequencies τ_m and decay amplitude d_m (the first term), and the damped harmonic oscillators in the infrared (five terms) and ultraviolet (6 terms) with resonance frequencies ω_j, decay amplitudes d_j and bandwidths g_j. The numerical values for the model constants in Eq. (4.7) are available in the literature (Nguyen, 2000; Nguyen and Schulze, 2004).

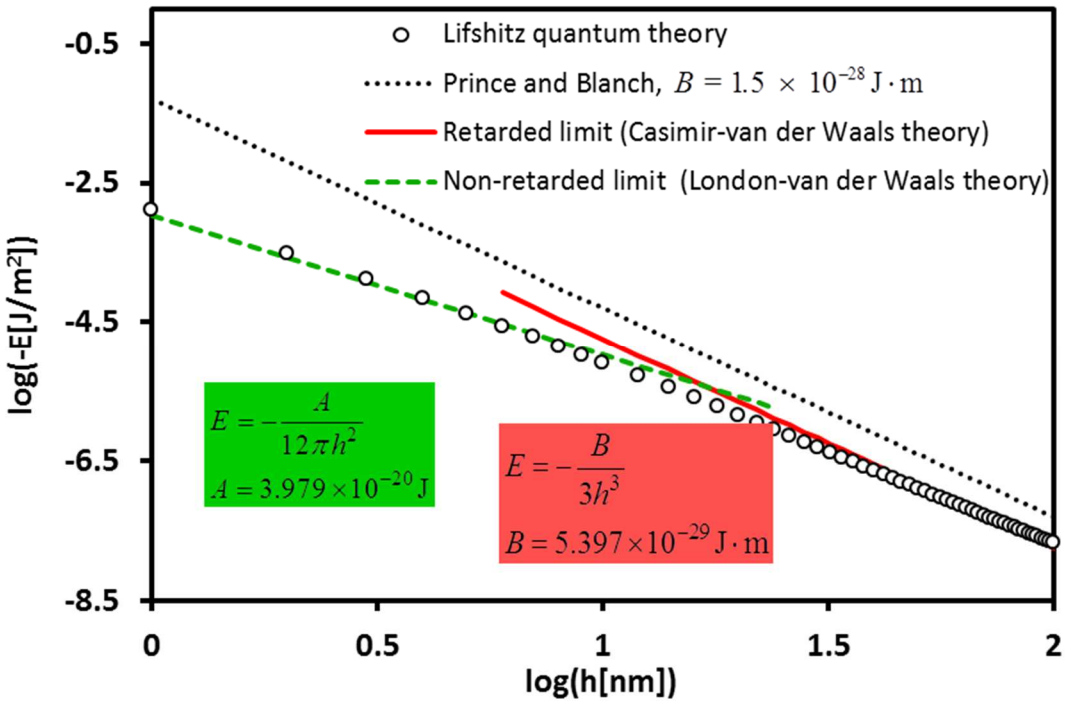

Figure 4.1. Numerical results (points) and its short-ranged (non-retarded) limit (green dashed line) and long-ranged (retarded) limit (red solid line) for the van der Waals interaction energy versus film thickness. The black dotted line shows the energy predicted by Prince and Blanch with B=1.5 $\times$ $10^{-28}\,\mathrm{J \cdot m}$.

Equation (4.4) can be numerically integrated using the Gauss-Laguerre quadrature (Nguyen and Schulze, 2004). The numerical results are compared with the results of Prince and Blanch for the van der Waals energy in Figure 4.1. It is noted that the zero point on the horizontal axis of the logarithmic scale corresponds to 1 nm distance. However, the plots in Figure 4.1 are specifically for the van der Waals interaction energies and do not contain the Born repulsion (effective at 0.3 nm) which is typically considered in calculating the total interaction energy between two surfaces. Shown in Figure 4.1 are also the two limits established from the Lifshitz theory for the short-ranged (London-van der Waals) and long-ranged (Casimir-van der Waals) interaction energy, which gives $A = 3.979 \times 10^{-20}\,\mathrm{J}$ and $B = 5.397 \times 10^{-29}\,\mathrm{J \cdot m}$ for a film of pure water between two bubbles. The value obtained for B from the numerical results is evidently significantly smaller than the value $B = 1.5 \times 10^{-28}\,\mathrm{J \cdot m}$ assigned by Prince and Blanch by a relative error of 178%. This difference leads to an over-prediction of the van der Waals energy by Prince and Blanch as can be observed in Figure 4.1. The results presented in Figure 4.1 also show that there is a transition from the non-

retarded to retarded van der Waals attractions at a separation distance between 10 and 20 nm which is in agreement with the literature (Israelachvili, 2005).

It is noted that the zero-frequency term contribution to the van der Waals attraction described by Eq. (4.4) is essentially an electrostatic interaction and can be screened out by the salt ions inside the intervening water films (Nguyen and Schulze, 2004). This screening effect can be included in Eq.(4.4) by multiplying the zero frequency term by a factor of $(1+2\kappa h)\exp(-2\kappa h)$ where κ is the Debye constant defined as follows:

$$\kappa = \left\{ \frac{2000CF^2z^2}{\varepsilon\varepsilon_0 R_g T} \right\}^{1/2} \tag{4.8}$$

where F is the Faraday constant, z is the ion valence of the symmetric z:z salt, C is the salt concentration, ε_0 and $\varepsilon = 80$ are the dielectric constants of the vacuum and water permittivity, respectively.

The dependence of B on salt concentration can be calculated from retarded limit of the Lifshitz theory with the zero-frequency term multiplied by the factor of $(1+2\kappa h)\exp(-2\kappa h)$. The results are shown in Figure 4.2. Evidently, B decreases with increasing salt concentration up to 0.001 M and then remains unchanged at a value of $B = 3.492 \times 10^{-29}\,\mathrm{J\cdot m}$. We consider this value for the retarded Hamaker constant in saline liquid films since transition concentrations of salts are larger than 0.01 M. The value obtained for B for saline water films is significantly smaller than the value assigned by Prince and Blanch ($B = 1.5 \times 10^{-28}\,\mathrm{J\cdot m}$) in predicting the salt concentration by a relative error of 330%.

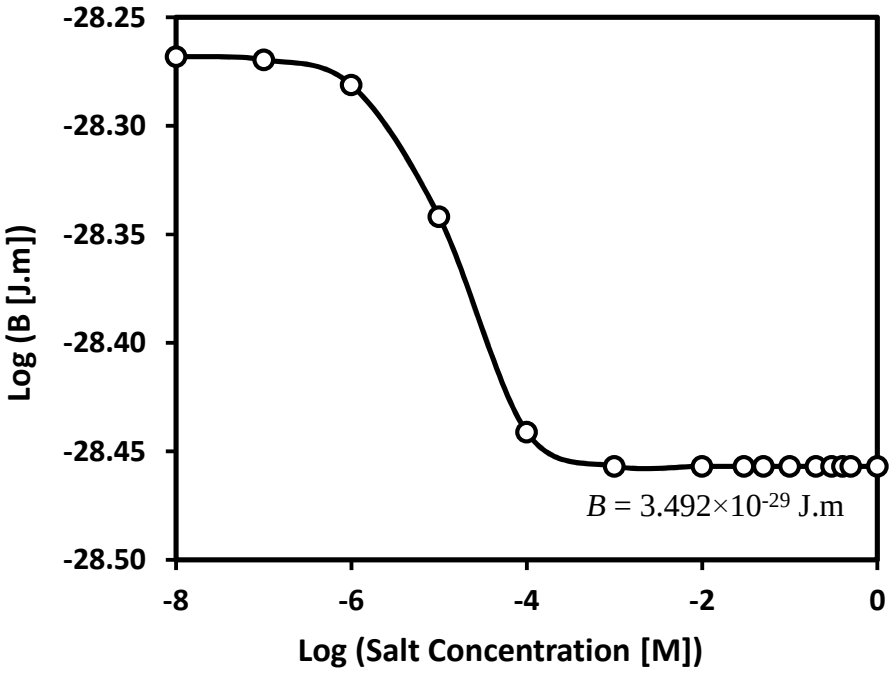

Figure 4.2.Dependence of the retarded Hamaker constant *B* on salt concentration

4.5 VALIDATION OF THE AVAILBLE MODELS USING THE CORRECTED VALUES FOR HAMAKER CONSTANTS

Having obtained the accurate values for the Hamaker constants from the numerical results for saline water films, the predictions described by Eqs. (4.2) and (4.3) can be compared with the available experimental data. The comparison is shown in Figure 4.3 and Table 4.2. For consistency the same experimental data shown in Table 4.1 are used for comparison in Figure 4.3. Since the models described by Eqs. (4.2) and (4.3) requires the bubble radius to calculate the critical salt concentration, the absence of the bubble size in many reports on the critical concentration in the literature limits further validation of the models. However, the experimental and predicted data obtained by two independent methods in Tables 4.1 and 4.2 evidently show that both theories developed based on the van der Waals attraction significantly under-predict the experimental results. The difference between the model predictions increases with increasing the critical salt concentration. This significant difference between the model predictions and experimental data indicates that van der Waals attractions are not sufficiently strong to counterbalance the opposing force owing to the Gibbs-Marangoni stress to correctly produce the critical salt concentration detected by the experiments. Perhaps, stronger attractions than van der Waals attractions are needed to correctly

explain the available experimental results for the critical salt concentration. Hydrophobic attraction inferred from the force measurements between two hydrophobic surfaces has been argued for some time (Hampton and Nguyen, 2012; Meyer et al., 2006; Nguyen and Nguyen, 2010) but faces similar uncertainty of the classical Hamaker theory. Significantly, hydrophobic attraction between two air bubbles is more difficult to measure than its counterpart between two solid surfaces.

Table 4.2. Summary of results for salts critical concentration as calculated using Eqs. (4.2) and (4.3) and the corrected values for the Hamaker constants, and the experimental conditions given in Table 4.1.

	Critical salt concentration, C_{cr} [M]		
Salt	Eq. (4.2) with $A = 3.979 \times 10^{-20}$ J	Eq. (4.3) with $B = 3.492 \times 10^{-29}$ J.m	Experimental results
$MgSO_4$	0.016	0.020	0.032
$MgCl_2$	0.022	0.027	0.055
$CaCl_2$	0.020	0.026	0.055
Na_2SO_4	0.034	0.043	0.061
LiCl	0.063	0.079	0.160
NaCl	0.058	0.072	0.170
NaBr	0.094	0.123	0.220
KCl	0.080	0.101	0.230
KCl	0.077	0.095	0.210
K_2SO_4	0.038	0.046	0.080
KOH	0.050	0.062	0.170
$CuSO_4$	0.047	0.057	0.070
KI	0.226	0.278	0.630
KNO_3	0.148	0.182	0.410

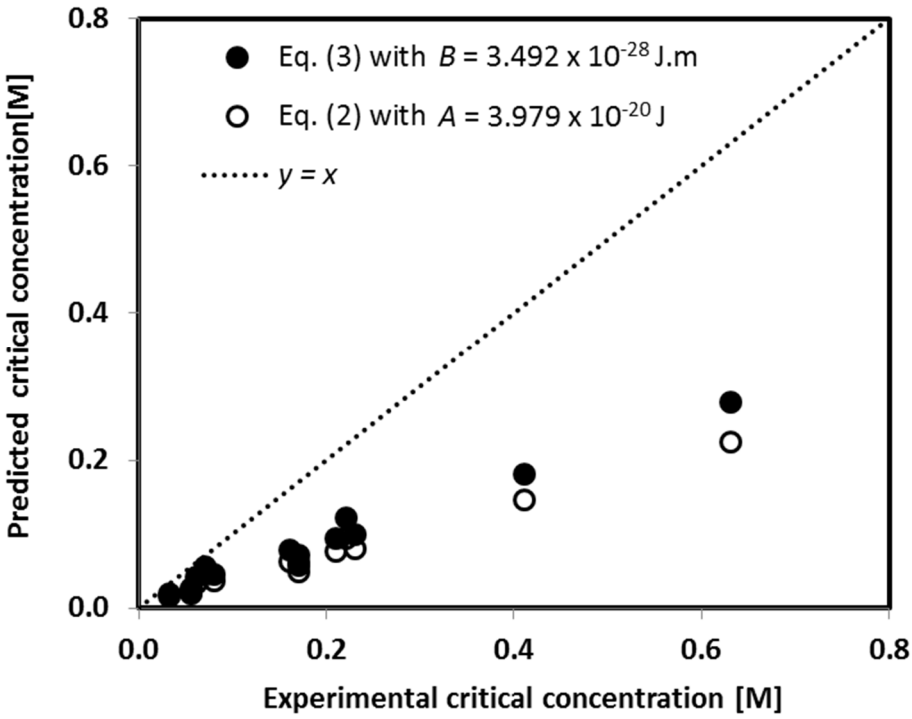

Figure 4.3. Comparison of the experimental results (Lessard and Zieminski, 1971; Marrucci and Nicodemo, 1967) with Marrucci's model described by Eq. (4.2) with with $A = 3.979 \times 10^{-20}$ J, and Prince and Blanch's model described by Eq. (4.3) with $B = 3.492 \times 10^{-29}$ J.m (Table 4.2).

4.6 CONCLUSION

It is concluded that the effect of van der Waals attraction on the critical salt concentration for bubble coalescence inhibition is significantly weaker than previously hypothesized. The models based on van der Waals attractions significantly under-predict the experimental critical concentration. This failure of the van der Waals attraction in predicting the critical salt concentration demands further theoretical developments and understanding of bubble coalescence in salt solutions and saline water.

ACKNOWLEDGEMENTS

The authors gratefully acknowledge the financial support from the Australian Research Council (Grant DP0985079).

REFERENCES

Christenson, H.K., Bowen, R.E., Carlton, J.A., Denne, J.R.M., Lu, Y., Electrolytes that Show a Transition to Bubble Coalescence Inhibition at High Concentrations. The Journal of Physical Chemistry C, 2007, **112(3)**, 794-796.

Christenson, H.K., Yaminsky, V.V., Solute effects on bubble coalescence. Journal of Physical Chemistry, 1995, **99(25)**, 10420.

Craig, V.S.J., Ninham, B.W., Pashley, R.M., Effect of electrolytes on bubble coalescence. Nature, 1993, **364(6435)**, 317-319.

Hampton, M.A., Nguyen, A.V., 2012. The nanobubble story, In *Encyclopedia of Surface and Colloid Science*, ed. Somasundaran, P., 2nd ed. Taylor and Francis, London, pp. 1-15.

Henry, C.L., Craig, V.S.J., The link between ion specific bubble coalescence and Hofmeister effects is the partinioning of ions within the interface. Langmuir, 2010, **26(9)**, 6478-6483.

Henry, C.L., Dalton, C.N., Scruton, L., Craig, V.S.J., Ion-Specific Coalescence of Bubbles in Mixed Electrolyte Solutions. The Journal of Physical Chemistry C, 2006, **111(2)**, 1015-1023.

Hofmeier, U., Yaminsky, V.V., Christenson, H.K., Observations of solute effects on bubble formation. J. Colloid Interface Sci., 1995, **174(1)**, 199-210.

Horn, R.G., Del Castillo, L.A., Ohnishi, S., Coalescence map for bubbles in surfactant-free aqueous electrolyte solutions. Advances in Colloid and Interface Science, 2011, **168(1-2)**, 85-92.

Israelachvili, J.N., *Intermolecular and Surface Forces*. 2005, Academic Press, London.

Karakashev, S.I., Nguyen, P.T., Tsekov, R., Hampton, M.A., Nguyen, A.V., Anomalous ion effects on rupture and lifetime of aqueous foam films formed from monovalent salt solutions up to saturation concentration. Langmuir, 2008, **24(20)**, 11587-11591.

Kirkpatrick, R.D., Lockett, M.J., The influence of approach velocity on bubble coalescence. Chemical Engineering Science, 1974, **29(12)**, 2363-2373.

Klassen, V.I., Mokrousov, V.A., *An Introduction to the Theory of Flotation*. 1963, Butterworths, London.

Kracht, W., Finch, J.A., Bubble break-up and the role of frother and salt. International Journal of Mineral Processing, 2009, **92(3-4)**, 153-161.

Kunz, W., Specific ion effects in colloidal and biological systems. Current Opinion in Colloid & Interface Science, 2010, **15**, 34-39.

Kurniawan, A.U., Ozdemir, O., Nguyen, A.V., Ofori, P., Firth, B., Flotation of coal particles in MgCl2, NaCl, and NaClO3 solutions in the absence and presence of Dowfroth 250. International Journal of Mineral Processing, 2011, **98(3-4)**, 137-144.

Laskowski, J.S., *Coal flotation and fine coal utilisation*. 2001, Elsevier, Amsterdam.

Lessard, R.R., Zieminski, S.A., Bubble coalescence and gas transfer in aqueous electrolytic solutions. Ind. Eng. Chem. Fun., 1971, **10(2)**, 260-269.

Marrucci, G., A theory of coalescence. Chemical Engineering Science, 1969, **24(6)**, 975-985.

Marrucci, G., Nicodemo, L., Coalescence of gas bubbles in aqueous solutions of inorganic electrolytes. Chem. Eng. Sci., 1967, **22(9)**, 1257-1265.

Meyer, E.E., Rosenberg, K.J., Israelachvili, J.N., Recent progress in understanding hydrophobic interactions. Proc. Natl. Acad. Sci. U. S. A. , 2006, **103**, 15739-15746.

Nguyen, A.V., Improved Approximation of Water Dielectric Permittivity for Calculation of Hamaker Constants. J. Colloid Interface Sci., 2000, **229(2)**, 648-651.

Nguyen, A.V., Harvey, P.A., Evans, G.M., Jameson, G.J., 2003. Coal flotation in electrolyte solutions, In *22nd Int. Miner. Process. Congr.*, Cape Town, South Africa, pp. 594 - 605.

Nguyen, A.V., Schulze, H.J., *Colloidal science of flotation*. 2004, Marcel Dekker, New York.

Nguyen, P.T., Hampton, M.A., Nguyen, A.V., Birkett, G., The influence of gas velocity, salt type and concnetration on transition concentration for bubble coalescence inhibition and gas holdup. Chemical Engineering Science, 2012, **90**, 33-39.

Nguyen, P.T., Nguyen, A.V., Drainage, rupture, and lifetime of deionized water films: effect of dissolved gases. Langmuir, 2010, **26(5)**, 3356-3363.

Ozdemir, O., Du, H., Karakashev, S.I., Nguyen, A.V., Celik, M.S., Miller, J.D., Understanding the role of ion interactions in soluble salt flotation with alkylammonium and alkylsulfate collectors. Advances in Colloid and Interface Science, 2011, **163(1)**, 1-22.

Prince, M.J., Blanch, H.W., Transition electrolyte concentrations for bubble coalescence. AIChE J., 1990, **36(9)**, 1425-1429.

Quinn, J.J., Kracht, W., Gomez, C.O., Gagnon, C., Finch, J.A., Comparing the effect of salts and frother (MIBC) on gas dispersion and froth properties. Minerals Engineering, 2007, **20(14)**, 1296-1302.

Weissenborn, P.K., Pugh, R.J., Surface tension of aqueous solutions of electrolytes: Relationship with ion hydration, oxygen solubility, and bubble coalescence. Journal of Colloid and Interface Science, 1996, **184(2)**, 550-563.

Yaminsky, V.V., Ohnishi, S., Vogler, E.A., Horn, R.G., Stability of aqueous films between bubbles. Part 1. the effect of speed on bubble coalescence in purified water and simple electrolyte solutions. Langmuir, 2010, **26(11)**, 8061-8074.

CHAPTER 5

A NOVEL METHODOLOGY FOR PREDICTING CRITICAL SALT CONCENTRATION OF BUBBLE COALESCENCE INHIBITION

Mahshid Firouzi and Anh V. Nguyen

Published in “The Journal of Physical Chemistry C”, 2014, 118-2, 1021-1026

5.1 ABSTRACT

Bubble coalescence in some salt solutions can be inhibited if the salt concentration reaches a critical concentration C_{cr}. There are three models available for C_{cr} in the literature, but fail to predict C_{cr} correctly. The first two models employ the van der Waals attraction power laws to establish C_{cr} from the discriminant of quadratic or cubic polynomials. To improve the two models, the third model uses the same momentum balance equation of the previous models, but different intermolecular force generated by water hydration with exponential decaying. The third prediction for C_{cr} requires the experimental input for film rupture thickness and is incomplete. We show further in this paper that the third model is incorrect. We propose a novel methodology for determining C_{cr} which resolves the mathematical uncertainties in modelling C_{cr} and can explicitly predict it from any relevant intermolecular forces. The methodology is based on the discovery that C_{cr} occurs at the local maximum of the balance equation for the capillary pressure, disjoining pressure and pressure of the Gibbs-Marangoni stress. The novel generic approach is successfully validated using non-linear equations for complicated disjoining pressure.

KEYWORDS: saline water, Gibbs-Marangoni effect, disjoining pressure, van der Waals attractions, electrical double-layer interactions

5.2 INTRODUCTION

Inorganic salts are known to significantly influence bubble coalescence in liquids, bubble size and distribution, gas holdup, gas-liquid interfacial area and bubble rise velocity, all of which critically govern many important devices (e.g., bubble columns, distillation towers and bioreactors) and industrial processes (e.g., dissolved air flotation used to prepare seawater fed to desalination plants, and induced air flotation used to recover valuable minerals from the earth's crust) (Bournival et al., 2012; Kracht and Finch, 2009; Kurniawan et al., 2011; Leja, 1982; Nguyen et al., 2003; Nguyen and Schulze, 2004; Nguyen et al., 2012; Paulson and Pugh, 1996; Quinn et al., 2007). The foaminess of ocean waves on the beach exemplifies the significant effect of salts in reducing bubble coalescence in nature. The experiments show that bubble coalescence can be significantly inhibited beyond a critical salt concentration, C_{cr} (also termed the transition concentration) (Christenson et al., 2008;

Craig et al., 1993; Hofmeier et al., 1995; Lessard and Zieminski, 1971; Marrucci and Nicodemo, 1967; Nguyen et al., 2012; Quinn et al., 2007). It is referred to as the critical concentration here because bubbles and liquid films undergo a transition from coalescence to non-coalescence at the critical moment when the opposing forces are balanced.

Despite the maturity of experimental techniques and evidence, a full theoretical understanding of inhibition of bubble coalescence in salt solutions is still lacking. So far, there are three models available in the literature to predict the critical salt concentrations (Chan and Tsang, 2005; Marrucci, 1969; Prince and Blanch, 1990). All of these models are based on the finding that at C_{cr}, salts can alter the interfaces of the intervening liquid films between bubbles, such that they change from mobile interfaces at low salt concentration to the immobile interfaces at high salt concentration [&]. Consequently, at C_{cr} the film drainage changes from the inertial regime at low salt concentration to the viscous regime at high salt concentration (Chan and Tsang, 2005; Parkinson and Ralston, 2010; Prince and Blanch, 1990; Yaminsky et al., 2010). At the transition from the inertial to viscous drainage regime, the pressure of the Gibbs-Marangoni stress can be sufficiently large to counterbalance the driving force of film rupture by the capillary pressure and attractive disjoining pressure. For example, Marrucci (1969) considered the London-van der Waals attraction in the pressure balance, and the corresponding expression for C_{cr} is obtained from the discriminant of the cubic polynomial as follows (Prince and Blanch, 1990):

$$C_{cr} = 0.084 \upsilon R_g T \left(\frac{\sigma A^2}{R} \right)^{1/3} \left(\frac{\partial \sigma}{\partial C} \right)^{-2} \tag{5.1}$$

where υ is the number of ions produced upon salt dissociation, R_g is the gas constant, T is the absolute temperature, A is the non-retarded Hamaker constant, R is the bubble radius, and σ and $\partial\sigma / \partial C$ are the surface tension and the surface tension gradient with respect to salt concentration, respectively.

Although the electromagnetically non-retarded London-van der Waals attraction is strong, it is very short-ranged, i.e., shorter than 10 nm, while gas bubbles in saline water normally coalesce at the film thickness larger than 40 nm. Therefore, it is argued that the electromagnetically retarded Casimir-van der Waals attraction acting over the distance of the rupture thickness of the film should be used in modelling the critical salt concentration (Prince and Blanch, 1990). The quadratic polynomial of the modified theory gives the following prediction for C_{cr} (Prince and Blanch, 1990):

$$C_{cr} = 0.707 \upsilon R_g T \left(\frac{\sigma B}{R} \right)^{1/2} \left(\frac{\partial \sigma}{\partial C} \right)^{-2} \tag{5.2}$$

where B is the retarded Hamaker constant. The authors also examined the effect of inertial drainage on C_{cr}, obtaining another prediction similar to Eq.(5.2), where the numerical constant is replaced by 1.181. It is noted that an exact value for the Hamaker constants in Eqs. (5.1) and (5.2) is difficult to determine. Indeed, using the advanced Lifshitz theory on van der Waals interaction energy we have recently shown (Firouzi and Nguyen, 2013) that the Hamaker constants were not correctly calculated by previous authors and both Eqs. (5.1) and (5.2) under-estimate the experimental results for C_{cr}.

In 2005, Chan and Tsang (2005) were not able to compare the two models for C_{cr} with their experimental results and modified the previous models by replacing the van der Waals attractions by the repulsive hydration forces. They argued that the Gibbs-Marangoni tangential stress produced by the surface tension gradient would not be strong enough to inhibit the bubble coalescence. Their prediction for C_{cr} is a function of the thickness of the film at rupture, h_{rup}, as follows:

$$C_{cr} = \upsilon \sigma R_g T \left(\frac{h_{rup}^2}{2R} \right) \left(\frac{\partial \sigma}{\partial C} \right)^{-2} \tag{5.3}$$

Since the film rupture thickness is usually unknown, the third model requires further experimental work to determine the thickness as the model input. The third model is incomplete because C_{cr} can usually be obtained using simple devices like a bubble column (Nguyen et al., 2012) and independent measurements of film rupture thickness are not required. We show below that this model is also incorrect.

In this paper, we present a new, generic method for predicting C_{cr} from the same starting equation of momentum balance for liquid flow inside thin films. This method resolves the mathematical uncertainties and incorrectness in modelling C_{cr} and can be used with complicated equations for intermolecular forces which likely play the key role in the bubble coalescence affair. Indeed, the failure of the third model is due to the fact that the proposed pressure balance equation cannot be broken down at the transition, which can be proved by using the new methodology. The outcome of our novel approach is the ability to explicitly predict C_{cr} from the known surface tension

of salt solutions and its concentration gradient, and the physical properties of air bubbles such as size and intermolecular forces.

5.3 MODEL DEVELOPMENT

The starting point of many modelling works in the area of bubble coalescence and thin liquid film drainage is the momentum balance as described by the Navier-Stokes equation for low Reynolds number flows within thin liquid films. This is a well-established area, known as the lubrication theory. Therefore, we do not repeat all the derivations here (details are available in Appendix 2) and consider the available generic result for pressure balance equation at the transition (Chan and Tsang, 2005; Prince and Blanch, 1990):

$$\frac{4C}{h^2 \upsilon R_g T}\left(\frac{\partial \sigma}{\partial C}\right)^2 - \frac{2\sigma}{R} + \Pi(h) = 0 \tag{5.4}$$

where $\Pi(h)$ is the disjoining pressure, h is the averaged film thickness, the first term is the pressure of the Gibbs-Marrangoni stress and the second term is the capillary pressure. In Eq. (5.4), the inertial effect on the film drainage is ignored.

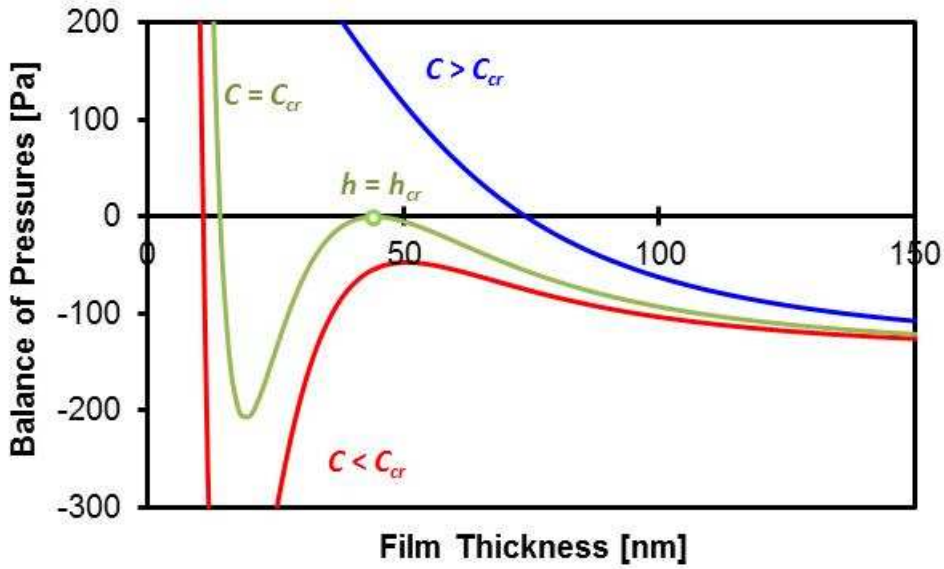

Figure 5.1**.** Variation of balance of pressure as described by the left hand side of Eq. (5.4) versus film thickness at three characteristic salt concentrations, i.e., small concentration ($C < C_{cr}$), high concentration ($C > C_{cr}$) and critical concentration ($C = C_{cr}$). The model parameters include: $R = 0.001\ \mathrm{m}$, $\nu = 2$, $\Pi(h) = -10000 \times \exp(-h/10)$ [Pa], $C_{cr} = 0.000629\ \mathrm{M}$ $T = 293\ \mathrm{K}$, $\sigma = 0.072\ \mathrm{N}$ and $\partial\sigma / \partial C = 0.001\ \mathrm{N \cdot m^{-1} \cdot M^{-1}}$.

Now the new modelling approach is developed based on the following analysis of Eq. (5.4) and discovery (occurrence of the C_{cr} at the local maximum of equation (5.4)). It is noted that when *h* is very large, the Gibbs-Marangoni pressure (first term) and the disjoining pressure (third term) of Eq. (5.12) approach zero, and the balance of pressures on the left hand side of Eq. (5.12) becomes negative (i.e., is equal to $-2\sigma / R$). Likewise as *h* approaches zero $1/h^2$ approaches infinity, and the balance of pressures becomes a large positive value. For intermediate values of film thickness, $10\ \mathrm{nm} < h < 100\ \mathrm{nm}$, the change in the balance of pressures depends to a significant extent on the variation of the disjoining pressure versus *h* as well as the salt concentration. For example, for a low salt concentration and an attractive (negative) disjoining pressure, the balance of pressures can increase from the negative value of $-2\sigma / R$ to a local maximum, pass through a local minimum and then increase to a large positive value (infinity) when the film thickness *h* decreases from a very large value (infinity) to a small value (zero). Shown in Figure 5.1 is the typical variation of the balance of pressures on the left hand side of Eq. (5.4) versus the film thickness and salt concentration. Without loss of generality, a single exponential dependence of the attractive disjoining pressure on the film

thickness, i.e., $\Pi = -A\exp\left(-h/\lambda\right)$, is used for the illustration in Figure 5.1. If the salt concentration is high, the balance of pressures does not exhibit any local maximum or minimum, i.e., it increases monotonically from the negative value of $-2\sigma/R$ (at $h \to \infty$) to $+\infty$ (at $h \to 0$) as shown in Figure 5.1.

The variation of the balance of pressures as illustrated in Figure 5.1, in conjunction with the available experimental observations, is important for our interpretation of the stability of aqueous films of salt solutions. Firstly, the aqueous films of salt solutions (surfactant-free films) are relatively thick and often rupture before becoming a very thin film of a thickness less than 20 nm. For those films of low salt concentrations ($C < C_{cr}$), the balance of pressures is negative and, therefore, Eq. (5.4) cannot be satisfied, i.e., it has no real solution for *h*. This nonexistence of a solution for *h* means that a (meta-) stable or (quasi-) equilibrated film cannot exist under the condition of low salt concentration. For high salt concentrations ($C > C_{cr}$), Eq. (5.4) can be satisfied, i.e., it has a real solution for *h* for the film stability, which is the horizontal coordinate of the intercept of the blue curve in Figure 5.1 with the horizontal axis – the existence of the solution for *h* means that a (meta-) stable or (quasi-) equilibrated film exists under the condition of high salt concentration. Critically, the transition from unstable to stable films occurs when Eq. (5.4) is just met, i.e., the curve of the balance of pressures just locally touches the horizontal axis as illustrated by the green curve in Figure 5.1. This condition can happen when the local maximum is equal to zero and can mathematically be described as follows:

$$\frac{4C_{cr}}{h_{cr}{}^{2}\upsilon R_g T}\left(\frac{\partial\sigma}{\partial C}\right)^{2}_{C=C_{cr}} - \frac{2\sigma}{R} + \Pi\left(h_{cr}\right) = 0 \tag{5.5}$$

$$-\frac{8C_{cr}}{h_{cr}{}^{3}\upsilon R_g T}\left(\frac{\partial\sigma}{\partial C}\right)^{2}_{C=C_{cr}} + \Pi'\left(h_{cr}\right) = 0 \tag{5.6}$$

$$\frac{24C_{cr}}{h_{cr}{}^{4}\upsilon R_g T}\left(\frac{\partial\sigma}{\partial C}\right)^{2}_{C=C_{cr}} + \Pi''\left(h_{cr}\right) < 0 \tag{5.7}$$

where h_{cr} is the (critical) thickness of the transition from its instability to stability, and the single or double primes describe the first and second derivatives of the disjoining pressure with respect to *h*. Equations (5.6) and (5.7) describe the position of the local maximum while Eq. (5.5) describes the condition where the value of the local maximum is equal to zero.

Equations (5.13) and (5.14) can be simultaneously solved for C_{cr} and h_{cr}. Mathematically, the two equations describe the necessary condition for finding a solution for C_{cr} and h_{cr}, while Eq. (5.7) is a sufficient condition for the local maximum to occur. Eqs. (5.6) and (5.7) have not been established previously. If Eq. (5.6) is not used, the solution of Eq. (5.5) for C_{cr} is uncertain because h_{cr} is unknown and many pairs of numerical values for C_{cr} and h_{cr} can be found to satisfy Eq. (5.5). This is the critical point of the previous papers (Chan and Tsang, 2005; Marrucci, 1969) which require experimental data for h_{cr} to remove the mathematical uncertainty. Eq. (5.7) provide a quick and helpful check whether or not a solution for C_{cr} exists mathematically. Indeed, the third modelling approach taken by Chan and Tsang (2005) fails to satisfy Eq. (5.7) and is proved to be incorrect as described in the following section.

5.4 FURTHER EVALUATIONS AND APPLICATIONS

Equations (5.5) to (5.7) present the new model prediction for determining C_{cr}. The new model also allows for the prediction of the critical film thickness, h_{cr}, of the transition from instability to stability of saline water film drainage or vice versa. The model is generic because it can be used *i*) to predict C_{cr} when a complicated/nonlinear isotherm for the disjoining pressure is employed, and *ii*) to establish the simple solutions for C_{cr} which were previously obtained from different simple models, such as those described by Eqs. (5.1) and (5.2). The details are shown below.

When the non-retarded van der Waals disjoining pressure, $\Pi = -A/6\pi h^3$ (here the non-retarded Hamaker constant, *A*, is a positive number), is used, Eqs. (5.5) to (5.7) gives

$$\frac{4C_{cr}}{h_{cr}{}^2 \upsilon R_g T}\left(\frac{\partial\sigma}{\partial C}\right)^2_{C=C_{cr}} - \frac{2\sigma}{R} - \frac{A}{6\pi h_{cr}{}^3} = 0 \tag{5.8}$$

$$-\frac{8C_{cr}}{h_{cr}{}^3 \upsilon R_g T}\left(\frac{\partial\sigma}{\partial C}\right)^2_{C=C_{cr}} + \frac{A}{2\pi h_{cr}{}^4} = 0 \tag{5.9}$$

$$\frac{24C_{cr}}{h_{cr}{}^4 \upsilon R_g T}\left(\frac{\partial\sigma}{\partial C}\right)^2_{C=C_{cr}} - \frac{2A}{\pi h_{cr}{}^5} < 0 \tag{5.10}$$

Solving these equations for the critical salt concentration and film thickness yields

$$C_{cr} = \left(\frac{3}{512\pi^2}\right)^{1/3} \upsilon R_g T \left(\frac{A^2\sigma}{R}\right)^{1/3} \left(\frac{\partial\sigma}{\partial C}\right)^{-2}_{C=C_{cr}} \tag{5.11}$$

$$h_{cr} = \left(\frac{AR}{24\pi\sigma}\right)^{1/3} \tag{5.12}$$

$$-\left(\frac{3A^2\sigma}{R\pi^2}\right)^{1/3} < 0 \tag{5.13}$$

Equation (5.11) is identical to Eq. (5.1) and the inequality (5.13) is automatically met, confirming the validity of the new model.

Likewise, for the retarded van der Waals disjoining pressure, $\Pi = -B / h^4$, solving Eqs. (5.5) to (5.7) yields

$$C_{cr} = \upsilon R_g T \left(\frac{B\sigma}{2R}\right)^{1/2} \left(\frac{\partial\sigma}{\partial C}\right)^{-2}_{C=C_{cr}} \tag{5.14}$$

$$h_{cr} = \left(\frac{BR}{2\sigma}\right)^{1/4} \tag{5.15}$$

$$-16\left(\frac{\sigma B}{2R}\right)^{1/2} < 0 \tag{5.16}$$

Again, Eq. (5.14) is identical to Eq. (5.2) and the inequality (5.16) is automatically met, validating the new model again.

Finally, when the repulsive hydration disjoining pressure, $\Pi = (W / \lambda)\exp(-h / \lambda)$, as proposed by Chan and Tsang (2005) is used, inserting the hydration disjoining pressure into Eqs. (5.5) to (5.7) gives

$$\frac{4C_{cr}}{h_{cr}{}^2 \upsilon R_g T}\left(\frac{\partial\sigma}{\partial C}\right)^2_{C=C_{cr}} - \frac{2\sigma}{R} + \frac{W}{\lambda}\exp\left(-\frac{h_{cr}}{\lambda}\right) = 0 \tag{5.17}$$

$$-\frac{8C_{cr}}{h_{cr}{}^3 \upsilon R_g T}\left(\frac{\partial\sigma}{\partial C}\right)^2_{C=C_{cr}} - \frac{W}{\lambda^2}\exp\left(-\frac{h_{cr}}{\lambda}\right) = 0 \tag{5.18}$$

$$\frac{24C_{cr}}{h_{cr}{}^{4}\upsilon R_g T}\left(\frac{\partial\sigma}{\partial C}\right)^{2}_{C=C_{cr}}+\frac{W}{\lambda^{3}}\exp\left(-\frac{h_{cr}}{\lambda}\right)<0 \tag{5.19}$$

where W is the pre-exponential (force) constant (positive) and λ is the decay length of the hydration force. Since the left hand side of Eq. (5.18) is always negative and inequation (5.19) is always positive, Eq. (5.18) and inequation (5.19) cannot be satisfied by any real values of the salt concentration and film thickness, and therefore no real solutions for C_{cr} and h_{cr} can be found from Eqs. (5.17) to (5.19). As a result, the proposal by Chan and Tsang (Chan and Tsang, 2005) to replace the van der Waals attractions by the repulsive hydration forces is physically inconsistent and cannot be justified (The hydration force is also very short range, i.e., the decay length of the hydration force is shorter than 2 nm (Butt, 1991; Cevc et al., 1995; Pashley, 1981, 1982; Pashley and Israelachvili, 1984) and cannot inhibit film rupture between two bubbles which occurs when the thickness is significantly larger than 2 nm).

Likewise, not only the repulsive hydration disjoining pressure, but any other (single or combined) repulsive disjoining pressure cannot be the main driving force for inhibiting the bubble coalescence in salt solutions. This is because in the case of the repulsive disjoining pressure being a decreasing function of the film thickness, first derivative of the pressure term in Eq. (5.6) is negative and the left hand side of Eq. (5.6) is negative, making Eq. (5.6) unsolvable mathematically. In the other cases, when a single repulsive disjoining pressure together with another attractive disjoining pressure provides a combined (summed) disjoining pressure with its first derivative being positive, Eq. (5.6) can be satisfied and a mathematical solution to the new model Eqs. (5.5) to (5.7) can be found. This case is demonstrated in the following.

In many cases, the disjoining pressure can have a number of components with compatible magnitudes at compatible separation distances, e.g., the van der Waals pressure and the electric double-layer pressure at relatively high salt concentrations. No model for C_{cr} in these complicated cases is available in the literature. Here we show that the new model proposed in this paper can be used with the complicated/nonlinear disjoining pressure. We consider the disjoining pressure as a sum of the retarded van der Waal interaction and the electrical double-layer interaction, i.e.,

$$\Pi=-\frac{B}{h^{4}}+64000CR_gT\tanh^{2}\left(\frac{z\psi F}{4R_gT}\right)\exp(-\kappa h) \tag{5.20}$$

where F is the Faraday constant, z is the ion valence of the symmetric z:z salt and ψ is the potential of the air-salt solution interface. The Debye constant is defined as

$$\kappa = \left\{ \frac{2000CF^2 z^2}{\varepsilon\varepsilon_0 R_g T} \right\}^{1/2} \tag{5.21}$$

where ε_0 and $\varepsilon = 80$ are the dielectric constants of the vacuum and water permittivity, respectively. In Eq. (5.20), the superposition approximation for the double-layer interaction (Nguyen and Schulze, 2004) is used for thick films of salt solutions, and the unit of mol/L is used for the salt concentration. Substituting Eq. (5.20) into Eqs. (5.5) to (5.7) gives

$$\frac{4C_{cr}}{h_{cr}{}^2 \upsilon R_g T}\left(\frac{\partial\sigma}{\partial C}\right)^2_{C=C_{cr}} - \frac{2\sigma}{R} - \frac{B}{h_{cr}{}^4} + 64000 C_{cr} R_g T \tanh^2\left(\frac{z\psi F}{4R_g T}\right)\exp(-\kappa h_{cr}) = 0 \tag{5.22}$$

$$-\frac{8C_{cr}}{h_{cr}{}^3 \upsilon R_g T}\left(\frac{\partial\sigma}{\partial C}\right)^2_{C=C_{cr}} + \frac{4B}{h_{cr}{}^5} - 64000\kappa C_{cr} R_g T \tanh^2\left(\frac{z\psi F}{4R_g T}\right)\exp(-\kappa h_{cr}) = 0 \tag{5.23}$$

$$\frac{24C_{cr}}{h_{cr}{}^4 \upsilon R_g T}\left(\frac{\partial\sigma}{\partial C}\right)^2_{C=C_{cr}} - \frac{20B}{h_{cr}{}^6} + 64000\kappa^2 C_{cr} R_g T \tanh^2\left(\frac{z\psi F}{4R_g T}\right)\exp(-\kappa h_{cr}) < 0 \tag{5.24}$$

Equations (5.22) to (5.23) can be solved by applying a numerical technique. Using MATLAB code developed by our team, Eqs. (5. 22) to (5.24) are successfully solved simultaneously. The retarded Hamaker constant can be determined accurately by fitting the retarded van der Waals disjoining pressure, $\Pi = -B / h^4$, with the exact data of the Lifshitz theory and the full dielectric spectrum for water (Nguyen, 2000; Nguyen and Schulze, 2004), giving $B = 3.492\times10^{-29}$ Jm (The zero-frequency term in salt solutions of high concentration is negligibly small and is not considered here) (Firouzi and Nguyen, 2013). As an example, NaCl is used for the numerical calculation of C_{cr} and h_{cr}. The numerical solutions obtained for films of NaCl solutions are C_{cr}= 45 mM and h_{Cr}=25.6 nm for R = 1.8 mm[&&]. The additional experimental data needed in the calculation for NaCl solution films are as follows. The potential of the interface between air and NaCl solutions can be measured by microelectrophoresis using a Rank-Brothers zeta meter MK II (Rank Brothers Ltd, Cambridge, England) and fine air bubbles of 20 μm in diameter. Shown in Figure 5.2 are the experimental results (points) and the empirical approximation (line) for the modelling:

$\psi = 1.097(\log C)^2 + 17.110 \log C + 0.155$, where the units of potential and concentration are mV and mol/L, respectively. At 23 ºC, Eq. (5.21) gives $\kappa = 3.239\sqrt{C}$, where the units of the Debye constant and concentration are given in nm^{-1} and mol/L, respectively. As shown in Figure 5.3, the surface tension for NaCl solutions at 23 ºC can be approximated by $\sigma = 0.0724 + 1.704 \times 10^{-3} C$, where the units for surface tension and concentration are N/m and mol/L, respectively.

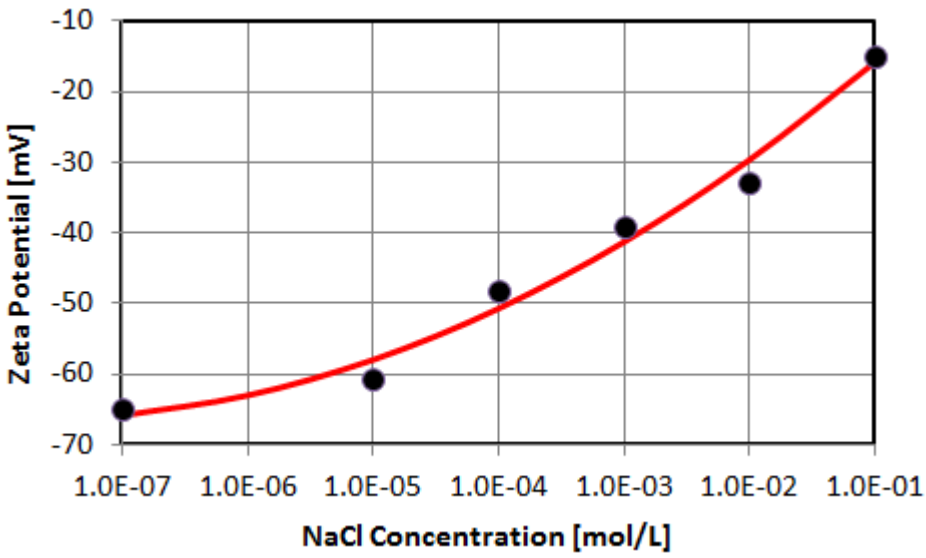

Figure 5.2. Zeta potential of air-NaCl interface versus NaCl concentration at pH=5.8.

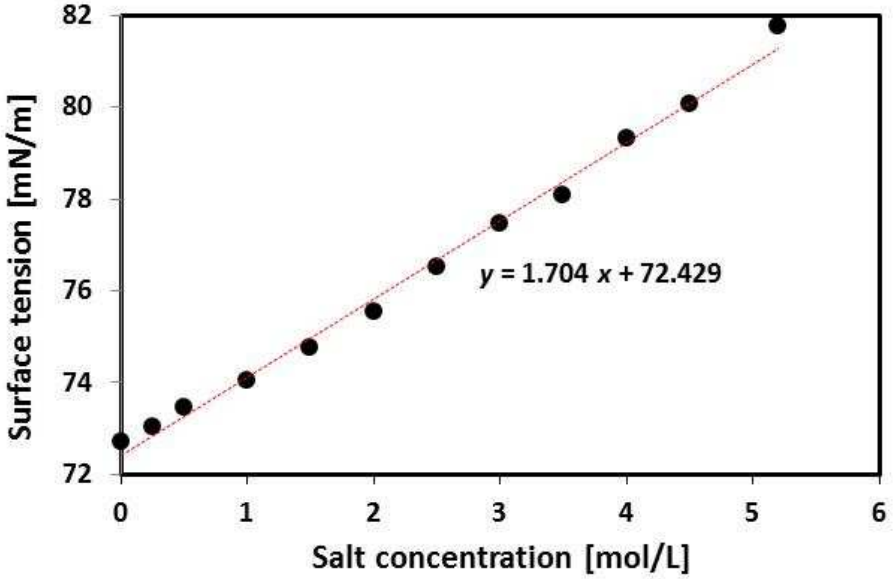

Figure 5.3. Surface tension of NaCl solutions versus concentration up to saturation at 23 ^{o}C (Ozdemir et al., 2009).

The calculated result for $C_{cr} = 0.045\,\text{mol/L}$ is significantly different from the experimental results of 0.175 mol/L for NaCl solutions and for the bubble radius of 1.8 mm, as reported by Lessard and Zieminski (Lessard and Zieminski, 1971). The calculated result of $h_{cr} = 25.626\,\text{nm}$ is also too small compared with the experimental results for salt solution films (Karakashev et al., 2008). This significant difference indicates that there may be another attractive disjoining pressure, much stronger than the retarded van der Waals attraction, causing the film to rupture at larger thicknesses. Indeed, similar to the retarded van der Waals attraction, an empirical power-law dependence of hydrophobic attraction on thickness was reported for the foam films stabilized by surfactants (Wang and Yoon, 2004). Therefore, here we allow the force parameter *B* in Eqs. (5.22) - (5.24) to change and it is found that if $B = 52\times10^{-29}\,\text{Jm}$, the model gives the same results for $C_{cr} = 0.175\,\text{mol/L}$ as experimentally determined for NaCl. Evidently, the new force parameter is greater by an order of magnitude than $B = 3.492\times10^{-29}\,\text{Jm}$ for the retarded van der Waals attraction. The new critical thickness is equal to $h_{cr} = 50.302\,\text{nm}$, which is within the range of the available experimental results (Karakashev et al., 2008). These new results show the weakness of the van der Waals attractions (which would cause the film rupture and bubble coalescence) in balancing the pressure of the Gibbs-Marangoni stress (which

would inhibit the film rupture and bubble coalescence) at the experimental critical concentrations. In the other words, to be able to predict the experimental critical concentration and thickness, which are far greater than the predictions of the available model using the weak van der Waals attractive disjoining pressures, strong attractive non-DLVO disjoining pressures are required. This demands further investigation and modification in the theoretical predictions of the critical concentration of salts.

5.5 CONCLUSIONS

In this paper we developed a novel methodology for predicting C_{cr}. We have shown that C_{cr} occurs at the local maximum of the pressure balance equation for capillary pressure, disjoining pressure and pressure of the Gibbs-Marangoni stress. We also showed that the previous simple predictions for C_{cr} could be obtained from our new, generic model described by Eqs. (5.5) - (5.7) when the van der Waals disjoining pressure is applied. We showed further that the hydration repulsive disjoining pressure could not be used to predict C_{cr} since the model equations have no solutions for C_{cr} and h_{cr} in this case, and the hydration repulsion is too short-ranged to affect the rupture of aqueous films of salt solutions at larger thicknesses. We successfully used the new model to demonstrate the solution for C_{cr} and h_{cr} when the retarded Casimir-van der Waals disjoining pressure and the electrical double-layer disjoining pressure were applied. Comparing the new model with the experimental results for C_{cr} and h_{cr} for NaCl solutions, it showed that the retarded van der Waals disjoining pressure would not be strong enough to cause the film to rupture at high NaCl concentrations. Indeed, if a strong hydrophobic attraction is used in the model, the matching of the model results and the experimental data for C_{cr} for NaCl solutions is obtained, also giving a physically consistent solution for h_{cr}. The pressure constant of the power-law dependence of hydrophobic attraction on film thickness is greater, by an order of magnitude, than the Hamaker constant for the retarded van der Waals attraction. Further investigation to elucidate the role of hydrophobic attraction in determining C_{cr} and h_{cr} is needed.

ACKNOWLEDGMENTS

The authors gratefully acknowledge the financial support from the Australian Research Council (Grant DP0985079). The assistance of Ms Kitty Tang in measuring the surface potential is warmly acknowledged.

REFERENCES

Bournival, G., Pugh, R.J., Ata, S., Examination of NaCl and MIBC as bubble coalescence inhibitor in relation to froth flotation. Miner. Eng., 2012, 25(1), 47-53.

Butt, H.J., Measuring electrostatic, van der Waals, and hydration forces in electrolyte solutions with an atomic force microscope. Biophys. J., 1991, 60(6), 1438-1444.

Cevc, G., Hauser, M., Kornyshev, A.A., Effects of the Interfacial Structure on the Hydration Force between Laterally Nonuniform Surfaces. Langmuir, 1995, 11(8), 3111-3118.

Chan, B.S., Tsang, Y.H., A theory on bubble-size dependence of the critical electrolyte concentration for inhibition of coalescence. J. Colloid Interface Sci., 2005, 286(1), 410-413.

Christenson, H.K., Bowen, R.E., Carlton, J.A., Denne, J.R.M., Lu, Y., Electrolytes that Show a Transition to Bubble Coalescence Inhibition at High Concentrations. Journal of Physical Chemistry C, 2008, 112(3), 794-796.

Craig, V.S.J., Ninham, B.W., Pashley, R.M., Effect of electrolytes on bubble coalescence. Nature, 1993, 364(6435), 317-319.

Firouzi, M., Nguyen, A.V., On the effect of van der Waals attractions on the critical salt concentration for inhibiting bubble coalescence (Accepted). Minerals Engineering, 2013.

Henry, C.L., Parkinson, L., Ralston, J.R., Craig, V.S.J., A Mobile Gas-Water Interface in Electrolyte Solutions. Journal of Physical Chemistry C, 2008, 112(39), 15094-15097.

Hofmeier, U., Yaminsky, V.V., Christenson, H.K., Observations of solute effects on bubble formation. J. Colloid Interface Sci., 1995, 174(1), 199-210.

Karakashev, S.I., Nguyen, P.T., Tsekov, R., Hampton, M.A., Nguyen, A.V., Anomalous ion effects on rupture and lifetime of aqueous foam films formed from monovalent salt solutions up to saturation concentration. Langmuir, 2008, 24(20), 11587-11591.

Kracht, W., Finch, J.A., Bubble break-up and the role of frother and salt. International Journal of Mineral Processing, 2009, 92(3-4), 153-161.

Kurniawan, A.U., Ozdemir, O., Nguyen, A.V., Ofori, P., Firth, B., Flotation of coal particles in MgCl2, NaCl, and NaClO3 solutions in the absence and presence of Dowfroth 250. International Journal of Mineral Processing, 2011, 98(3-4), 137-144.

Leja, J., Surface Chemistry of Froth Flotation. 1982, Plenum Press, New York, NY.

Lessard, R.R., Zieminski, S.A., Bubble coalescence and gas transfer in aqueous electrolytic solutions. Ind. Eng. Chem. Fun., 1971, 10(2), 260-269.

Marrucci, G., Theory of coalescence. Chemical Engineering Science, 1969, 24(6), 975-985.

Marrucci, G., Nicodemo, L., Coalescence of gas bubbles in aqueous solutions of inorganic electrolytes. Chem. Eng. Sci., 1967, 22(9), 1257-1265.

Nguyen, A.V., Improved Approximation of Water Dielectric Permittivity for Calculation of Hamaker Constants. J. Colloid Interface Sci., 2000, 229(2), 648-651.

Nguyen, A.V., Harvey, P.A., Evans, G.M., Jameson, G.J., 2003. Coal flotation in electrolyte solutions, In 22nd Int. Miner. Process. Congr., Cape Town, South Africa, pp. 594 - 605.

Nguyen, A.V., Schulze, H.J., Colloidal science of flotation. 2004, Marcel Dekker, New York.

Nguyen, P.T., Hampton, M.A., Nguyen, A.V., Birkett, G., The influence of gas velocity, salt type and concnetration on transition concentration for bubble coalescence inhibition and gas holdup. Chemical Engineering Science, 2012, 90, 33-39.

Ozdemir, O., Karakashev, S.I., Nguyen, A.V., Miller, J.D., Adsorption and surface tension analysis of concentrated alkali halide brine solutions. Minerals Engineering, 2009, 22(3), 263-271.

Parkinson, L., Ralston, J., The Interaction between a Very Small Rising Bubble and a Hydrophilic Titania Surface. The Journal of Physical Chemistry C, 2010, 114(5), 2273-2281.

Pashley, R.M., Hydration forces between mica surfaces in aqueous electrolyte solutions. J. Colloid Interface Sci., 1981, 80(1), 153-162.

Pashley, R.M., Hydration forces between mica surfaces in electrolyte solutions. Advances in Colloid and Interface Science, 1982, 16, 57-62.

Pashley, R.M., Israelachvili, J.N., DLVO and hydration forces between mica surfaces in magnesium(2+), calcium(2+), strontium(2+), and barium(2+) chloride solutions. J. Colloid Interface Sci., 1984, 97(2), 446-455.

Paulson, O., Pugh, R.J., Flotation of Inherently Hydrophobic Particles in Aqueous Solutions of Inorganic Electrolytes. Langmuir, 1996, 12(20), 4808-4813.

Prince, M.J., Blanch, H.W., Transition electrolyte concentrations for bubble coalescence. AIChE Journal, 1990, 36(9), 1425-1429.

Quinn, J.J., Kracht, W., Gomez, C.O., Gagnon, C., Finch, J.A., Comparing the effect of salts and frother (MIBC) on gas dispersion and froth properties. Miner. Eng., 2007, 20(14), 1296-1302.

Wang, L., Yoon, R.-H., Hydrophobic Forces in the Foam Films Stabilized by Sodium Dodecyl Sulfate: Effect of Electrolyte. Langmuir, 2004, 20(26), 11457-11464.

Yaminsky, V.V., Ohnishi, S., Vogler, E.A., Horn, R.G., Stability of aqueous films between bubbles. Part 1. The effect of speed on bubble coalescence in purified water and simple electrolyte solutions. Langmuir, 2010, 26(11), 8061-8074.

[&] It is noted that the bubble rise velocity is mainly affected by buoyancy which is significantly stronger than the effect of inorganic salts. The changes in boundary conditions affected by salts are too weak to be detected by changes in the bubble rise velocity (Henry et al., 2008). Indeed, the boundary condition affected by salts can be probed by changes in the interfacial physics and intermolecular forces governing liquid film drainage between two approaching (colliding) bubbles. The important role of salts in thin liquid film drainage is discussed in the recent literature (Henry et al., 2008): “We must acknowledge that there are differences between a single bubble rising in a quiescent fluid and the thinning of a film between two colliding bubbles. Diffusion of electrolyte from the bulk to the interface, which arrests any induced surface tension gradient, is likely to be different, particularly if the film is very thin. Additionally, the presence of surface forces may influence the distribution of ions in a thin film”. The transition from mobile to immobile air-water interfaces in salt

solutions is established by experiments with colliding bubbles (Parkinson and Ralston, 2010). Immobile (no-slip) boundary condition at the film interface between air and KCl solutions is confirmed when the bubble approaches the solid surface. It is also confirmed that the bubbles terminal velocities in the same KCl solutions displays full slip boundary condition at the air-solution interface of air bubbles in KCl solutions. It is further suggested that a surface tension gradient can be established during drainage of a thin liquid film even in the case of very clean air-water interface (Yaminsky et al., 2010). Indeed, the radial plug flow in the thin liquid film results in a non-uniform ion distribution in the surface which leads to a surface tension gradient sufficiently large to alter the air-bubble interface from mobile to partially mobile or immobile interface. Evidently, the effect of salts on film drainage and instability is significant and cannot be contrasted by the bubble rise velocity.

&& The bubble radius of R = 1.8 mm is as reported by Lessard and Zieminski (1971). The effect of bubble radius on the calculated critical concentration of NaCl is relatively weak. For example, for R = 1.8, 2 and 2.05 mm, the calculated critical concentrations of NaCl are 0.045, 0.043 and 0.042 mol/L, respectively. The concentration variation is within experimental errors.

.

CHAPTER 6

CRITICAL SALT CONCENTRATION IN BUBBLE COALESCENCE INHIBITION: EFFECT OF DISSOLVED GASES AND HYDROPHOBIC ATTRACTION

Mahshid Firouzi and Anh V. Nguyen

Submitted to “The Journal of Physical Chemistry C”, July 2014

6.1 ABSTRACT

Some salts can inhibit bubble coalescence above a critical concentration, called the "transition concentration". The available models fail to predict these critical salt concentrations correctly. In this paper, a novel model for predicting the transition concentration reveals the critical role of hydrophobic attractions and gas solubility in bubble coalescence in salt solutions. The hydrophobic disjoining pressure is predicted by the phenomenological theory for hydrophobic attractions developed by Eriksson et al. The model parameters of hydrophobic strength and decay length were obtained using our experimental results for the critical concentration and film thickness of NaF, NaBr, NaI, NaCl, KCl and LiCl aqueous solutions. The Pitzer theory for the solution activity was applied to predict the critical salt concentration. A power law correlation was proposed to evaluate the hydrophobic strength as a function of the salting-effect coefficient representing the salt type. The strength was shown to increase with increasing gas (oxygen) solubility in brine solutions. The decay length of hydrophobic attractions was obtained as 15.78±0.09 nm for the salt solutions, which agrees with the previous results obtained for different systems.

KEYWORDS: critical film thickness, gas solubility, saline water, Gibbs-Marangoni effect, disjoining pressure, hydrophobic attraction, van der Waals attractions

6.2 INTRODUCTION

Inhibition of bubble coalescence by salts has been applied in many areas such as surface and colloid chemistry, biology, biochemistry, tertiary oil recovery, foam fractionation and mineral flotation. The idea of the stabilizing effect of common salts such as NaCl at concentrations above a transition (critical) concentration on bubble coalescence has stemmed from the comparison of foaminess of the ocean with fresh water. The stabilizing effect of salts has been experimentally investigated by different techniques, including 1) monitoring the bubble population by measuring the solution turbidity or bubble size distribution in a bubble column (Craig et al., 1993; Marrucci and Nicodemo, 1967; Nguyen et al., 2012), 2) contacting a pair of bubbles and determining the percentage of coalescence by counting the number of coalescing bubbles compared to the total number of contacted bubbles (Christenson et al., 2007; Kirkpatrick and Lockett, 1974; Lessard and Zieminski, 1971) and 3) measuring the lifetime of the thin liquid film of salt solutions between bubbles using an optical interferometric method (Firouzi and Nguyen, 2014a; Karakashev et al., 2008). Electric double layer repulsions (Miklavcic, 1996), hydration repulsions (Chan and Tsang, 2005; Tsao and Koch, 1994), the Gibbs-Marangoni effect (Christenson et al., 2007; Marrucci and Nicodemo, 1967;

Yaminsky et al., 2010), gas solubility and hydrophobic attractions (Craig et al., 1999; Nguyen and Nguyen, 2009; Weissenborn and Pugh, 1996) have been proposed to explain the inhibition of bubble coalescence in salt solutions. However, to date there is no consensus on a mechanism to explain the inhibiting effect of all salts on bubble coalescence.

Despite many experimental investigations on bubble coalescence in salt solutions, there are few theoretical studies on the modelling of the inhibiting effect of salts. The first theoretical model to predict the critical salt concentration was proposed by Marrucci (1969). This model is based on balancing the capillary pressure and the non-retarded London-van der Waals attraction with an opposing force owing to a change in the surface excess of salts, called the Gibbs-Marangoni stress. The Gibbs-Marangoni stress caused by surface tension gradient can tangentially immobilize the film surfaces at high salt concentration. Thus, the transition from the inertial (at low salt concentration) to viscous (at high salt concentration) drainage inside the thin film occurs at the critical salt concentration. The second model proposed by Prince and Blanch (1990) modified the first model by incorporating the effect of inertia and replacing the non-retarded London-van der Waals attraction by the retarded Casimir-van der Waals attraction. The predicted critical salt concentrations are in close agreement with the experimental results. However, they determine the “unknown” retarded Hamaker constant based on the best fit of the model into the experimental results of Marrucci & Nicodemo (1967) and Lessard & Zieminski (1971). Recently, we accurately determined the Hamaker constants by employing the advanced Lifshitz theory on van der Waals interaction energy (Firouzi and Nguyen, 2014b). By considering these Hamaker constants, we demonstrated that these two models significantly under-predict the experimental critical concentration of salts.

In 2005, Chan and Tsang (2005) argued that the Gibbs-Marangoni tangential stress produced by the surface tension gradient would not be sufficiently strong to inhibit bubble coalescence and the van der Waals force would also be weak relative to the Laplace pressure (Typically, it is only equal to about 2% of the Laplace pressure). Therefore, they modified the previous models by replacing the van der Waals attractions by the repulsive hydration force. It was recently shown that the consideration of repulsive hydration forces as well as any other (single or combined) repulsive disjoining pressure as the main driving force for inhibiting bubble coalescence in salt solutions would be physically inconsistent (Firouzi and Nguyen, 2013). Thus, the failure of the available models in predicting the critical salt concentration highlights the urgent need of revising the available theories on bubble coalescence in salt solutions. We previously demonstrated that considering another attraction with a power law dependence on the film thickness similar to van der Waals attractions and

assigning a value of 5.2×10^{-28} J.m to the force constant would result in a critical thickness and concentration very close to the experimental values for NaCl solutions (Firouzi and Nguyen, 2013). The required force constant which is one order of magnitude larger than the retarded Hamaker constant ($B = 3.492\times10^{-29}$ J.m) indicates that another attractive disjoining pressure, stronger than the retarded van der Waals attraction, should be taken into account in the models.

Force measurements between hydrophobic surfaces confirm the existence of significantly stronger attractions (in range and strength) than van der Waals attractions. These attractions are referred to as hydrophobic forces and are ascribed to such mechanisms as bridging sub-microscopic bubbles, induced cavitation, electrostatic forces and rearrangement of water structure (Craig et al., 1999; Hampton and Nguyen, 2010; Stevens et al., 2005; Yaminsky and Ninham, 1993). Therefore, in view of the experimental evidence it could be hypothesised that the missing attractions in the theoretical models are hydrophobic attractions. This paper aims to modify the theoretical models to predict the critical concentration and film thickness of salt solutions by incorporating hydrophobic attractions.

6.3 THEORETICAL ANALYSIS

6.5.1 PREDICTION OF CRITICAL SALT CONCENTRATION

By analysing the film drainage in the same generic way presented initially by Marrucci (1969), we can derive the following pressure balance equation at the transition from viscous to inertial drainage:

$$-\frac{4\Gamma}{h^2}\frac{d\sigma}{dC}-\frac{2\sigma}{R}+\Pi(h)=0 \tag{6.1}$$

where $d\sigma/dC$ is the surface tension gradient with respect to the salt molar concentration, *C*, *h* is the film thickness, Γ is the Gibbs surface excess, and $2\sigma/R$ and $\Pi(h)$ are the capillary and disjoining pressures, respectively. The Gibbs surface excess (adsorption) is calculated from the Gibbs adsorption isotherm (Marrucci and Nicodemo, 1967):

$$\Gamma=-\frac{1}{\upsilon R_g T}\frac{d\sigma}{d\ln(a)} \tag{6.2}$$

where *a* is the activity of the salt solution. For dilute solutions (< 1 mM), the solution activity coefficient, γ, is close to 1 and the activity is numerically equal to the salt concentration. For high salt concentrations, the salt solution activity can be related to the concentration using the Pitzer theory

(Harvie and Weare, 1980; Kim and Frederick, 1988; Pitzer, 1973), which gives $a = \gamma m$, where m is the salt concentration in molality (mole per kilogram of solvent). For the activity coefficient of ions dissociated from single salts described as *MX*, the Pitzer theory at 25°C gives:

$$\ln\gamma = -\left|z_M z_X\right| 0.392\left[\frac{\sqrt{I}}{1+b\sqrt{I}} + \frac{2}{b}\ln\left(1+b\sqrt{I}\right)\right] + 4m\left(\frac{\upsilon_M \upsilon_X}{\upsilon}\right)\left(B_{MX} + \frac{I}{2}B'_{MX}\right) + 6m^2\left(\frac{\upsilon_M \upsilon_X}{\upsilon}\right)\upsilon_M z_M \frac{C^{\phi}_{MX}}{2\left|z_M z_X\right|^{1/2}} \tag{6.3}$$

where z and υ are the charge and stoichiometric coefficients of the salt ions, and *M* and *X* refer to a cation and anion respectively. B_{MX} and B'_{MX} describe the interaction parameters for the oppositely charged ions which are functions of the solution ionic strength, *I*, as follows:

$$B_{MX} = \beta_0 + \beta_1 f\left(\alpha_1\sqrt{I}\right) + \beta_2 f\left(\alpha_2\sqrt{I}\right) \tag{6.4}$$

$$B'_{MX} = \frac{\beta_1 f'\left(\alpha_1\sqrt{I}\right) + \beta_2 f'\left(\alpha_2\sqrt{I}\right)}{I} \tag{6.5}$$

where $f(x) = 2\left[1-(1+x)\exp(-x)\right]/x^2$ and $f'(x) = 2\left[1-\left(1+x+0.5x^2\right)\exp(-x)\right]/x^2$. β_i for i = 0, 1, and 2 and C^{ϕ}_{MX} are the Pitzer coefficients. For monovalent salts, only the first two terms of Eqs. (6.4) and (6.5) are considered and $\alpha_1 = 2$. For higher valence type electrolytes, such as 2-2 electrolytes, the full equations are to be used and $\alpha_1 = 1.4$ and $\alpha_2 = 12$ (Kim and Frederick, 1988).

Substituting Eq.(6.2) for the expression for surface excess into Eq. (6.1) yields

$$\frac{4C\phi}{h^2 \upsilon R_g T}\left(\frac{d\sigma}{dC}\right)^2 - \frac{2\sigma}{R} + \Pi(h) = 0 \tag{6.6}$$

where $\phi = 1/\left(1 + d\ln\gamma / d\ln C\right)$.

Figure 6.1 shows the surface tension of some monovalent salts versus salt concentration. The results show that the slope of salt surface tension versus salt concentration, $K = d\sigma / dC$, is constant in the investigated range of salt concentrations of interest. Therefore, *K* is considered as a constant for salts to determine the critical salt concentrations which are of the order of 0.1 M for most of the monovalent salts. Since *K* is a key factor in our calculations, we obtained the most reliable experimental values for each salt by collecting the experimental data available in the literature and applying least-square regression analysis. The results are presented in Table A3.1 in Appendix 3.

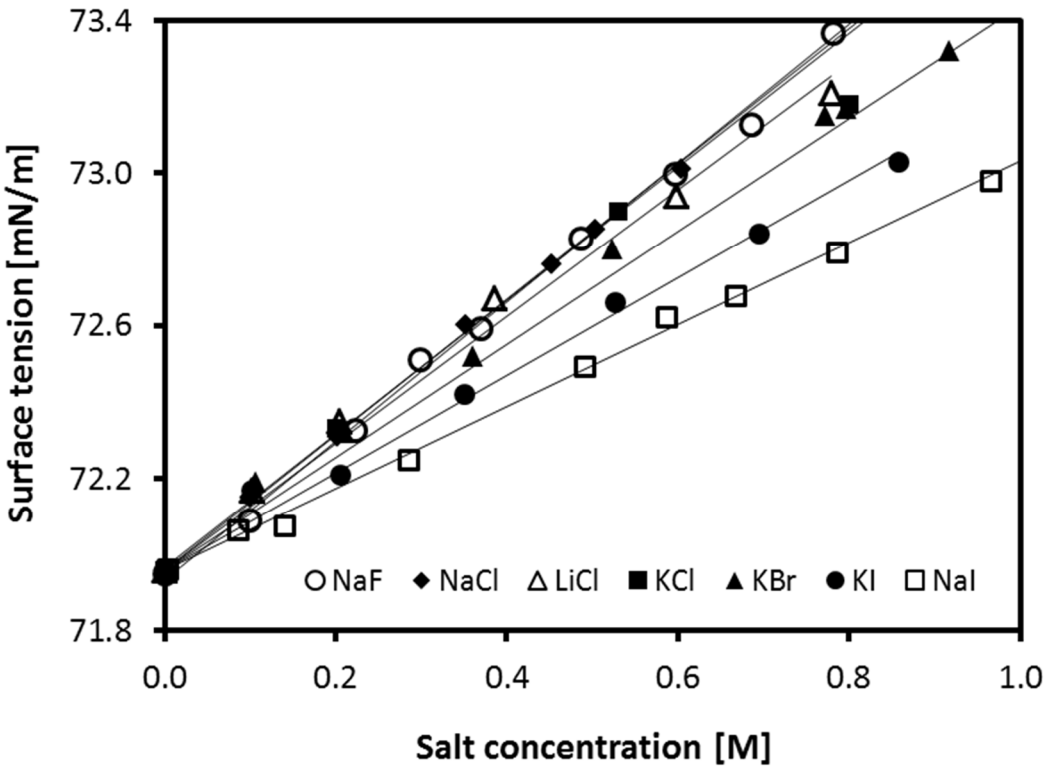

Figure 6.1. Surface tension of monovalent salts versus salt concentration at 20°C. Data are taken from (Aveyard and Saleem, 1976; Matubayasi et al., 2001).

Our generic modelling approach (Firouzi and Nguyen, 2013) shows that the transition from unstable to stable films occurs when the local maximum of Eq. (6.6) is equal to zero and can mathematically be described as follows:

$$\frac{4C_{cr}\phi}{h_{cr}^{2}\upsilon R_g T}K^2-\frac{2\sigma}{R}+\Pi\left(h_{cr}\right)=0 \tag{6.7}$$

$$\frac{8C_{cr}\phi}{h_{cr}^{3}\upsilon R_g T}K^2-\Pi'\left(h_{cr}\right)=0 \tag{6.8}$$

$$\frac{24C_{cr}\phi}{h_{cr}^{4}\upsilon R_g T}K^2+\Pi''\left(h_{cr}\right)<0 \tag{6.9}$$

where C_{cr} and h_{cr} are the critical concentration and film thickness of liquid films (referred to as the critical thickness of rupture of saline liquid films) at the transition from stability to instability. $\Pi\left(h_{cr}\right)$ is the disjoining pressure evaluated at the critical thickness. $\Pi'\left(h_{cr}\right)$ and $\Pi\left(h_{cr}\right)''$ are the first and

second derivatives of disjoining pressure with respect to film thickness, evaluated at the critical film thickness.

Van der Waals (vdW) attractions, electrostatic double layer (EDL) repulsions, hydration repulsions and hydrophobic attractions form the components of the disjoining pressure within the liquid film between two bubbles, referred to as the foam film. The hydration repulsions which arise from the strongly bound and uniformly oriented first layer of water molecules are very short-ranged, with the decay length shorter than 2 nm (Israelachvili and Wennerstrom, 1996; Pashley, 1982). Therefore, these short-ranged repulsions cannot inhibit rupture of the foam film, which occurs within a range of tens of nanometres (Weissenborn and Pugh, 1996). The EDL repulsions are much weaker than vdW attractions in the range of film thickness and salt concentration encountered during the coalescence of bubbles. Therefore, EDL repulsions need not be considered in modelling and predicting the critical salt concentration (Sagert and Quinn, 1978). The effect of vdW and hydrophobic attractions on bubble coalescence in salt solutions is discussed in detail in the following section.

6.5.2 VAN DER WAALS FORCE

Van der Waals (vdW) attractions are considered as short-ranged (London-) and long-ranged (Casimir-) van der Waals attractions. Although the non-retarded London-van der Waals attraction is strong, it is very short-ranged, i.e., shorter than 10 nm (Israelachvili, 2005). Coalescence of gas bubbles normally occurs at the thickness of saline water films greater than 30 nm. Therefore, the retarded Casimir-van der Waals attraction is the appropriate prediction for the contribution of vdW attractions and results in the following expression for the disjoining pressure in Eq. (6.7):

$$\Pi\left(h_{cr}\right) = -\frac{H}{h_{cr}^{\ 4}} \tag{6.10}$$

where H is the retarded Hamaker constant. The H value was previously evaluated to be $H = 5.397 \times 10^{-29}\,\mathrm{J \cdot m}$ by applying the advanced Lifshitz theory on a water film between two air bubbles (Firouzi and Nguyen, 2014b). It was also shown that the H value for foam films of salt solutions decreased to $H = 3.492 \times 10^{-29}\,\mathrm{J \cdot m}$ owing to the screening effect of salts on the zero-frequency term.

6.5.3 HYDROPHOBIC FORCE

Hydrophobic attractions are believed to be considerably stronger than vdW attractions (Meyer et al., 2004; Pashley and Craig, 1997). Hydrophobic forces between macroscopic (solid) hydrophobic surfaces have generally been found to increase with the hydrophobicity of the surfaces, as conventionally defined by the water contact angle. The first direct measurements of the hydrophobic force showed that the attraction has a very long range and decays exponentially as $\Pi_h(H) = K_h \exp(-h/l)$ where l is the decay length and K_h is a constant (Israelachvili and Pashley, 1982). Since the first measurements, experimental data have shown that the attraction between hydrophobic surfaces is strong and long-ranged and can be empirically described by a double exponential function of two decay lengths as $\Pi_h = K_h \exp(-h/l) + K_h^* \exp(-h/l^*)$. Alternatively, the measured hydrophobic attraction can be described by a power law similar to vdW interactions (Claesson et al., 1986; Yoon et al., 1997) as $\Pi_h = K_{232}/h^3$, where the empirical constant, K_{232}, is obtained from the best fit to experimental data. These empirical correlations have no real physical basis, and they only describe the difference between DLVO prediction and experimental data for surface forces (Attard et al., 2002; Christenson and Claesson, 2001; Hampton and Nguyen, 2010; Nguyen et al., 2003; Steitz et al., 2003; Yang et al., 2003). To examine the effect of these strong attractions, we use the phenomenological theory for the hydrophobic attraction developed by Eriksson et al. (Eriksson et al., 1989). The following equation can be established for the hydrophobic disjoining pressure by differentiating Eq. (28) of Eriksson et al.'s paper (Eriksson et al., 1989):

$$\Pi_{Hyd} = \frac{-B}{4\pi\lambda} \frac{1}{\sinh^2(h/2\lambda)} \tag{6.11}$$

where B and λ are the strength and decay length of the hydrophobic disjoining pressure, respectively. This model is based on the mean-field theory employing the idea that the hydrophobic attractions arise from the structural changes within a liquid film between two hydrophobic surfaces (Eriksson et al., 1989).

Expressing the disjoining pressure in Eqs. (6.7)- (6.9) as the sum of retarded vdW attraction and hydrophobic attraction gives the following final governing equations:

$$\frac{4C_{cr}\phi}{h_{cr}^2 \upsilon R_g T} K^2 - \frac{2\sigma}{R} - \frac{H}{h_{cr}^4} - \frac{B}{4\pi\lambda} \operatorname{csch}^2\left\{\frac{h_{cr}}{2\lambda}\right\} = 0 \tag{6.12}$$

$$\frac{8C_{cr}\phi}{h_{cr}{}^{3}\upsilon R_g T}K^2 - \frac{4H}{h_{cr}{}^{5}} - \frac{B}{4\pi\lambda^2}\operatorname{csch}^3\left\{\frac{h_{cr}}{2\lambda}\right\}\cosh\left\{\frac{h_{cr}}{2\lambda}\right\} = 0 \tag{6.13}$$

$$\frac{24C_{cr}\phi}{h_{cr}{}^{4}\upsilon R_g T}K^2 - \frac{20H}{h_{cr}{}^{6}} - \frac{B}{8\pi\lambda^3}\operatorname{csch}^4\left\{\frac{h_{cr}}{2\lambda}\right\}\left[2+\cosh\left\{\frac{h_{cr}}{\lambda}\right\}\right] < 0 \tag{6.14}$$

The effect of each of these components of the disjoining pressure on the critical salt concentration is analyzed and discussed in Section 6.4.

6.4 EXPERIMENTAL METHOD

Thin liquid film interferometry with the experimental setup outlined in (Firouzi and Nguyen, 2014a; Karakashev et al., 2008) was utilized to study the effect of salts on bubble coalescence. The necessary details of the experimental setup are explained as follows.

A cylindrical glass tube called the film holder with an inner diameter of 4 mm housed in an enclosed glass cell was used to produce the liquid film. A biconcave droplet of the investigated salt solution was created inside the film holder. A small amount of the liquid was kept in the cell to saturate the environment inside the glass cell. Before each test, the setup was left for about one hour to reach thermal equilibrium so as to avoid film thinning due to evaporation. A digital nano-pump connected to the film holder through a glass capillary tube was used to control the amount of the liquid in the droplet and to bring the surfaces of the biconcave droplet towards each other to form a film. The pump was stopped once the biconcave surfaces were close enough to form a film and allow the pressure difference along the film surface to drive the film drainage. A metallurgical microscope was used to observe the interferograms created by the reflection of the white light from the air- liquid interfaces. The interferograms were recorded for off-line processing. All salts were obtained from Sigma-Aldrich (Australia) with purity higher than 99.5% and further purified by either roasting at 500°C for 4 hours or foam fractionation by bubbling the solutions with nitrogen gas for 2-3 minutes to remove organic trace contaminants. Pure deionised (DI) water with resistivity of 18.2 MΩ.cm was produced from tap water purified by a reverse osmosis unit and then with a Milli-Q system (Millipore).

The film thickness and radius were determined by analyzing the recorded interferograms using a MATLAB program written by our group. The colourful interferograms were filtered with the wavelength $\lambda' = 546\,\text{nm}$ to produce monochromatic interferograms. The film thickness (h) was calculated by using the average light intensity from each image to obtain the temporal profile of the

film thickness. The *h* profile was obtained from the ratio of the measured intensities, *I*, and the maximum and minimum intensities (I_{max} and I_{min}) using the interferometric equation (Nguyen and Schulze, 2004).

$$h = \frac{\lambda'}{2\pi n}\left[\delta\pi \pm \arcsin\sqrt{\frac{\Delta(1+r)^2}{(1-r)^2 + 4r\Delta}}\right] \tag{6.15}$$

where the Fresnel reflection coefficient, $r = (n-1)^2/(n+1)^2$, for the air-solution interface is a function of the water refractive index, *n*, and δ = 0, 1, 2, ... is the order of the interference patterns; and $\Delta = (I - I_{min})/(I_{max} - I_{min})$ (Nguyen and Schulze, 2004). Each experiment for a particular salt type and concentration was repeated at least 20 times to obtain statistically reliable data.

6.5 RESULTS AND DISCUSSION

6.5.1 EXPERIMENTAL RESULTS

It has been experimentally shown that liquid films with radii larger than 50 µm are not homogenous and plane parallel (Manev et al., 1997). Therefore, to avoid any external disturbances followed by surface corrugations and dimpling during the film drainage, the nano-pump was stopped just before the formation of a liquid film (with the maximum suction rate of 100 nL/s). Figure 6.2 shows the film thickness profile of 0.125 M LiCl solutions across the film radius during its evolution. The drainage time was normalized relative to the lifetime of the film measured from the instant of the film formation (the first interferogram) until the film ruptured. It is shown that the film radii are almost constant and smaller than 50 µm during the film drainage which ensures that the film drainage is not influenced by the suction rate as the initial driving force. The results also show that the film is reasonably plane-parallel after the initial dynamic stages of the film drainage, quantitatively at the drainage time normalized by the film lifetime t* > 0.3. Therefore, under this condition the disturbing effect of hydrodynamics on the film drainage can be eliminated theoretically. Figure 6.3 shows the effect of different suction rates on film drainage of 0.195 M NaBr solutions from the moment of the formation of the film until its rupture. As shown in this figure, the suction rate of the nano-pump in

the investigated range does not affect the film drainage significantly. The results show that increasing the suction rate has an initial effect on the film drainage for $t^* < 0.1$, but for $t^* > 0.1$ the difference in the film thickness profiles is just within the experimental error.

It was also noted that for each salt there is a critical concentration above which the liquid films last for up to almost 10 s, unlike the films at concentrations below the critical salt concentration which rupture instantly or last for less than 0.2 s. The critical salt concentration increased according to the salt type following the order: NaF < NaCl < LiCl < KCl < NaBr < NaI. Critical concentrations of the investigated salts are compared with the literature data in Table 6.1. Different experimental methods, salt purity and interface approach speed (suction rate) can be the reasons for the difference between the reported critical concentrations in the literature and this work. As shown in Table 6.1, the critical concentration of NaCl of this work is close to that of Karakashev et al. (2008) which was conducted under similar conditions using the same method. Shown in Table 6.1 is also the critical thickness (at which the film ruptured) of saline liquid films.

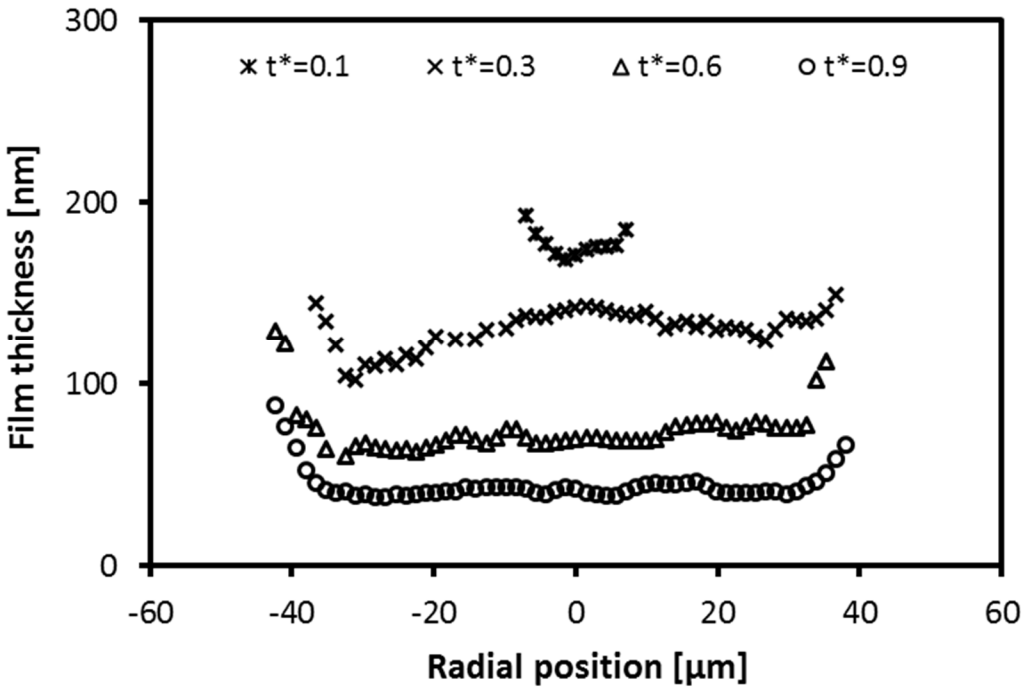

Figure 6.2. Film thickness profile of LiCl 0.125 M at different times and the suction rate of 100 nL/s.

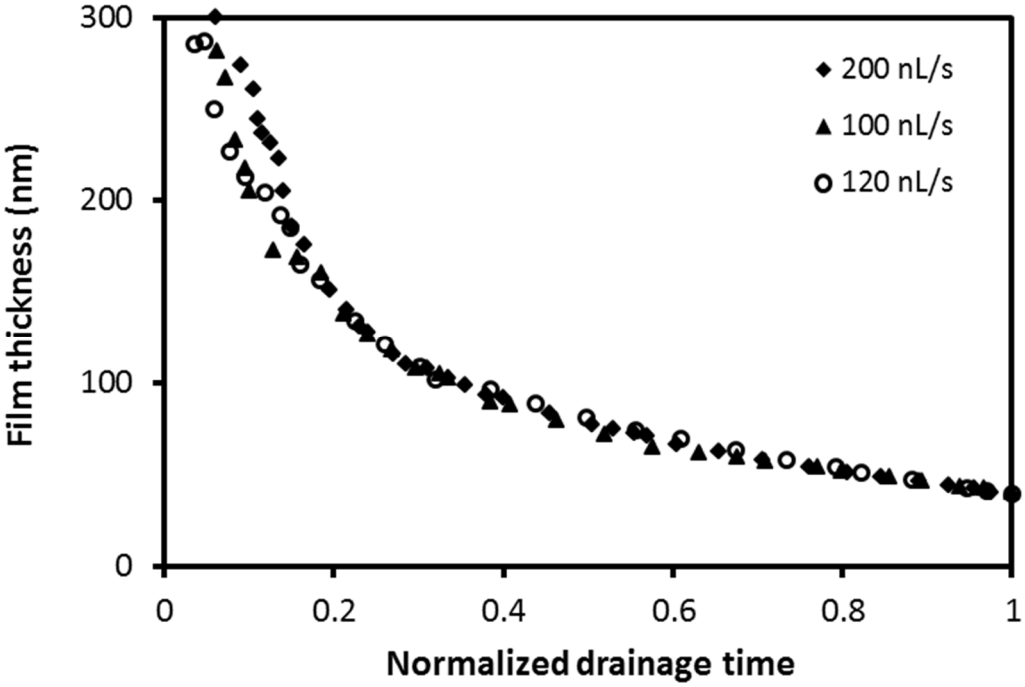

Figure 6.3. Transient profiles of film thickness of 0.195 M NaBr solution at suction rates of 100, 120 and 200 nL/s.

Table 6.1. Critical concentrations and rupture thicknesses of the saline water films at their critical concentrations at u = 10 µm/s.

Salt	Critical concentration [M]		h_{cr} ±SE [nm]
	Literature	This work	
NaF	Not available	0.080±0.0025*	33.12±0.43
NaCl	0.175[a], 0.075[b], 0.208[c], 0.1[d]	0.115±0.0025	35.62±0.61
LiCl	0.160[a], 0.1[d]	0.125±0.0025	35.96±0.12
KCl	0.23[a], 0.12[b]	0.150±0.0025	38.14±0.98
NaBr	0.22[a]	0.195±0.0025	40.01±0.70
NaI	>1[a]	0.345±0.0025	43.06±1.43

[a] Lessard and Zieminski (Lessard and Zieminski, 1971)
[b] Craig et al. (1993)
[c] Christenson et al. (2007)
[d] Karakashev et al. (2008)
* The critical salt concentrations were obtained in 0.005 M concentration interval which can result in an error of ±0.0025 M.

6.5.2 EFFECT OF VAN DER WAALS ATTRACTIONS

Traditionally, only van der Waals attractions have been considered in the modelling of the salt critical concentration (Marrucci, 1969; Prince and Blanch, 1990). The effect of vdW attractions on the critical salt concentration can be evaluated by ignoring the last term for the hydrophobic attraction in Eqs. (6.12)- (6.14). Figure 6.4 compares the predicted critical salt concentrations with the experimental results from this work (table 6.1) and literature (table 4.1) for the critical salt concentration (Karakashev et al., 2008; Lessard and Zieminski, 1971). The significant difference between the model predictions and the experimental data for the critical salt concentrations shown in Figure 6.4 indicates that vdW attractions are rather weak to balance the pressures in Eq. (6.6) for predicting the critical salt concentrations. Therefore, hydrophobic attractions which are believed to be significantly stronger than vdW attractions are considered in the model to predict the critical salt concentration. The details are discussed in the following sections.

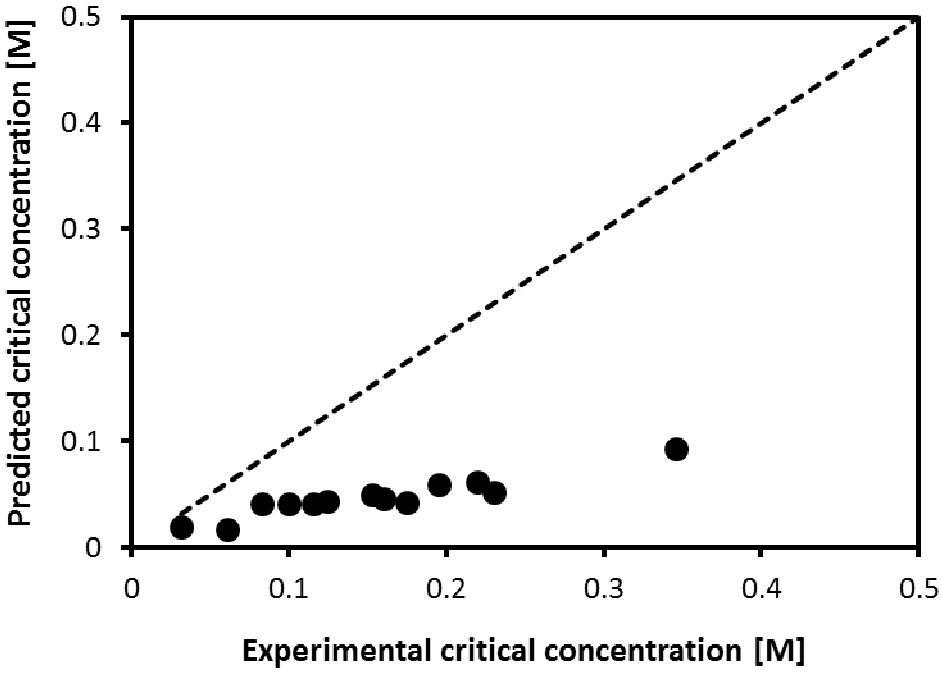

Figure 6.4**.** Comparison of the theoretical critical concentrations by considering the long-ranged retarded Casimir-van der Waals attraction $\left(H = 3.492\times 10^{-29}\,\text{J.m}\right)$ with the experimental results shown in tables 6.1 and 4.1 (the dashed line represents a perfect match with experimental data).

6.5.3 EFFECT OF HYDROPHOBIC ATTRACTIONS

To evaluate the impact of hydrophobic attractions on the critical salt concentration, the hydrophobic strength (B) and decay length (λ) in Eq. (6.11) are required. The following sections focus on determining these parameters to predict the critical concentration of salts.

6.5.3.1 USING THE AVAILABLE HYDROPHOBIC PARAMETERS

For expected hydrophobic attractions in pure water sandwiched between two hydrophobized mica surfaces, B and λ were predicted to be 0.5 mN/m and 15.8 nm respectively (Eriksson et al., 1989). In another study (Nguyen & Nguyen, 2009) the model suggested by Eriksson et al. (Eriksson et al., 1989) was employed to predict hydrophobic attractions in DI water films between two bubbles (foam films). By setting λ=15.8 nm, the hydrophobic strength was predicted to be B = 0.09 mN/m which is calculated using $B = 4\pi\lambda B'$, where $B' = 440$ Pa (Nguyen & Nguyen, 2009). These values for the hydrophobic strength and decay length were incorporated into Eqs. (6.12)- (6.14) as the initial guess and the final equations (containing both the hydrophobic and Casimir-van der Waals attractions) could be solved simultaneously for the critical salt concentration and film thickness.

Figure 6.5 compares the theoretical critical concentration and film thickness of investigated salt solutions with the experimental results of this work. The theoretical critical concentration and thickness of salt solutions using the B and λ values for the water film between hydrophobized mica surfaces are significantly overestimated in comparison to the experimental data. In contrast, when the B value for the foam films of DI water is used, the theoretical critical salt concentrations are very close to the experimental results. However, the critical film thickness of salt solutions is almost constant around 44 nm regardless of the salt type, unlike the experimental results where film thickness decreases with increasing K, which is specific to the salt type. Assigning the same hydrophobic strength and length to all saline liquid films in the model could be the reason for predicting the same critical thickness. Therefore, the next section examines this issue by allowing the hydrophobic strength and length to change with each of the different salts, i.e., the hydrophobic attraction parameters can be determined using the experimental results of this work for the critical salt concentration and film thickness.

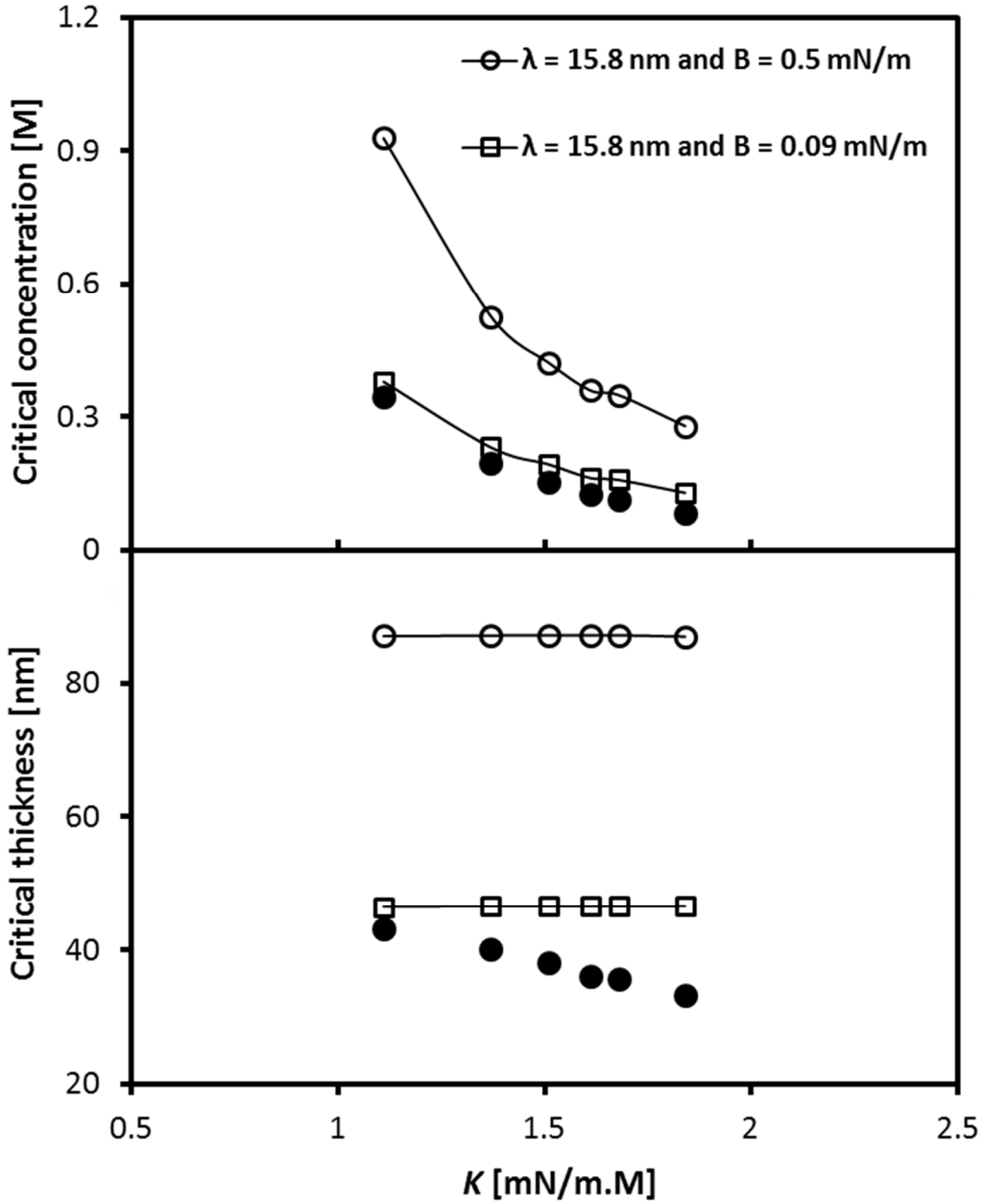

Figure 6.5**.** Comparison of the experimental (filled circles) and the theoretical (empty symbols) critical salt concentration and film thickness versus *K* using the available hydrophobic strengths and decay lengths (Eriksson et al., 1989, Nguyen & Nguyen, 2009).

6.5.3.2 DETERMINING HYDROPHOBIC PARAMETERS USING THE EXPERIMENTAL DATA

Conversely, knowing the critical salt concentration and film thickness from the experimental results shown in Table 6.1, Eqs. (6.12) to (6.13) were solved simultaneously for *B* and λ. The results for *B* and λ values versus the critical concentration of salts are shown in Figure 6.6. Interestingly, the

predicted decay lengths of hydrophobic attractions in each salt solution are close to 15.78 nm. This decay length is very close to λ=15.8 nm predicted for the water film between two hydrophobized mica surfaces (Eriksson et al., 1989) and solutions of sodium dodecyl sulfate (SDS) in the presence of 0.3 M NaCl between two bubbles (Angarska et al., 2004). Indeed, λ is expected to be the same for all hydrophobic surfaces under identical solution conditions since it is a bulk property and characterizes the propagation of the hydrogen-bond ordering effect on water molecular structure between the film surfaces (Eriksson et al., 1989). Predicting almost identical λ values in the liquid films of water and aqueous solutions of low SDS and salt concentrations indicates that the hydrogen-bond ordering effect of the salts and SDS at the investigated concentrations is independent of the critical concentrations. Unlike the λ, the predicted hydrophobic strength (which characterizes the surface hydrophobicity) (Angarska et al., 2004, Eriksson et al., 1989) changes noticeably for different salt solutions. The results show that the evaluated B values for the salts in this work are closer to the B value for the water films between two bubbles (Nguyen & Nguyen, 2009) compared to that between two hydrophobized mica surfaces (Eriksson et al., 1989). To predict the experimental critical salt concentration and film thickness, Eqs (6.12) to (6.13) were solved again by assigning 15.78 nm to the decay length and using our experimental results for C_{Cr} to determine B values of the salt solutions. To examine the relationship between the predicted B and hydrophobicity of the surfaces (which is explained in detail in the following section), the B values were plotted versus the salting-effect coefficient (K_s) of the salts. A power law relationship $B = 9.115\times10^{-6}\times K_s^{-0.930}$ was found between the values of B and K_s. Incorporating this correlation into Eqs. (6.12) to (6.13) and setting λ=15.78 nm, these equations were solved for the critical salt concentration and film thickness of liquid films. Figure 6.7 compares the predictions of this work and the models proposed by Marrucci (1969) and Prince & Blanch (1990) relative to the experimental critical salt concentrations from this work and the literature. Since the bubble radius is required by the models in calculating the critical salt concentration, the absence of the bubble size in many reports on the critical salt concentration in the literature limits further validation of the model. The results in Figure 6.7 evidently show that both theories developed based on the vdW attraction significantly under-predict the experimental results compared to the predictions of this work, which are in close agreement with the experimental data from this work and the literature.

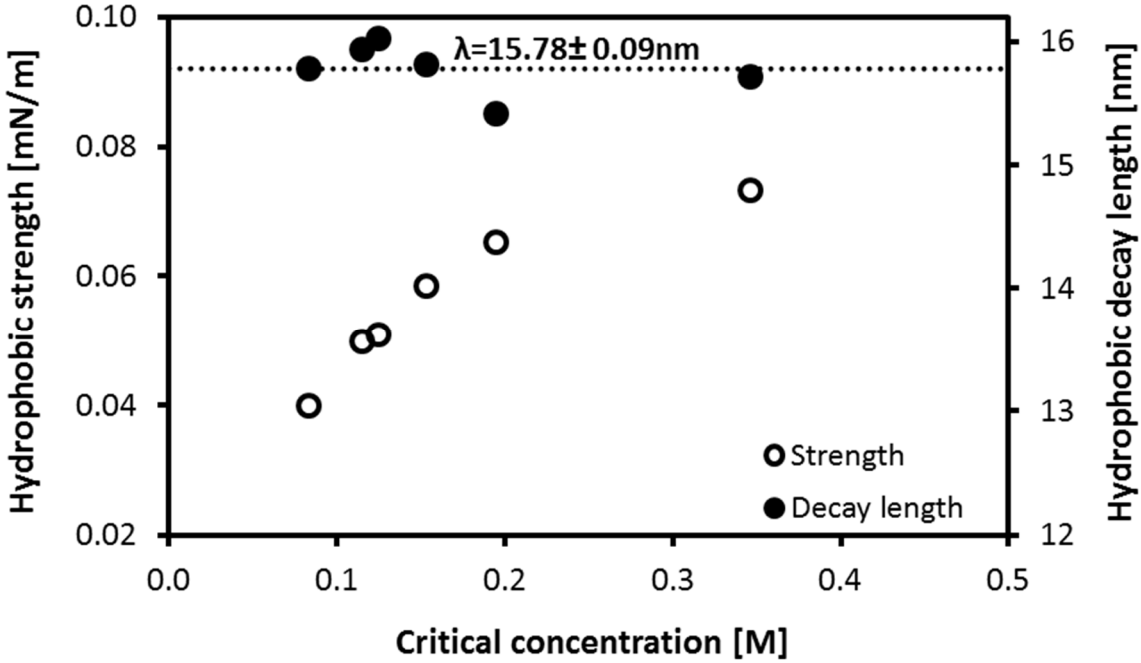

Figure 6.6**.** Predicted hydrophobic strength and decay length using the experimental results for h_{cr} and C_{cr}

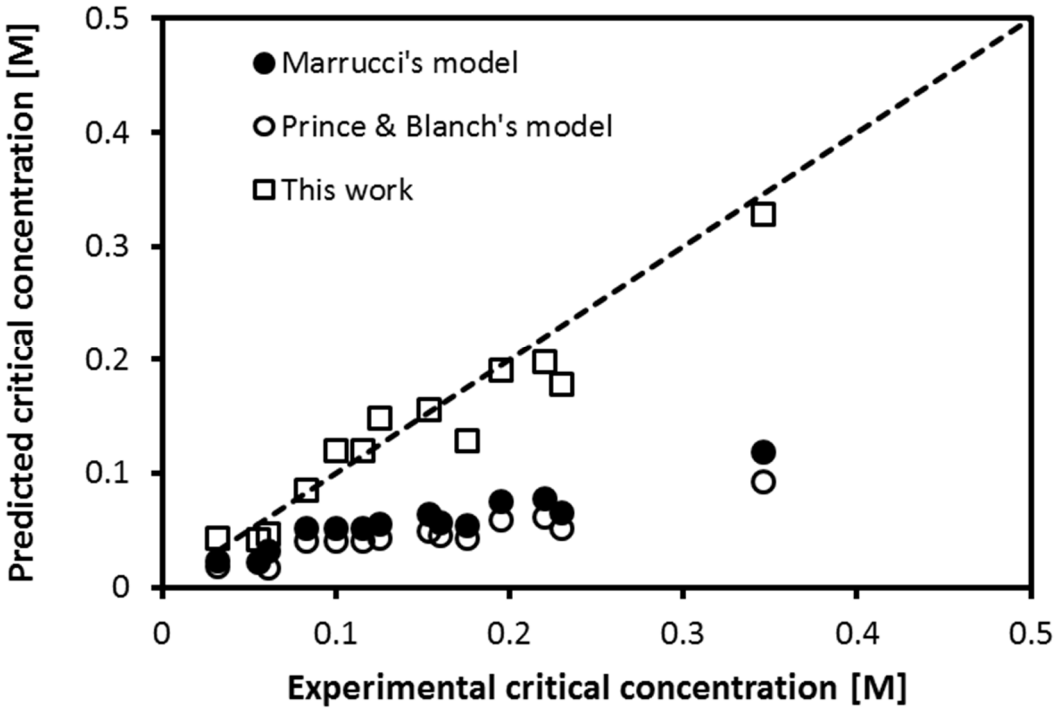

Figure 6.7. Comparison of the theoretical and experimental critical salt concentration of this work and the literature (Karakashev et al., 2008; Lessard and Zieminski, 1971) (the dashed line represents a perfect match with experimental data).

6.5.4 EFFECT OF GAS SOLUBILITY

There is evidence in the literature indicating the importance of dissolved gases in hydrophobic attractions. Experimental studies in this regard outline that the strength of hydrophobic attractions decreases considerably in (partially) degassed water relative to normal water between hydrophobized solid surfaces (Considine et al., 1999; Mastropietro and Ducker, 2012; Meyer et al., 2004; Stevens et al., 2005). Bridging of nano-bubbles on the hydrophobized surfaces has been proposed as the origin of the long-ranged hydrophobic attractions between the solid surfaces. However, this explanation cannot be applied for the thin liquid film between two bubbles (foam film) since neither of the surfaces is solid. The increase in local disruption of hydrogen bonds of water molecules due to the migration of dissolved gases has been suggested as the mechanism responsible for the long-ranged hydrophobic attractions in foam films (Nguyen & Nguyen, 2010). Indeed, the migration of dissolved gases decreases the effective viscosity of the water film, which results in a faster drainage of the liquid film owing to the increase in surface mobility. Salts are known to reduce the solubility of gases which play a significant role in bubble coalescence via hydrophobic attractions (Craig et al., 1993; Henry et al., 2006; Weissenborn and Pugh, 1996). The effect of salts on gas solubility is described by the Setchenov equation $\log\left(S^o / S\right) = K_s.C$ where S^o and S are the solubility of gas in pure water and saline solutions respectively, K_s is the salting-effect coefficient and C is the salt concentration in molar (Narita et al., 1983). It was previously demonstrated that the salting-effect coefficient increases linearly with the surface tension gradient with respect to the concentration of investigated salts ($K = d\sigma / dC$) (Weissenborn and Pugh, 1996). This relationship implies that salts with a higher K which have a smaller critical concentration (shown in Figure 6.5), salt out more strongly dissolved gases and, therefore, affect bubble coalescence inhibition at a lower concentration. It was also suggested that the fluctuations (migration) of dissolved gases influence the surface tension due to the ion hydration and consequent change in water structure. This relationship can be explained by the

hydration of ions where large ions like I^- with the loose hydration shell have a relatively large space between water molecules, which can accommodate more gas molecules. In contrast, small ions with high charge density bind the water molecules firmly and cause a reduction in the number of dissolved gases due to the compaction of water molecules (Weissenborn and Pugh, 1996, Tromans, 2000). The higher the number of dissolved gases, the more hydrogen bonding disruption is expected, which results in lower surface mobility and tension and higher hydrophobic attractions. The change of water volume upon the addition of one mole salt at constant temperature and pressure (referred to as the partial molar volume of salt) has been proven to be very useful in illuminating ion-water interactions in solutions (Millero, 1972). Depending on the ion size and charge, the volume change can be positive or negative. The higher the charge and the smaller the radius of the ion, the firmer the water molecules are packed around the ion than in bulk water, which causes a decrease in the net volume of the system due to the ordering effect of the ion on water structure. Figure 6.8 shows the relationship between the partial molar volume, ϕ_V^o of salts at infinite dilution and the predicted hydrophobic strength with $K = d\sigma / dC$. ϕ_V^o is an indicative measure of ion-solvent and solvent-solvent interactions in the absence of ion-ion interactions which can represent the effect of ions on water structure.

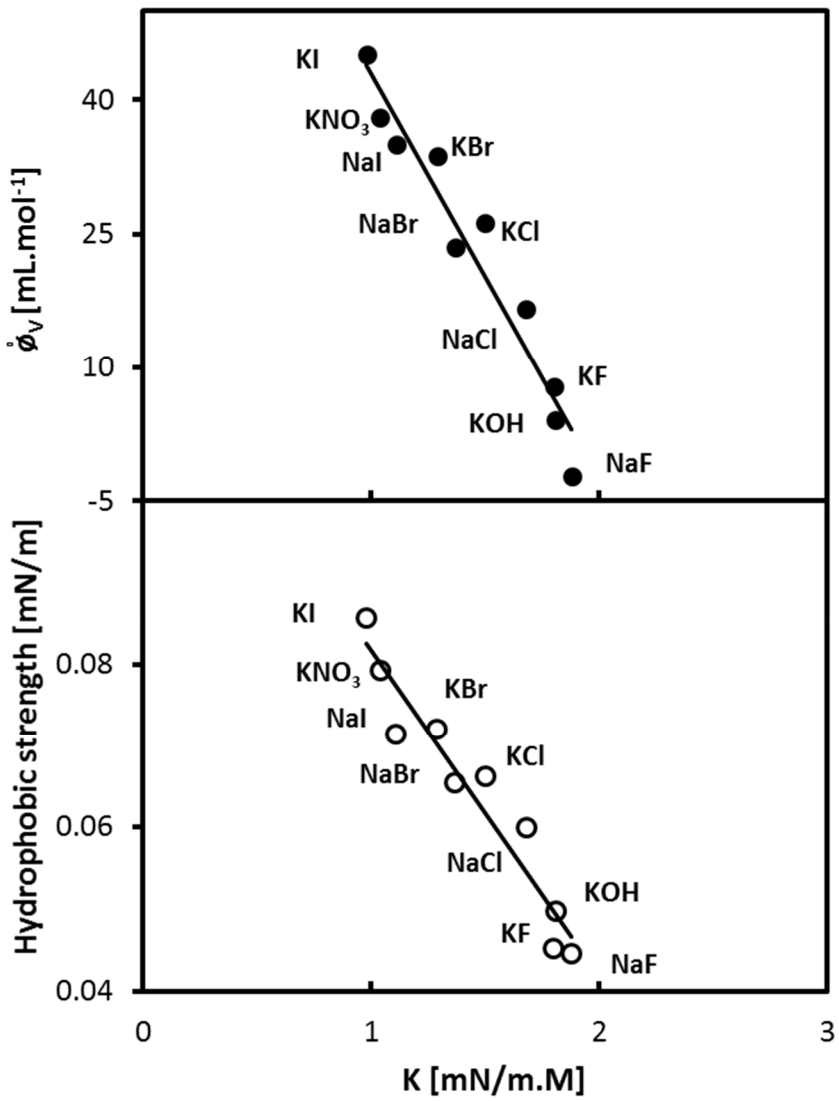

Figure 6.8. Change of partial molar volume of salts at infinite dilution and hydrophobic strength with *K*. The partial molar volume data are taken from (Millero, 1972).

The results in Figure 6.8 show a decreasing trend for the ϕ_V^o and *B* with increasing *K* for the 1:1 salts when the size of either the cation or anion decreases, which results in lower gas solubility and, therefore, weaker hydrophobicity. These results align with the results of sum frequency generation spectroscopy (Liu et al., 2004) and molecular dynamic simulation (Horinek et al., 2009; Jungwirth and Tobias, 2002) regarding the enhancement of large ions such as I^- at the air-water

interface (hydrophobic surface), which is attributed to the natural hydrophobicity of these ions compared to small hydrophilic ions like F^-. Therefore, the increasing trend of hydrophobic strength shown in Figure 6.8 with increasing hydrophobicity of the air-salt solution interface is in agreement with our expectation.To show the effect of gas solubility on the hydrophobic strength and pressure, oxygen solubility in each salt solution relative to pure water, S/S_0 was calculated at the salt critical concentration by using the Setchenov equation. The hydrophobic strength (B) and pressure (Π_{hyd}) of liquid films of salt solutions between two bubbles versus S/S_0 are shown in Figure 6.9(S/S_0 was calculated using the Setchenov equation).The results shown in Figure 6.9 do not indicate any noticeable effect of dissolved gases on the hydrophobic strength and pressure in the salt solutions within the range of the critical salt concentrations (less than 0.3 M) in which the gas solubility does not change significantly.

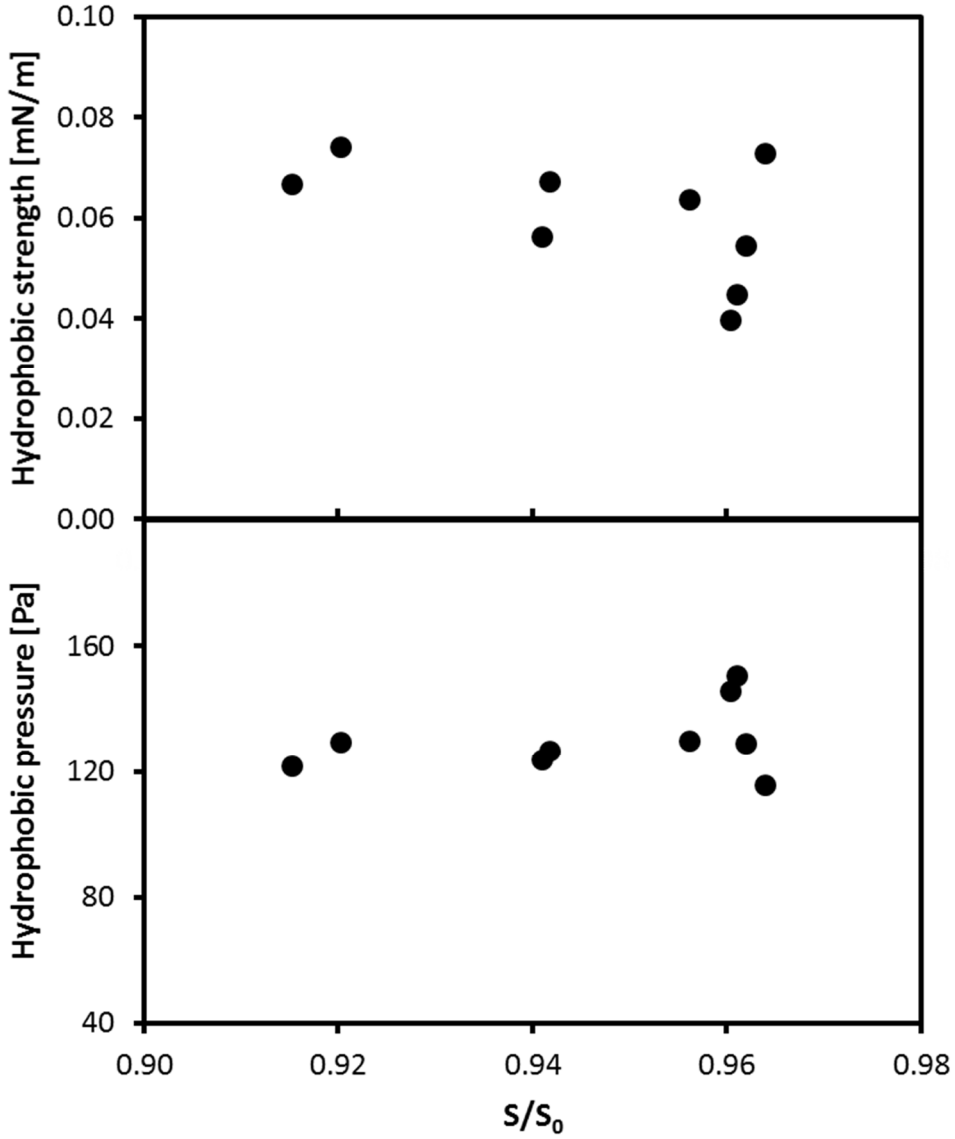

Figure 6.9. Predicted hydrophobic strength and pressure versus gas (oxygen) solubility in salt solutions at critical salt concentrations.

6.6 CONCLUSION

The importance of hydrophobic attractions in coalescence of bubbles in salt solutions was demonstrated by incorporating the hydrophobic attraction into the prediction of the critical (transition) salt concentration. Hydrophobic attractions were incorporated into the model by employing Eriksson et al.'s phenomenological theory. The model parameters, including the hydrophobic strength and decay length, were determined by using the experimental results for the critical concentration and thickness of saline liquid films between two bubbles. The experimental

investigation of the critical salt concentration was undertaken by applying the interferometric technique. Using the experimental results for the critical salt concentration and film thickness of liquid films of investigated salts, we obtained an average decay length of 15.78±0.09 nm. This value agrees with the values previously reported for liquid films of water, and low salt and dilute SDS concentration solutions. A power law correlation between the hydrophobic strength and the salting-effect coefficient representing the salt type was established. According to this correlation, salts with smaller salting-out coefficients and hence higher gas solubility were found to have a larger hydrophobic strength, which is attributed to the hydrophobicity of these ions. The predictions of the proposed model for the critical concentration of salts agree with the experimental data of this work and the literature.

ACKNOWLEDGEMENTS

This research is supported under Australian Research Council's DP Projects funding scheme (project number DP0985079).

REFERENCES

Angarska, J.K., Dimitrova, B.S., Danov, K.D., Kralchevsky, P.A., Ananthapadmanabhan, K.P., Lips, A., Detection of the Hydrophobic Surface Force in Foam Films by Measurements of the Critical Thickness of the Film Rupture. Langmuir, 2004, **20(5)**, 1799-1806.

Attard, P., Moody, M.P., Tyrrell, J.W.G., Nanobubbles: the big picture. Phys. A: Stat. Mech. Appl., 2002, **314(1-4)**, 696-705.

Aveyard, R., Saleem, S.M., Interfacial tensions at alkane-aqueous electrolyte interfaces. Journal of the Chemical Society, Faraday Transactions 1: Physical Chemistry in Condensed Phases, 1976, **72(0)**, 1609-1617.

Chan, B.S., Tsang, Y.H., A theory on bubble-size dependence of the critical electrolyte concentration for inhibition of coalescence. Journal of Colloid and Interface Science, 2005, **286(1)**, 410-413.

Christenson, H.K., Bowen, R.E., Carlton, J.A., Denne, J.R.M., Lu, Y., Electrolytes that Show a Transition to Bubble Coalescence Inhibition at High Concentrations. The Journal of Physical Chemistry C, 2007, **112(3)**, 794-796.

Christenson, H.K., Claesson, P.M., Direct measurements of the force between hydrophobic surfaces in water. Adv. Colloid Interface Sci., 2001, **91(3)**, 391-436.

Claesson, P.M., Blom, C.E., Herder, P.C., Ninham, B.W., Interactions between water-stable hydrophobic Langmuir-Blodgett monolayers on mica. J. Colloid Interface Sci., 1986, **114(1)**, 234-242.

Considine, R.F., Hayes, R.A., Horn, R.G., Forces Measured between Latex Spheres in Aqueous Electrolyte: Non-DLVO Behavior and Sensitivity to Dissolved Gas. Langmuir, 1999, **15(5)**, 1657-1659.

Craig, V.S.J., Ninham, B.W., Pashley, R.M., Effect of electrolytes on bubble coalescence. Nature, 1993, **364(6435)**, 317-319.

Craig, V.S.J., Ninham, B.W., Pashley, R.M., Direct Measurement of Hydrophobic Forces: A Study of Dissolved Gas, Approach Rate, and Neutron Irradiation. Langmuir, 1999, **15(4)**, 1562-1569.

Eriksson, J.C., Ljunggren, S., Claesson, P.M., A phenomenological theory of long-range hydrophobic attraction forces based on a square-gradient variational approach. Journal of the Chemical Society, Faraday Transactions 2: Molecular and Chemical Physics, 1989, **85(3)**, 163-176.

Firouzi, M., Nguyen, A.V., Novel Methodology for Predicting the Critical Salt Concentration of Bubble Coalescence Inhibition. The Journal of Physical Chemistry C, 2013, **118(2)**, 1021-1026.

Firouzi, M., Nguyen, A.V., Effects of monovalent anions and cations on drainage and lifetime of foam films at different interface approach speeds. Advanced Powder Technology, 2014a, **In press**.

Firouzi, M., Nguyen, A.V., On the effect of van der Waals attractions on the critical salt concentration for inhibiting bubble coalescence. Minerals Engineering, 2014b, **58**, 108-112.

Hampton, M.A., Nguyen, A.V., Nanobubbles and the nanobubble bridging capillary force. Adv. Colloid Interface Sci., 2010, **154(1-2)**, 30-55.

Harvie, C.E., Weare, J.H., The prediction of mineral solubilities in natural waters: the Na-K-Mg-Ca-Cl-SO4-H2O system from zero to high concentration at 25° C. Geochimica et Cosmochimica Acta, 1980, **44(7)**, 981-997.

Henry, C.L., Dalton, C.N., Scruton, L., Craig, V.S.J., Ion-Specific Coalescence of Bubbles in Mixed Electrolyte Solutions. The Journal of Physical Chemistry C, 2006, **111(2)**, 1015-1023.

Horinek, D., Herz, A., Vrbka, L., Sedlmeier, F., Mamatkulov, S.I., Netz, R.R., Specific ion adsorption at the air/water interface: The role of hydrophobic solvation. Chemical Physics Letters, 2009, **479(4–6)**, 173-183.

Israelachvili, J., Pashley, R., The hydrophobic interaction is long range, decaying exponentially with distance. Nature, 1982, **300(5890)**, 341-342.

Israelachvili, J., Wennerstrom, H., Role of hydration and water structure in biological and colloidal interactions. Nature, 1996, **379(6562)**, 219-225.

Israelachvili, J.N., *Intermolecular and Surface Forces*. 2005, Academic Press, London.

Jungwirth, P., Tobias, D.J., Ions at the Air/Water Interface. The Journal of Physical Chemistry B, 2002, **106(25)**, 6361-6373.

Karakashev, S.I., Nguyen, P.T., Tsekov, R., Hampton, M.A., Nguyen, A.V., Anomalous ion effects on rupture and lifetime of aqueous foam films formed from monovalent salt solutions up to saturation concentration. Langmuir, 2008, **24(20)**, 11587-11591.

Kim, H.T., Frederick, W.J., Evaluation of Pitzer ion interaction parameters of aqueous electrolytes at 25.degree.C. 1. Single salt parameters. Journal of Chemical & Engineering Data, 1988, **33(2)**, 177-184.

Kirkpatrick, R.D., Lockett, M.J., The influence of approach velocity on bubble coalescence. Chemical Engineering Science, 1974, **29(12)**, 2363-2373.

Lessard, R.R., Zieminski, S.A., Bubble coalescence and gas transfer in aqueous electrolytic solutions. Ind. Eng. Chem. Fun., 1971, **10(2)**, 260-269.

Liu, D., Ma, G., Levering, L.M., Allen, H.C., Vibrational spectroscopy of aqueous sodium halide solutions and air−liquid interfaces: observation of increased interfacial depth. The Journal of Physical Chemistry B, 2004, **108(7)**, 2252-2260.

Manev, E., Tsekov, R., Radoev, B., Effect of thickness non-homogeneity on the kinetic behaviour of microscopic foam film. Journal of Dispersion Science and Technology, 1997, **18(6-7)**, 769-788.

Marrucci, G., A theory of coalescence. Chemical Engineering Science, 1969, **24(6)**, 975-985.

Marrucci, G., Nicodemo, L., Coalescence of gas bubbles in aqueous solutions of inorganic electrolytes. Chem. Eng. Sci., 1967, **22(9)**, 1257-1265.

Mastropietro, D.J., Ducker, W.A., Forces between hydrophobic solids in concentrated aqueous salt solution. Physical Review Letters, 2012, **108(10)**, 106101.

Matubayasi, N., Tsunetomo, K., Sato, I., Akizuki, R., Morishita, T., Matuzawa, A., Natsukari, Y., Thermodynamic Quantities of Surface Formation of Aqueous Electrolyte Solutions: IV. Sodium Halides, Anion Mixtures, and Sea Water. Journal of Colloid and Interface Science, 2001, **243(2)**, 444-456.

Meyer, E.E., Lin, Q., Israelachvili, J.N., Effects of dissolved gas on the hydrophobic attraction between surfactant-coated surfaces. Langmuir, 2004, **21(1)**, 256-259.

Miklavcic, S.J., Deformation of fluid interfaces under double-layer forces stabilizes bubble dispersions. Physical Review E, 1996, **54(6)**, 6551-6556.

Millero, F.J., 1972. Water and aqueous solutions, in *structure, thermodynamics, and transport processes*, ed. Horne, R.A. Wiley-Interscience, New York, p. 519.

Narita, E., Lawson, F., Han, K.N., Solubility of oxygen in aqueous electrolyte solutions. Hydrometallurgy, 1983, **10(1)**, 21-37.

Nguyen, A.V., Nalaskowski, J., Miller, J.D., Butt, H.J., Attraction between hydrophobic surfaces studied by atomic force microscopy. International Journal of Mineral Processing, 2003, **72(1-4)**, 215-225.

Nguyen, A.V., Schulze, H.J., *Colloidal science of flotation*. 2004, Marcel Dekker, New York.

Nguyen, P.T., Hampton, M.A., Nguyen, A.V., Birkett, G., The influence of gas velocity, salt type and concnetration on transition concentration for bubble coalescence inhibition and gas holdup. Chem. Eng. Res. Des., 2012, **90**, 33-39.

Nguyen, P.T., Nguyen, A.V., Drainage, rupture, and lifetime of deionized water films: Effect of dissolved gases? Langmuir, 2009, **26(5)**, 3356-3363.

Nguyen, P.T., Nguyen, A.V., Drainage, rupture, and lifetime of deionized water films: Effect of dissolved gases. Langmuir, 2010, **26(5)**, 3356-3363.

Pashley, R.M., Hydration forces between mica surfaces in electrolyte solutions. Advances in Colloid and Interface Science, 1982, **16**, 57-62.

Pashley, R.M., Craig, V.S.J., Effects of electrolytes on bubble coalescence. Langmuir, 1997, **13(17)**, 4772-4774.

Pitzer, K.S., Thermodynamics of electrolytes. I. Theoretical basis and general equations. Journal of Physical Chemistry, 1973, **77(2)**, 268-277.

Prince, M.J., Blanch, H.W., Transition electrolyte concentrations for bubble coalescence. AIChE Journal, 1990, **36(9)**, 1425-1429.

Sagert, N.H., Quinn, M.J., The coalescence of gas bubbles in dilute aqueous solutions. Chemical Engineering Science, 1978, **33(8)**, 1087-1095.

Steitz, R., Gutberlet, T., Hauss, T., Kloesgen, B., Krastev, R., Schemmel, S., Simonsen, A.C., Findenegg, G.H., Nanobubbles and their precursor layer at the interface of water against a hydrophobic substrate. Langmuir, 2003, **19(6)**, 2409-2418.

Stevens, H., Considine, R.F., Drummond, C.J., Hayes, R.A., Attard, P., Effects of degassing on the long-range attractive force between hydrophobic surfaces in water. Langmuir, 2005, **21(14)**, 6399-6405.

Tromans, D., Modeling oxygen solubility in water and electrolyte solutions. Ind. Eng. Chem. Res., 2000, **39(3)**, 805-812.

Tsao, H.K., Koch, D.L., Collisions of slightly deformable, high Reynolds number bubbles with short-range repulsive forces. Physics of Fluids (1994-present), 1994, **6(8)**, 2591-2605.

Weissenborn, P.K., Pugh, R.J., Surface tension of aqueous solutions of electrolytes: Relationship with ion hydration, oxygen solubility, and bubble coalescence. Journal of Colloid and Interface Science, 1996, **184(2)**, 550-563.

Yaminsky, V.V., Ninham, B.W., Hydrophobic force: lateral enhancement of subcritical fluctuations. Langmuir, 1993, **9(12)**, 3618-3624.

Yaminsky, V.V., Ohnishi, S., Vogler, E.A., Horn, R.G., Stability of aqueous films between bubbles. Part 1. The effect of speed on bubble coalescence in purified water and simple electrolyte solutions. Langmuir, 2010, **26(11)**, 8061-8074.

Yang, J., Duan, J., Fornasiero, D., Ralston, J., Very small bubble formation at the solid-water interface. J. Phys. Chem. B, 2003, **107(25)**, 6139-6147.

Yoon, R.H., Flinn, D.H., Rabinovich, Y.I., Hydrophobic interactions between dissimilar surfaces. J. Colloid Interface Sci., 1997, **185(2)**, 363-370.

CHAPTER 7

CONCLUSIONS AND RECOMMENDATIONS FOR FUTURE WORK

7.1 CONCLUSIONS

This thesis aimed to investigate the effect of salts on bubble coalescence and the stability of thin liquids between bubbles both experimentally and theoretically.

In chapter 2, the current literature concerning the available experimental techniques, explanations for the inhibiting effect of salts and theoretical models to predict the critical salt concentrations were critically reviewed. Critical salt concentrations of NaCl as the most popular inhibiting salt determined via different experimental techniques were compared quantitatively. For a consistent comparison, the available data in the literature regarding the inhibiting effect of salts on bubble coalescence at different salt concentrations were converted to the "percentage coalescence" of bubbles. The transition (critical) concentration of NaCl was determined as the concentration at which the coalescence percentage was reduced by 95% from 100% in pure water to an asymptotic value of the coalescence percentage at a relatively high salt concentration. This concentration was called *TC95*. A linear correlation was demonstrated between the *TC95* of NaCl and the reciprocal of the square root of the bubble radius ($R^{-1/2}$). This correlation highlighted the importance of bubble size in bubble coalescence despite different experimental techniques, bubble approach speeds and salt purities. In this review of the literature, two major gaps were identified. The first is a systematic experimental investigation of the combined effects of a variety of salts in an extensive range of concentration and air-liquid interface approach speed on the stability of foam liquid films. The second gap concerns a physically consistent theoretical description of the behaviour of saline liquid films between bubbles to predict the critical concentration and film thickness of salt solutions.

To address the first issue, a systematic study of the effect of monovalent cations and anions including Li^+, Na^+, K^+, F^-, Cl^-, Br^- and I^- in a concentration range of 0-4 M at interface approach speeds of 10-300 μm/s on the stability of thin liquid films was conducted employing the micro-interferometric technique. The results showed that the lifetime of liquid films increased with increasing the size of either the cation or anion in the salt, which follows the order of NaF > LiCl > NaCl > KCl > NaBr > NaI. For each of the investigated salts, there was an abrupt increase in the film lifetime above the salt critical concentration. It was shown that there was a linear relationship between the non-dimensional specific adsorption energy (which could quantify the ion-specific effect on the water structure) of salts and their critical concentrations. The importance of the air-liquid interface (bubble) approach speed was also demonstrated. To mimic realistic conditions of bubble coalescence in a bubble column, the drainage of liquid films was studied under non-zero interface approach speed by continuously pumping out the liquid within the film holder until the film ruptured. It was shown

that for the foam films of deionized water there was a critical interface speed of 35 μm/s above which films rupture instantly and below which liquid films can last for a few seconds. The results showed that the fast approach of bubbles in salt solutions resulted in a faster increase in the film surface area and diameter following by formation of dimples compared to the uniform and planar liquid films at slow approach of bubbles.

To fill out the second identified gap in the literature, the available theoretical models to predict the critical salt concentration were scrutinized. To resolve the present uncertainties in the models regarding Hamaker constants, the advanced Lifshitz theory was employed. Calculating the van der Waals energy per area for the liquid film between bubbles resulted in $B = 3.492 \times 10^{-29}\,\mathrm{J \cdot m}$ for the retarded Hamaker constant in salt solutions. This value is significantly smaller than the value that was previously assigned to the retarded Hamaker constant to predict the critical salt concentration ($B = 1.5 \times 10^{-28}\,\mathrm{J \cdot m}$). The correct values of Hamaker constants were incorporated in the models and the models' predictions for the critical salt concentration were compared to the experimental results. The significant difference between the theoretical and experimental critical salt concentrations indicated that van der Waals attractions are not sufficient enough to counterbalance the opposing force owing to the Gibbs-Marangoni stress to predict the experimental critical salt concentration. It was also demonstrated that stronger attractions were required to predict the experimental critical concentration and film thickness of salt solutions. It was noted that a generic and physically consistent methodology was lacking for any further modification on the models. Therefore, a novel methodology was proposed to predict the critical salt concentration. The associated model was validated by applying the theory to establish the previous models obtained by the discriminant method. This methodology allows examination of the role of any complex and non-linear disjoining pressure in determining the critical salt concentration. Employing this methodology enabled us to modify the available models by incorporating hydrophobic attractions, which are believed to be significantly stronger than van der Waals attractions in terms of strength and range. The model proposed by Eriksson et al. for hydrophobic attractions was incorporated in the model to predict the critical salt concentration and film thickness. The hydrophobic model parameters, including the hydrophobic strength and decay length , were determined by employing the experimental data of this work for the critical salt concentration and film thickness. The decay length was predicted to be 15.78±0.09 nm which is in close agreement with the values previously reported for liquid films of water and solutions of low salt and SDS concentration. A power law correlation was introduced between the *B* and the salting-effect coefficient (*Ks*) of salts as a salt type indicator. The results showed that the *B* increases

with surface hydrophobicity. To show the effect of dissolved gasses on hydrophobic attractions and constants in salt solutions, the gas (oxygen) solubility was calculated at the critical salt concentration by using the Setchenov equation. The results did not show any significant effect of dissolved gasses on the hydrophobic attractions and constants in concentration range of the critical salt concentrations.

7.2 RECOMMENDATIONS FOR FUTURE WORK

There are a number of issues that could be pursued further from this study which would help to characterise the behaviour of thin liquid films in the absence of surfactants.

The abrupt increase in the film lifetime at salt concentrations above the critical concentration is attributed to the transition in the film drainage from viscous to inertial drainage. This transition is ascribed to the change in surface mobility from a mobile to immobile air-liquid interface owing to the Gibbs-Marangoni effect as a consequence of the non-uniform ion distribution at the interface. Despite the theoretical evidence for the required surface tension gradient for surface immobilization and experimental observations as well as Molecular Dynamic (MD) simulation results for ion distribution at the air-liquid interface, there is no quantitative measurement of the interface mobility. Therefore it is worthwhile to conduct a measurement of the surface mobility of air-liquid interface for different salt solutions.

- The experimental results showed that the film lifetime increased with the salt concentration above the critical concentrations, which was attributed to the decrease in hydrophobic attractions via dissolved gasses, thereby retarding the drainage and rupture of liquid films. For quantitative support, force measurement of salt solutions between two bubbles using Atomic Force Microscopy (AFM) is recommended.
- The experimental results of the drainage of liquid films under zero and non-zero interface approach speeds showed significantly different liquid film behaviours in terms of drainage rate (temporal thickness profile) and growth rate (temporal radius profile). However, there is no theoretical model available to predict the drainage rate of liquid films considering the change in the film size. All of the available models for drainage of liquid films have been derived for liquid films with constant radii smaller than 50 microns to avoid the complexity stemming from surface corrugations. Thus, modelling the drainage of expanding liquid films could be one important aspect of future study of thin liquid films.
- The proposed correlation for the hydrophobic strength of salts as a power law function of the salting-effect coefficient is based on our experimental results for critical concentration

and film thickness of sodium halide and alkali metal salts, which involves potential errors from our experimental measurements and film thickness calculations. Therefore force measurement for hydrophobic attractions in saline foam films at salts critical concentrations can be employed to modify this correlation.

APPENDICES

A1. APPENDIX 1

A1.1. PROCEDURE FOR DETERMINING THE THICKNESS OF FOAM FILMS

Here the optical interferometric method is used to calculate the film thickness. This method is based on determination of the change of the intensity of the light reflected from a film illuminated with a white light. The reflected light from the film surfaces undergoes a phase lag which depends on the local film thickness. As a result of the interference of the light a set of fringes with different colours (Newton rings) is formed. The interferometric images are recorded on a computer for off-line processing. The image analysis was previously done using software for digital processing, in this case Optimas. First a narrow strip passing through the centre of the interferograms was selected. Then the digital signals were converted into photocurrent versus redial distance using a user-defined macro developed in Optimas. Finally, the film thickness was calculated using the interferometric equation described as follows

$$h = \frac{\lambda}{2\pi n}\left[l\pi \pm \arcsin\sqrt{\frac{\Delta(1+r)^2}{(1-r)^2 + 4r\Delta}} \right] \qquad \text{(A1.1)}$$

Where λ is the wavelength of the monochromatic light, $\tilde{r} = (n-1)^2/(n+1)^2$ is the Fresnel reflection coefficient for the air-solution interface, n is the refractive index of water, l = 0, 1, 2, 3… is the order of the interference. $\Delta = (I - I_{\min})/(I_{\max} - I_{\min})$, where I is the instantaneous intensity of the photocurrent taken as an average over a small area on the monochromatic images, $I_{\min}$ and $I_{\max}$ are the minimum and maximum of the light intensity. The difference between the smallest minimum and the largest maximum of light intensity determines the image contrast. Figure A1.1 shows the light intensity and film thickness profiles of a typical dimpled foam film. Order of interference fringes is also shown which are determined by counting backwards from the end of the interferograms.

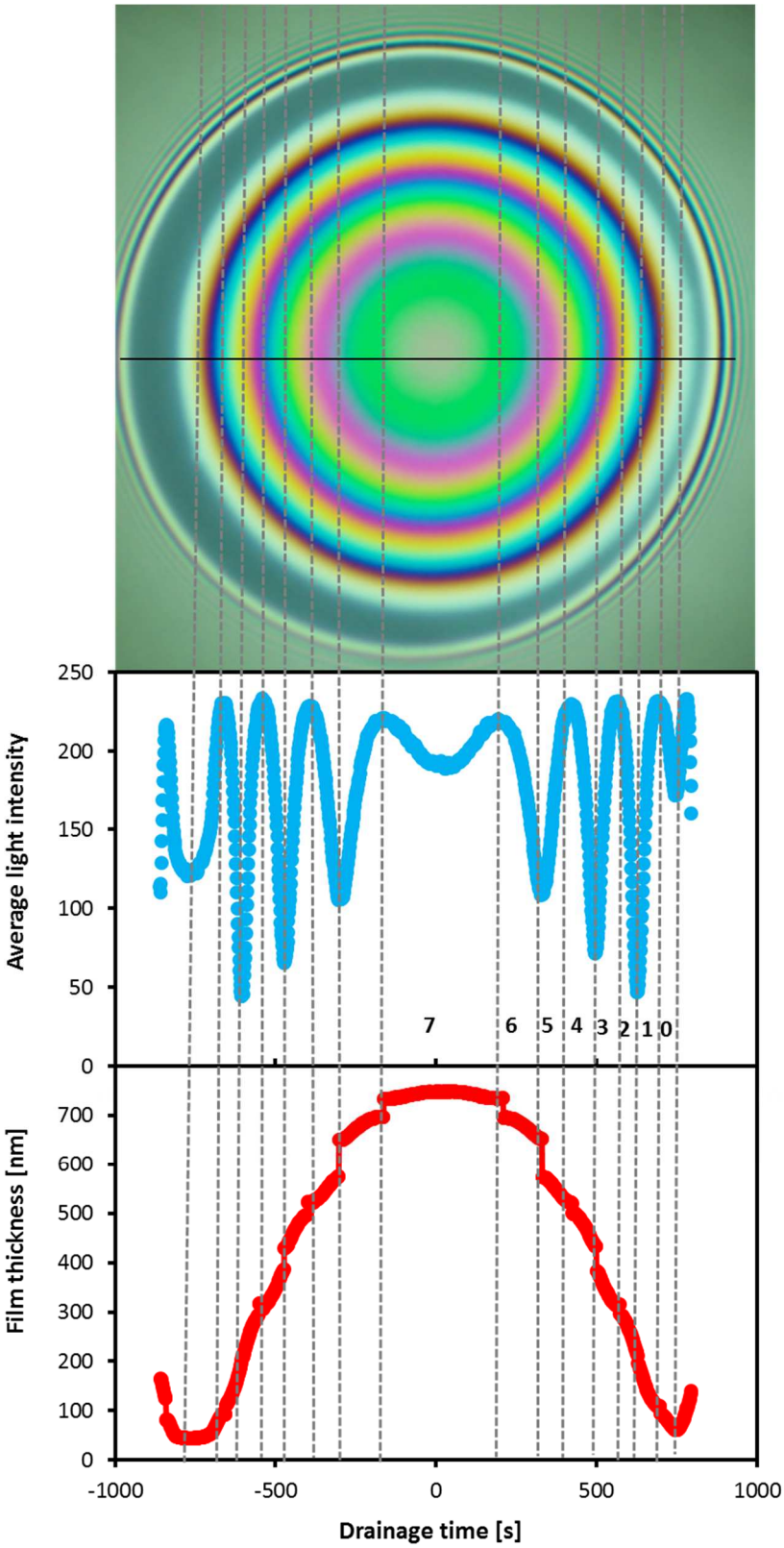

Figure A1.1.Light intensity and film thickness profile of a dimpled foam film

Since just one strip cannot represent the film thickness, more strips have to be analysed for film thickness calculation and for each of them the same procedure has to be repeated, which is very time consuming. Therefore, to improve the film thickness calculation in terms of time and precision, code was written in MATLAB which follows the same procedure as Optimas. First, the polychromatic images are converted to monochromatic interferograms. To determine the film radius, the centre of mass of the binary image (black and white) is obtained. Then by identifying the locations of non-zero pixels on the line passing through the centre of the image, the radius can be determined. Figure A1.2 illustrates the procedure for determining the film radius. After detecting the image boundary, radius and centre based on the value of the pixels on the line passing through the centre, the light intensity versus radial position graph can be plotted (Figure A1.3).

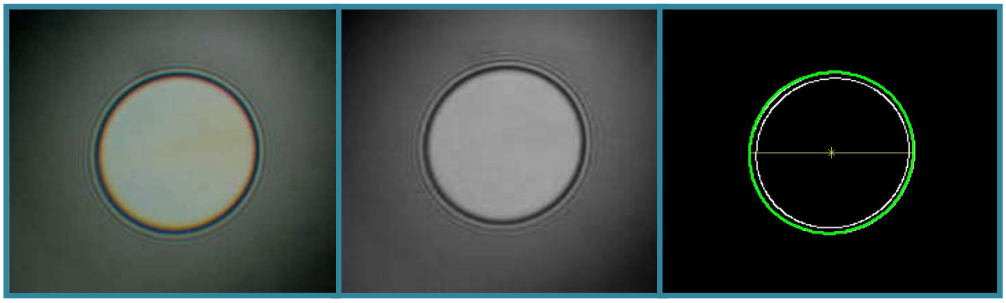

Polychromatic image Monochromatic image Binary image

Figure A1.2. Image processing procedure to find the light intensity profile on one strip

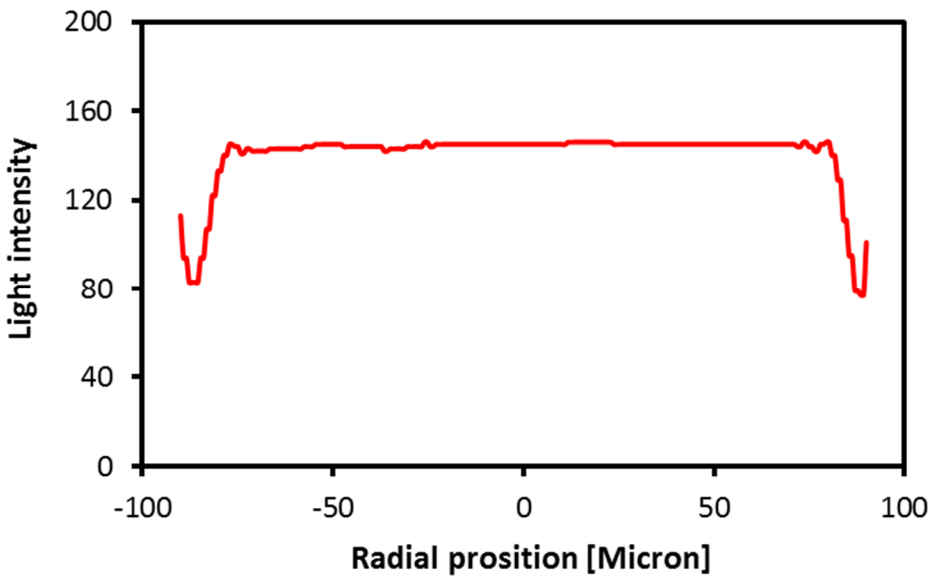

Figure A1.3. Light intensity profile versus radial location for the line shown in Figure A1.9

To choose another line on the film image, the position of the chosen strip is kept constant and the image is rotated with arbitrary small constant angular intervals. Figure A1. 4 illustrates the rotated image. The light intensity profile of each line is stored in an N by M matrix, where N is the number of the pixels on each line and M is the number of the strips. The same procedure is repeated for each of the extracted images (interferograms). Figure A1. 5 illustrates the extracted light intensity and calculated film thickness profiles versus radial position for 1° angular intervals. Finally, by having a temporal light intensity profile (the average of the light intensity profiles for each image), the maximum and minimum values of light intensity are identified to calculate the film thickness using the interferometric equation. Figure A1.6 and Figure A1.7 show the sequential interferograms of a foam film and its temporal intensity and film thickness profiles respectively.

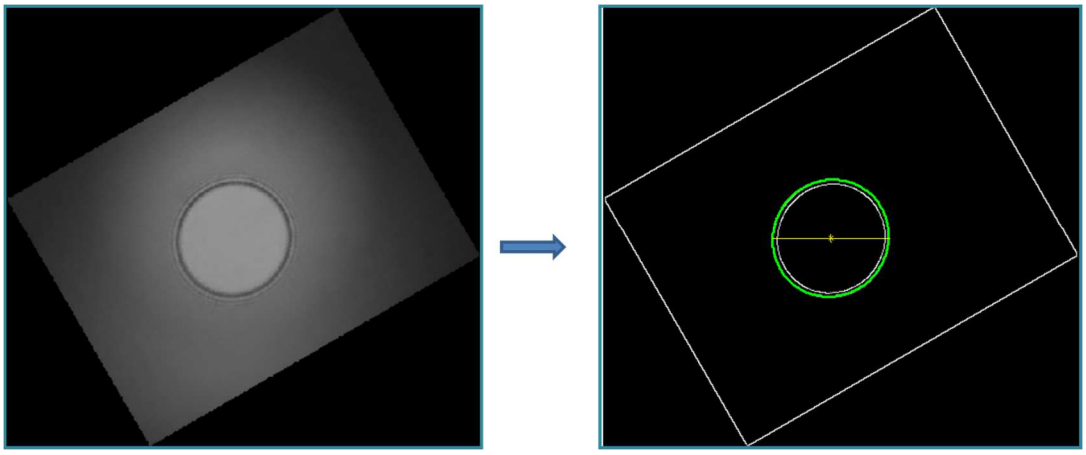

Figure A1. 4. The rotated image to determine the light intensity profile, $\theta = 30^{\circ}$

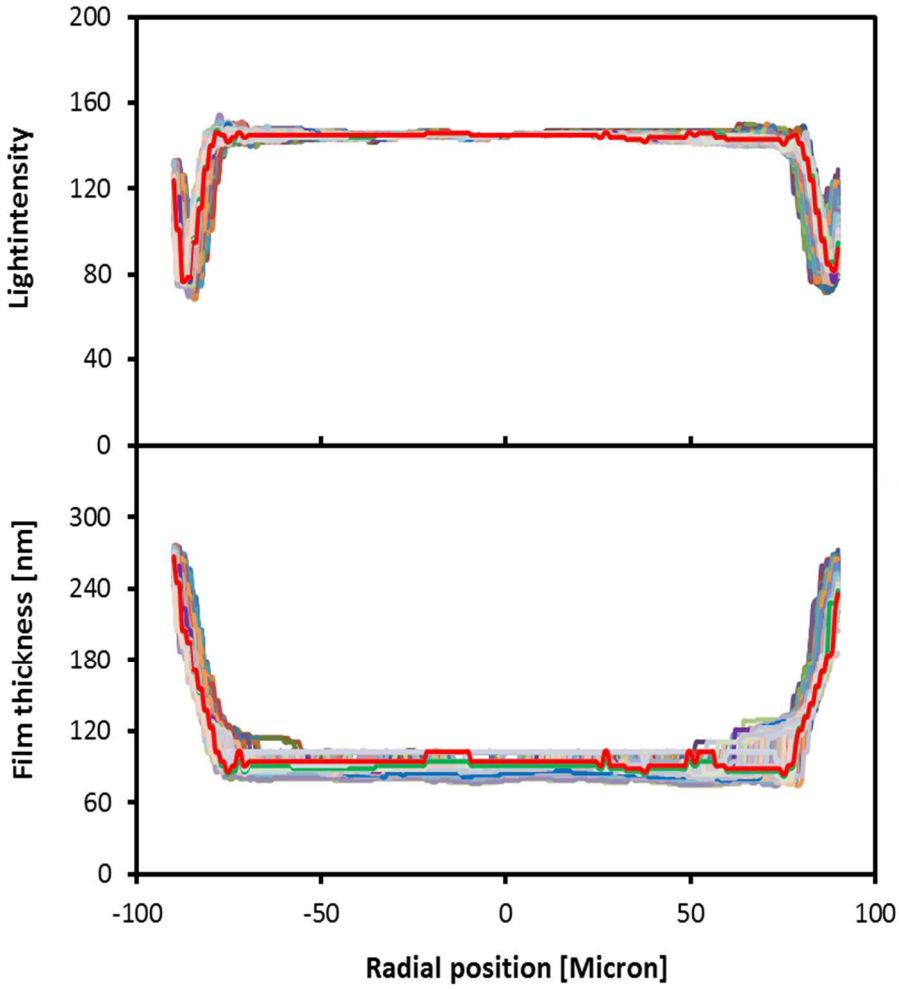

Figure A1. 5. Light intensity and film thickness profiles of 180 lines, the angular interval = 1° (the red line, represents the average film thickness)

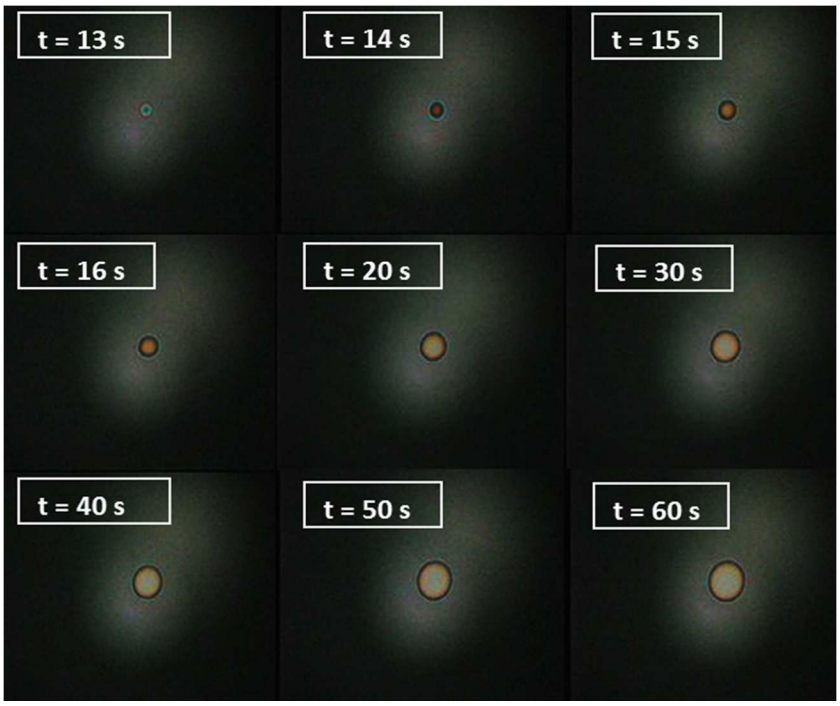

Figure A1.6. Sequential interferograms of a foam film

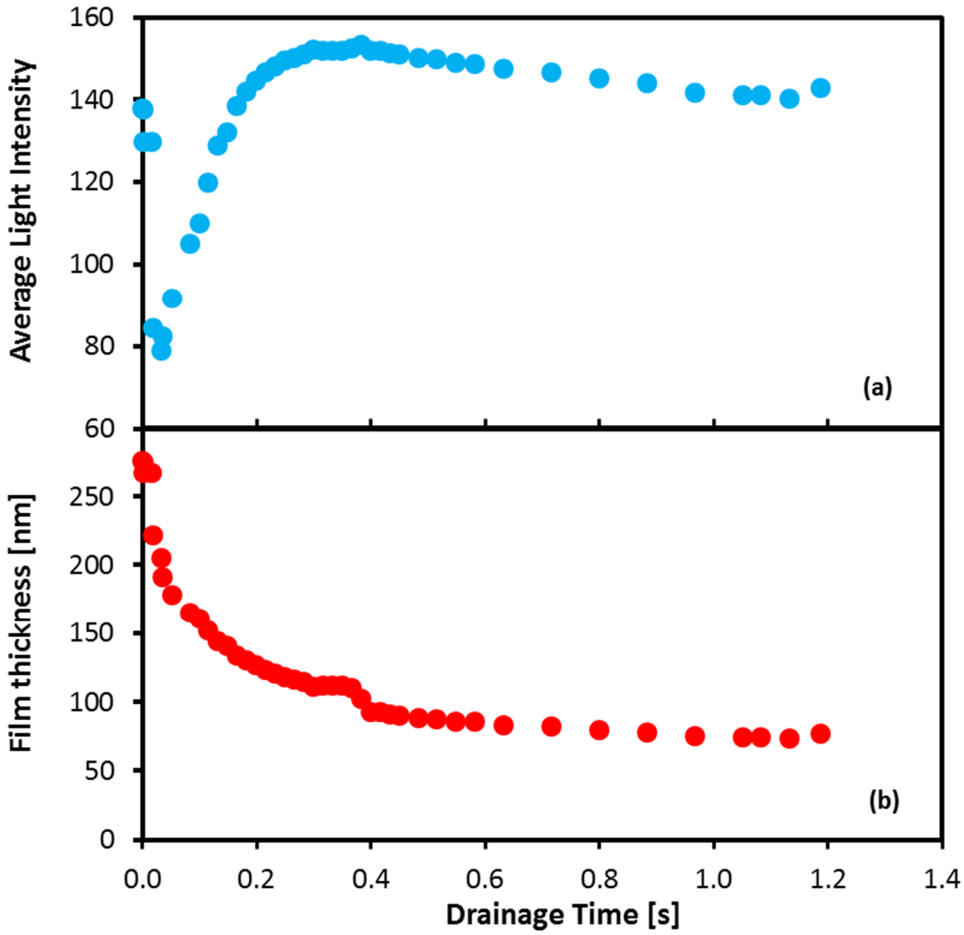

Figure A1.7**.** Temporal profile of (a) light intensity and (b) film thickness of a foam film

A2. APPENDIX 2

A2.1. MODEL DEVELOPMENT FOR DETERMINING THE CRITICAL SALT CONCENTRATION AND FILM THICKNESS

The equations governing the film drainage can be described using a cylindrical co-ordinate system (r, φ, z) with the origin located in the middle plane of the film and the z-axis aligned with the axis of the rotational symmetry of the film as shown in Figure A2.1.

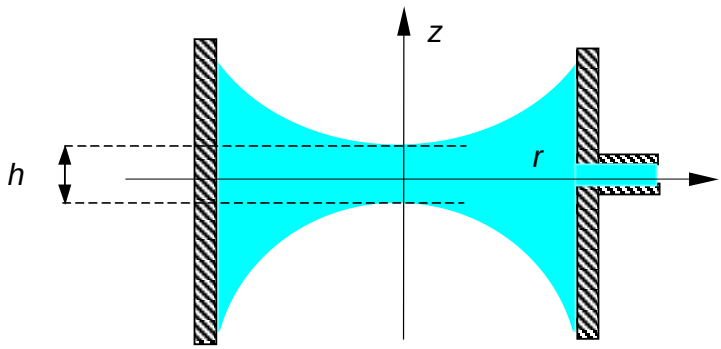

Figure A2.1.Schematic of a liquid film in the film holder in the Scheludko-Exerowa cell

The lubrication approximation of the continuity and Navier-Stokes equations gives the following predictions for the radial, u, and, axial, v, liquid velocities inside the film

$$u(z,r)=U(r)+\frac{1}{2\mu}\left(z^2-\frac{h^2}{4}\right)\frac{\partial p}{\partial r} \tag{A2.1}$$

$$v(r,z)=\left(\frac{h^2 z}{8}-\frac{z^3}{6}\right)\frac{1}{\mu r}\frac{\partial}{\partial r}\left(r\frac{\partial p}{\partial r}\right)-\frac{z}{r}\frac{\partial}{\partial r}(rU) \tag{A2.2}$$

where p is the pressure inside the film, μ is the bulk liquid viscosity, U is the radial velocity of the film surface, and h is the thickness of the (plane parallel) film, which can be determined from the equations for surfactant mass balance inside the film and at the film surfaces. Since the Péclet number of mass transfer of salt inside the film is small, the mass balance inside the film can be described by the diffusion equation: $\frac{1}{r}\frac{\partial}{\partial r}\left(r\frac{\partial C}{\partial r}\right)+\frac{\partial^2 C}{\partial z^2}=0$.Furthermore, for liquid films, the concentration does not significantly change along the film thickness and can be described by the cross-section averaged concentration ϕ. The first integration of the diffusion equation from the film middle plane gives

$$\frac{\partial C}{\partial z}=-\frac{z}{r}\frac{\partial}{\partial r}\left(r\frac{\partial \phi}{\partial r}\right) \tag{A2.3}$$

Along the film surface, the tangential stress of liquid flow is balanced by the Gibbs-Marangoni stress which gives

$$\pm\mu\left(\frac{\partial u}{\partial z}\right)_{z=\pm h/2}=\frac{\partial\sigma}{\partial r} \tag{A2.4}$$

where σ is the surface tension. Inserting Eq. (A2.1) into Eq. (A2.4)

$$\frac{\partial p}{\partial r}=\frac{2}{h}\frac{\partial\sigma}{\partial r}=\frac{2}{h}\frac{\partial\sigma}{\partial C}\frac{\partial C}{\partial r}\cong\frac{2}{h}\frac{d\sigma_0}{dC_0}\frac{d\phi}{\partial r} \quad \text{(A2.5)}$$

where the surface tension gradient with respect to salt concentration is approximated by the linear slope of the surface tension version salt concentration, $d\sigma_0 / dC_0$, in solution as experimentally observed for the halide salts.

The tangential surface velocity can be established from the mass balance at the film surface described by $\frac{1}{r}\frac{\partial}{\partial r}\left(r\Gamma U\right)=\mp D\left(\frac{\partial C}{\partial z}\right)_{z=\pm h/2}$, where Γ is the salt surface excess and D is the salt diffusion coefficients. Inserting Eq. (A2.3) into the surface mass balance equation and integrating the obtained equation gives

$$U=\frac{h}{2}\frac{D}{\Gamma}\frac{d\phi}{dr} \tag{A2.6}$$

The force, $F=\pi R^2\left[P_\sigma-\Pi\left(h\right)\right]$ acting on the film surface can also be determined by integrating the normal component of the pressure tensor over the film surface area, giving

$$F=2\pi\int_0^R\left[p\left(r\right)-p_\infty-2\mu\frac{\partial v}{\partial z}\right]_{z=\pm h/2}rdr \tag{A2.7}$$

where p_∞ is the pressure at the film periphery (in the bulk solution). The velocity derivative in Eq. (A2.7) can be calculated using (A2.7) can be calculated using Eq.(A2.2) which yields

$$F=4\pi\mu RU\left(R\right)+\pi\int_0^R r^2\frac{dp}{dr}dr \tag{A2.8}$$

$$F=4\pi\mu\frac{h}{2}\left(R\frac{D}{\Gamma}\frac{d\phi}{dr}\right)_R+\pi\int_0^R r^2\frac{2}{h}\frac{d\sigma_0}{dC_0}\frac{d\phi}{\partial r}dr \tag{A2.9}$$

Therefore, the first derivative of Eq.(A2.9) results

$$\frac{dF}{dR} = 4\pi\mu \frac{h}{2}\frac{d}{dR}\left\{ R\frac{D}{\Gamma}\left(\frac{d\phi}{dr}\right)_R \right\} + \pi R^2 \frac{2}{h}\frac{d\sigma_0}{dC_0}\left(\frac{d\phi}{dr}\right)_R \tag{A2.10}$$

Employing Gibbs' consideration of the solute (salt) mass balance within the film which is constant, gives

$$d\left[2\pi R^2\,\Gamma + \pi R^2 h C\right] = 0 \tag{A2.11}$$

where Γ is the salt excess averaged over the film surface and C is the salt concentration averaged over the film volume. These two averaged variables may depend on the film radius and thickness. Expanding Eq. (A2.11) gives

$$\frac{4\Gamma}{R} + 2\frac{d\Gamma}{dR} + h\frac{dC}{dR} = 0 \tag{A2.12}$$

Therefore, the solute concentration gradient at the film periphery can be estimated by

$$\left(\frac{d\phi}{dr}\right)_R = \frac{dC}{dR} = -\frac{4\Gamma}{Rh} - \frac{2}{h}\frac{d\Gamma}{dR} \tag{A2.13}$$

Inserting Eq. (A2.13) into Eq. (A2.9) gives

$$\frac{dF}{dR} = -4\pi\mu D\frac{d}{dR}\left\{\left(\frac{R}{\Gamma}\right)_R\left(\frac{2\Gamma}{R} + \frac{d\Gamma}{dR}\right)\right\} - \pi R^2 \frac{2}{h}\frac{d\sigma_0}{dC_0}\frac{4}{h}\left(\frac{\Gamma}{R} + \frac{d\Gamma}{2dR}\right) \tag{A2.14}$$

Rearranging the above equation gives

$$-\frac{2\mu D}{R}\frac{d}{dR}\left\{2 + \frac{R}{\Gamma}\frac{d\Gamma}{dR}\right\} - \frac{d\sigma_0}{dC_0}\frac{4}{h^2}\Gamma\left(1 + \frac{R}{\Gamma}\frac{d\Gamma}{2dR}\right) = P_\sigma - \Pi(h) \tag{A2.15}$$

Assuming that the surface-averaged excess weakly depends on the film radius, Eq. (A2.15) can be simplified to give

$$-\frac{4\Gamma}{h^2}\frac{d\sigma}{dC} = P_\sigma - \Pi(h) \tag{A2.16}$$

The Gibbs surface excess (Γ) is calculated from the Gibbs adsorption isotherm (Marrucci and Nicodemo, 1967):

$$\Gamma = -\frac{1}{\upsilon R_g T}\frac{\partial \sigma}{\partial \ln\left(f.C\right)} \tag{A2.17}$$

where f and C are the activity coefficient and concentration of the salt respectively. Considering f=1 for simplicity results in $\Gamma = -\frac{C}{\upsilon R_g T}\frac{d\sigma}{dC}$. Substituting the expression for the Gibbs surface excess into Eq.(A2.16) gives

$$\frac{4C}{h^2 \upsilon R_g T}\left(\frac{\partial \sigma}{\partial C}\right)^2 - \frac{2\sigma}{R} + \Pi\left(h\right) = 0 \tag{A2.18}$$

where $P_\sigma = \frac{2\sigma}{R}$ is the capillary pressure due to the curvature of bubbles (air-liquid interface).

A3.APPENDIX 3

A3.1. SURFACE TENSION GRADIENT WITH SALT CONCENTRATION OF SALTS

Table A3.1 shows the average surface tension gradient with concentration of different salts. The data are the results of least-square regression analysis of the literature data, including tabulated data and graphs of surface tension versus salt concentration from 0-1 M having a linear dependence of surface tension on molar concentration in the range of interest (0-1 M). All the experimental data are obtained at a constant temperature in the range of $20-30\,^{\circ}\mathrm{C}$ as temperature does not affect $K = d\sigma / dC$ significantly (Slavchov and Novev, 2012; Weissenborn and Pugh, 1996).

Salt molality (mole per kilogram of solvent), m, is converted to molar concentration (mole per litre of solution), C, using the following equation: $C = \rho_s \times m / (1 + m \times MW)$, where ρ_s and MW are the solution density (kg/L) and molecular weight of salt, respectively. Solution densities are taken from the data compiled by Novotny and Sohnel (1988).

Table A3.3. Average surface tension gradient with respect to the salt concentration

Salts	$K = d\sigma / dC \pm SE$ [mN/(mM)]	References
LiCl	1.61±0.06	(Abramzon and Gaukhberg, 1993b; Aveyard and Saleem, 1976; Jarvis and Scheiman, 1968; Matubayasi et al., 1999; Washburn, 2003a; Weissenborn and Pugh, 1996)
NaCl	1.68±0.07	(Abramzon and Gaukhberg, 1993a; Aveyard and Saleem, 1976; Jarvis and Scheiman, 1968; Johansson and Eriksson, 1974; Ozdemir et al., 2009; Washburn, 2003a)
KCl	1.51±0.04	(Abramzon and Gaukhberg, 1993b; Aveyard and Saleem, 1976; Johansson and Eriksson, 1974; Jones and Ray, 1937; Matubayasi et al., 1999; Ozdemir et al., 2009; Washburn, 2003a; Weissenborn and Pugh, 1996)
NaF	1.84±0.01	(Matubayasi et al., 2001; Weissenborn and Pugh, 1996)
NaBr	1.37±0.08	(Abramzon and Gaukhberg, 1993a; Aveyard and Saleem, 1976; Jarvis and Scheiman, 1968; Matubayasi et al., 2001; Washburn, 2003a; Weissenborn and Pugh, 1996)
NaI	1.11±0.04	(Abramzon and Gaukhberg, 1993a; Jarvis and Scheiman, 1968; Johansson and Eriksson, 1974; Matubayasi et al., 2001; Washburn, 2003a; Weissenborn and Pugh, 1996)
KBr	1.29±0.02	(Abramzon and Gaukhberg, 1993a; Washburn, 2003a)
KI	1.00±0.05	(Abramzon and Gaukhberg, 1993b; Johansson and Eriksson, 1974; Ozdemir et al., 2009)
KOH	1.81±0.05	(Abramzon and Gaukhberg, 1993b; Washburn, 2003a; Weissenborn and Pugh, 1996)
KNO_3	1.04±0.02	(Abramzon and Gaukhberg, 1993b; Matubayasi and Yoshikawa, 2007; Washburn, 2003b)
NH_4Cl	1.23±0.07	(Abramzon and Gaukhberg, 1993a; Jarvis and Scheiman, 1968; Matubayasi et al., 2010; Washburn, 2003a; Weissenborn and Pugh, 1996)
$CuSO_4$	1.83	(Washburn, 2003a)
$MgSO_4$	2.61±0.38	(Jarvis and Scheiman, 1968; Washburn, 2003a; Weissenborn and Pugh, 1996)

$ZnSO_4$	1.95	(Washburn, 2003a)
Na_2SO_4	2.76±0.11	(Abramzon and Gaukhberg, 1993b; Aveyard and Saleem, 1976; Jarvis and Scheiman, 1968; Matubayasi et al., 2001; Washburn, 2003a)
K_2SO_4	2.58	(Washburn, 2003a)
$MgCl_2$	3.32±0.27	(Jarvis and Scheiman, 1968; Matubayasi et al., 1999; Washburn, 2003a)
$LaCl_3$	4.8±0.55	(Abramzon and Gaukhberg, 1993b; Weissenborn and Pugh, 1996)

A3.2. AVERAGE SALTING-COEFFICIENT OF SALTS

Table A3. 4. Average salting-effect coefficient, K_s, of different salts at $T = 25\,^{\circ}\mathrm{C}$ and $P = 1\,\mathrm{bar}$

Salts	$K_S \pm SE$ [L mol^{-1}]	References
NaCl	0.145±0.002	(Battino et al., 1983; Cramer, 1980; MacArthur, 1915; Sherwood et al., 1991)
LiCl	0.11	(Battino et al., 1983)
KCl	0.129±0.021	(Battino et al., 1983; MacArthur, 1915)
NaBr	0.131	(Battino et al., 1983)
NaI	0.118	(Battino et al., 1983)
KBr	0.117±0.005	(Battino et al., 1983; MacArthur, 1915)
KI	0.093±0.001	(Battino et al., 1983; MacArthur, 1915)
KOH	0.181±0.007	(Geffcken, 1904; Shoor et al., 1969)
KNO_3	0.102±0.002	(Battino et al., 1983; MacArthur, 1915)
NaF	1.84	(Narita et al., 1983)
$MgSO_4$	0.281±0.008	(Battino et al., 1983; Millero et al., 2002)
Na_2SO_4	0.367±0.033	(Geffcken, 1904; MacArthur, 1915; Millero et al., 2002)
K_2SO_4	0.330±0.045	(Battino et al., 1983; MacArthur, 1915; Millero et al., 2002)